Louisiana State University

LSU Scholarly Repository

1995

Host-Guest Chemistry of Cofacial Binuclear Copper(II) and Zinc(II) Complexes of Bis(beta-Diketone) Ligands.

Laurie A. Brown
Louisiana State University and Agricultural & Mechanical College

Follow this and additional works at: https://repository.lsu.edu/gradschool_disstheses

Recommended Citation

INFORMATION TO USERS

This manuscript has been reproduced from the microfilm master. UMI films the text directly from the original or copy submitted. Thus, some thesis and dissertation copies are in typewriter face, while others may be from any type of computer printer.

The quality of this reproduction is dependent upon the quality of the copy submitted. Broken or indistinct print, colored or poor quality illustrations and photographs, print bleedthrough, substandard margins, and improper alignment can adversely affect reproduction.

In the unlikely event that the author did not send UMI a complete manuscript and there are missing pages, these will be noted. Also, if unauthorized copyright material had to be removed, a note will indicate the deletion.

Oversize materials (e.g., maps, drawings, charts) are reproduced by sectioning the original, beginning at the upper left-hand corner and continuing from left to right in equal sections with small overlaps. Each original is also photographed in one exposure and is included in reduced form at the back of the book.

Photographs included in the original manuscript have been reproduced xerographically in this copy. Higher quality 6" x 9" black and white photographic prints are available for any photographs or illustrations appearing in this copy for an additional charge. Contact UMI directly to order.

HOST-GUEST CHEMISTRY OF COFACIAL BINUCLEAR COPPER(II) AND ZINC(II) COMPLEXES OF BIS(BETA-DIKETONE) LIGANDS

A Dissertation

Submitted to the Graduate Faculty of the
Louisiana State University and
Agricultural and Mechanical College
in partial fulfillment of the
requirements for the degree of
Doctor of Philosophy

in

The Department of Chemistry

by
Laurie A. Brown
B.S., University of Southern Mississippi, 1990
December 1995

UMI Number: 9618273

UMI

Acknowledgments

In appreciation for a multitude of assistance during my graduate work, I would like to mention certain individuals.

First, thanks goes to Dr. Andrew Maverick, my research advisor, for his tireless efforts to teach me something about host-guest chemistry and his amiable personality which he managed to maintain even when faced with disagreeable data.

I also want to thank Dr. George Stanley for his computer and molecular modeling assistance, which he gave freely and always with a smile.

Thanks goes to the members of my Ph.D. committee: Dr. Robert Hammer, Dr. Brian Hales, Dr. Mary Barkley, and Dr. Philip Adams for their dedication to the training and development of new scientists.

I want to acknowledge those graduate students: Abdul Mohammed, Qin Yao, Maria Benites, Alicia James, Hui Fan, and Ralph Isovitsch and the undergraduate students: Jason Morvant, Ramon Rionda, and Greg Clethen with whom I have had the pleasure of working over the past five years.

This work could not have been accomplished without the assistance of Dr. Ravi Laxman, postdoc in our lab; Dr. Frank Fronczek, LSU Chemistry Department Crystallographer; Marcus Nauman and Dr. David Vargus, LSU Chemistry Department NMR Specialists; and Jeff Corkern, Rolly Singh, and Dr. Tracy McCarley, LSU Chemistry MS specialists.

For their prayers and encouragement, I would like to thank Vickie Sweet, James Gross, Jing Yan, Catherine and Johnny Clark, Laurie and Cheryl Castilaw, and Daniel, Bobby, and Andy Johnson.

I want to thank my parents, David and Patsy Brown, for instilling in me the desire to do my best at whatever I attempt and my brother Jason and his wife Sherry for supporting me in whatever that may be.

Last, I want the thank God for His Creation and all of its amazing properties which make science and exciting field in which to be.

Table of Contents

Abstract

We have been synthesizing cofacial binuclear copper(II) and zinc(II) complexes using bis(β-diketone) ligands in order to design a host complex which selectively binds guest molecules and demonstrates catalytic activity. The metal atoms are held by the chelating acetylacetonate groups, of the bis(β-diketone) ligands, in adjacent parallel planes separated by a cavity into which the guest molecule fits. The host-guest interactions are described. The synthesis of these complexes are discussed beginning with the synthesis of the substituted naphthalenes which bridge the metal-acetylacetonate planes.

We needed 2,7-dimethylnaphthalene-1-carbonitrile for the synthesis of the bis(β-diketone) ligand, NBAH$_2$-1-CN. After the first recrystallization of 2,7-dimethylnaphthalene-1-carbonitrile, it was found to exhibit unusual luminescence properties. The intense luminescence was found to be due to trace amounts of impurities which could be removed via column chromatography. Concentrated solutions of 2,7-dimethylnaphthalene-1-carbonitrile were found to emit excimer fluorescence. The fluorescence of solid samples and dilute solutions of 2,7-dimethylnaphthalene-1-carbonitrile was similar.

The methyl groups of 2,7-dimethylnaphthalene-1-carbonitrile derivatives were each brominated once in a free radical bromination to make 2,7-bis(bromomethyl)naphthalene-1-carbonitrile. Pure bis(bromomethyl)naphthalene-1-carbonitrile was needed to make the desired ligand, but the reaction often produced di- and tribrominated side products. The optimization of this reaction and the characterization of the side products are discussed.

The side chain Br groups in 2,7-bis(bromomethyl)naphthalene-1-carbonitrile were replaced by acetylacetonate (acac⁻) groups in order to achieve the desired bridging/chelating bis(β-diketone) ligand (NBAH$_2$-1-CN, 3,3'-[1-cyanonaphthalene-2,7-diylbis(methylene)]bis(2,4-pentanedione). NBAH$_2$-1-Br, 3,3'-[1-bromonaphthalene-2,7-diylbis(methylene)]bis(2,4-pentanedione)) was also synthesized in a similar manner from the corresponding bis(bromomethyl)naphthalene compound. The ligands were treated with copper(II) to form the green cofacial bimetallic complexes (Cu$_2$(NBA-1-X)$_2$, X = CN or Br). Small nitrogenous bases (Dabco (1,4-diazabicyclo[2.2.2]octane), pyrazine, aminopyrazine, and piperazine) were used as guest molecules, binding to the host complexes via the metal atoms. UV-Vis spectroscopy was used to monitor the host-guest interactions. These interactions are reported in the form of binding constants.

Cofacial bimetallic zinc(II) complexes were made using the NBAH$_2$ (3,3'-2,7-naphthalenediylbis(methylene))bis(2,4-pentanedione) ligand and Dabco, pyrazine, and piperazine as guests. These colorless complexes were found to luminesce at wavelengths similar to the NBAH$_2$ ligand. Luminescence, lifetime, and NMR spectroscopy data on these complexes are presented.

Chapter 1. Introduction

1.1 Host-Guest Chemistry in the Area of Molecular Recognition

The dynamic process by which one molecule recognizes and interacts with another having complementary features is known as molecular recognition.[1] Molecular recognition frequently involves the modeling of enzyme-substrate systems with the goal of gaining a better understanding of these naturally occurring systems or mimicking their activity. These goals are not mutually exclusive and, quite frequently, success in one results in achieving the other. In other words, if one sets out to synthesize a molecule which will mimic the catalysis occurring at the active site of an enzyme, it is highly probable that information of the structural orientation and electronic features necessary for catalysis will be determined.

These enzyme mimics, which are tools in the area of molecular recognition, can be referred to as host complexes.[2] Host complexes resembling enzyme active sites consist of one or more metal ions coordinated (bound) to a molecule via a dative bond, in which the majority of the electron density remains on the molecule. These coordinating molecules are also known as ligands. Some host complexes designed for molecular recognition are crown ethers and their derivatives,[2] cofacial diporphyrins,[3-18] cyclic polyaza compounds,[19-28] flexible binucleating Schiff base macrocycles,[29-34] planar polyketones,[35] and our cofacial bis(β-diketones)[36-39] (Figure 1.1). The molecules with which these hosts interact are known as guests.[2]

We have designed our complexes using β-diketone ligands because they are readily synthesized,[40] can be used with many bridging groups,[40] and form planar
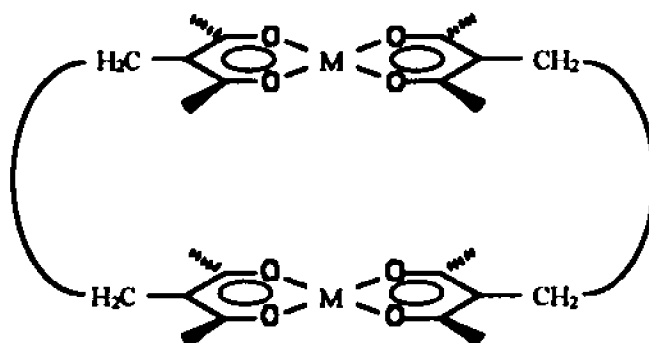
Figure 1.1. Representation of a cofacial binuclear bis(β-diketone) (M = metal ion).

complexes with many metals.[41] In our complexes, the β-diketones hold two metal atoms in parallel planes or cofacial to one another so that they direct coordination sites into the three-dimensional cavity generated by the ligand. It is within this cavity, at the metal coordination sites, where the guests bind. We have attached functional groups (X) (see **Figure 1.2**) to the bridging ligand frame to determine how these groups influence the binding of the guest molecules.
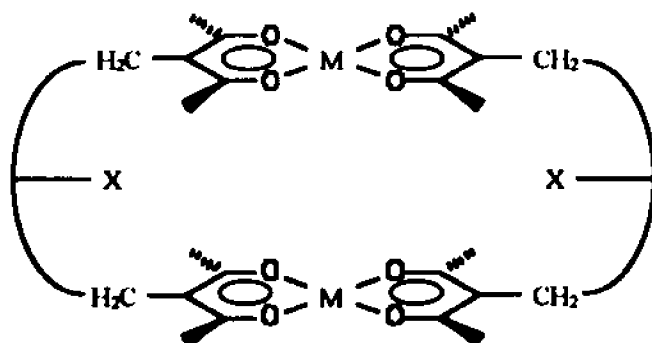
Figure 1.2. Representation of a cofacial binuclear bis(β-diketone) (M = metal ion, X = CN, Br).

An enzyme is highly efficient at recognizing its designated substrate and carrying out catalysis. Because of the large size and frequently complicated nature of the enzyme, it is difficult to know the structure of the active site during catalysis. We propose that our models will provide useful information concerning the function of the various substituents at the active site. Enzymatic systems such as alkaline phosphatase (Zn, hydrolysis of organophosphates),[42] hemocyanin (Cu, transports dioxygen),[43] and tyrosinase (Cu, activates dioxygen for hydroxylation of tyrosine)[44] each have two metal atoms playing a role in the catalytic activity at their active sites. The enzyme whose processes we are interested in mimicking initially is the zinc-containing enzyme alkaline phosphatase.

1.2 Alkaline Phosphatase

Alkaline phosphatase is a non-specific phosphomonoesterase that functions through a phosphoseryl intermediate to produce free inorganic phosphate or to transfer the phosphoryl group to other alcohols[42] with the overall reaction being

$$ROPO_3^{2-} + H_2O \rightarrow ROH + HPO_4^{2-}$$
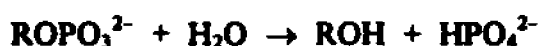
The *Escherichia coli* enzyme has two subunits, each of which has two Zn^{2+} at the active site (see Figure 1.3) and one Mg^{2+} nearby. Both Zn atoms bind the organophosphate undergoing hydrolysis. Once bound, the organophosphate is susceptible to nucleophilic attack by a serine residue coordinated to one of the zinc atoms (Figure 1.3). The acidic metal atoms and arginine (Arg) at the active site allow for the rapid phosphorylation of serine-102 by the bound organophosphate and the transfer of the phosphate group to an acceptor.
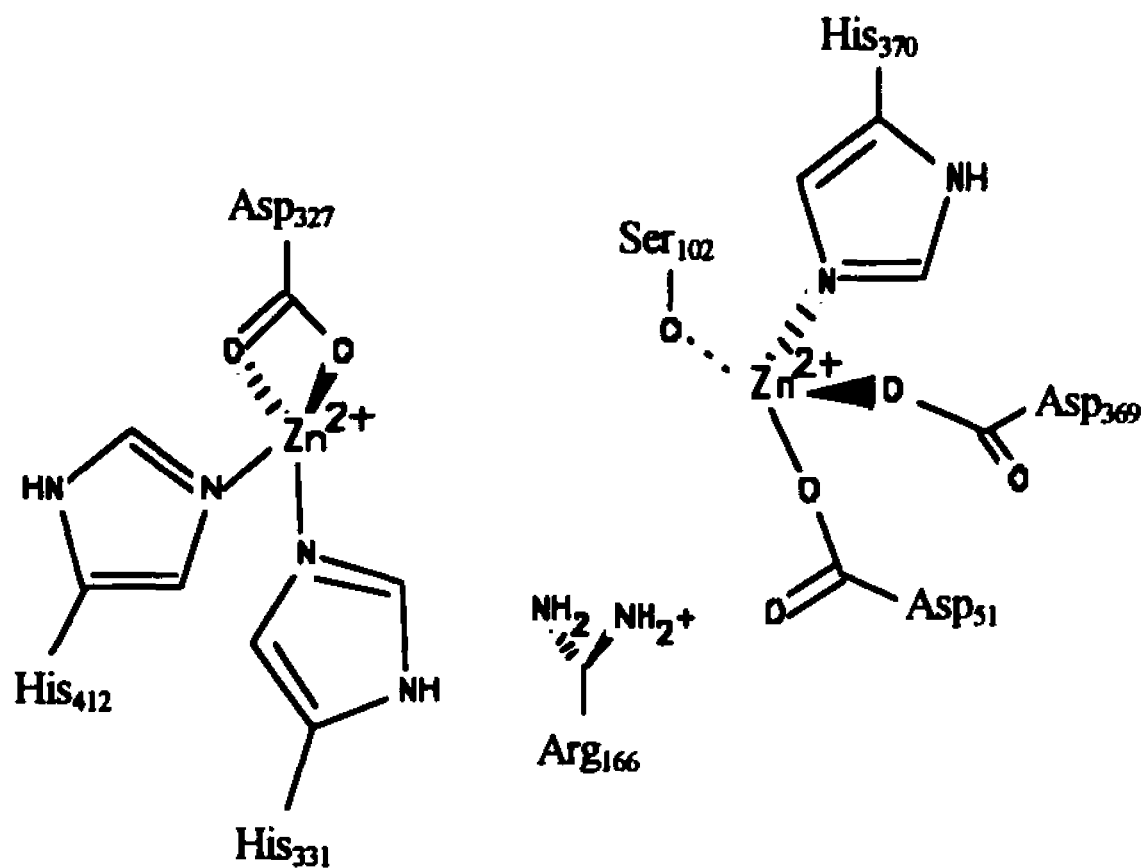
Figure 1.3. Active site of *E. coli* alkaline phosphatase.[42]

$$[\text{Zn-OH-Ser}] \underset{\text{H}^+}{\overset{-\text{H}^+}{\rightleftharpoons}} [\text{Zn-O-Ser}] \underset{-\text{ROPO}_3^{2-}}{\overset{\text{ROPO}_3^{2-}}{\rightleftharpoons}} [\text{ROPO}_3^{2-}\text{-Zn-O-Ser}] \overset{\text{H}^+}{\longrightarrow}$$

$$[\text{Zn-O(Ser)PO}_3^{2-}] + \text{ROH} \tag{1.1}$$

$$[\text{Zn-O(Ser)-PO}_3^{2-}] + \text{H}_2\text{O} \longrightarrow [\text{HPO}_4^{2-}\text{-Zn-OH-Ser}] \longrightarrow$$

$$[\text{Zn-O-Ser}] + \text{HPO}_4^{2-} \tag{1.2}$$
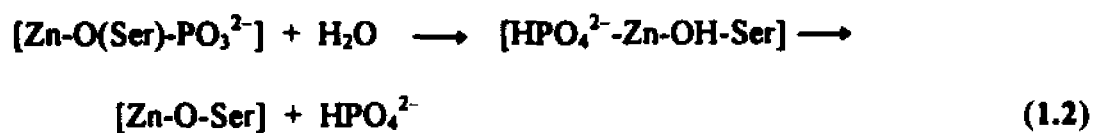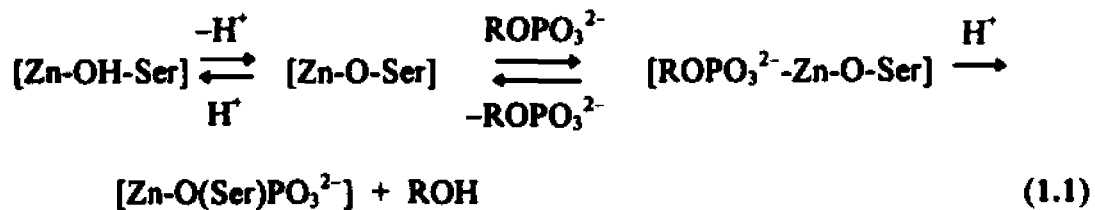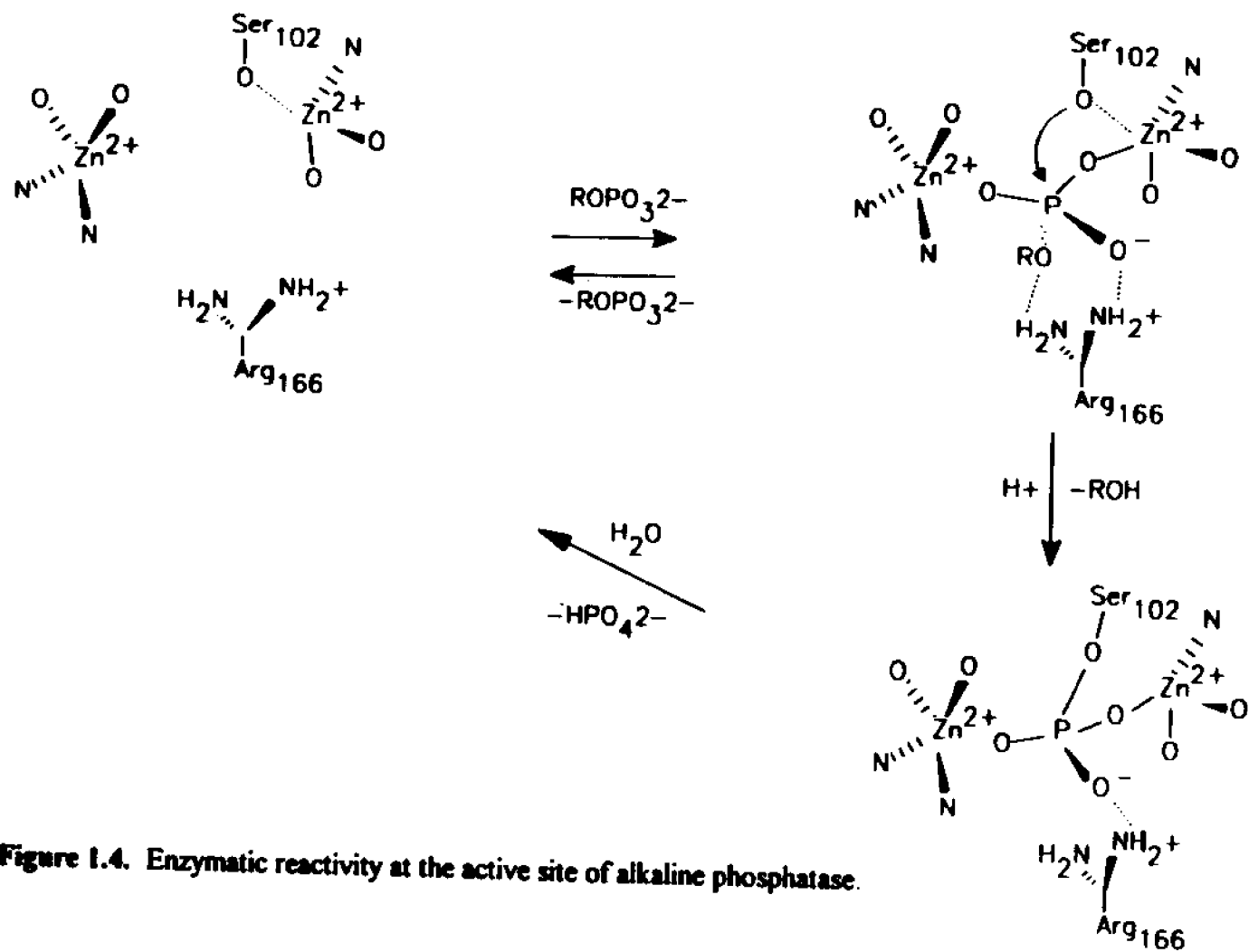
Figure 1.4. Enzymatic reactivity at the active site of alkaline phosphatase.

Most of the esterase model systems to date involve well-defined metal (e.g., Co^{3+}, Cu^{2+}, Ni^{2+}, Zn^{2+}, La^{3+}, and Ir^{3+}) complexes acting as "receptors" that are designed to accommodate, or recognize, specific guest molecules.[42] Although nucleophiles have been attached to metal-complexing ligands to increase reactivity, the combination of inwardly directed Lewis acidic metal sites and close-lying functional groups does not appear to have been achieved prior to our attempts. By using bis(β-diketone) ligands and their derivatives, we have attached different functional substituents to bridging naphthalenes, in an attempt to bring reactive groups into regions where interactions with the bound guest can occur as seen at the active site of the alkaline phosphatase enzyme.

1.3 Recent Models of Zn^{2+} and Cu^{2+} Containing Enzymes

Several model systems have been designed to study the features of Zn^{2+} and Cu^{2+} containing enzymes.[45-49] The macrocyclic amine complexes of Kimura[45-48] and Breslow[49] serve as models of Zn^{2+} containing enzymes. The amine complexes of Karlin et. al.[50-52] have properties resembling those of a couple of Cu^{2+} containing enzymes. Although, these systems provide useful information they lack certain features provided by our complexes.

Kimura et. al. have designed a series of macrocyclic oxo polyamine ligands (see Figure 1.5) in an effort to determine the role of Zn^{2+} at the enzyme active site.[45-48] His models attempt to circumvent the well-known difficulties of Zn^{2+} complexes:[48] (i) Zn^{2+}, having a complete d-shell, has few observable chemical properties which can be used to

preventing construction of a well-defined reactive site as seen in a Zn^{2+} containing enzyme. (iii) There are few ligands which allow for the study of the ligand-Zn^{2+} interactions without the presents of another metal atom.
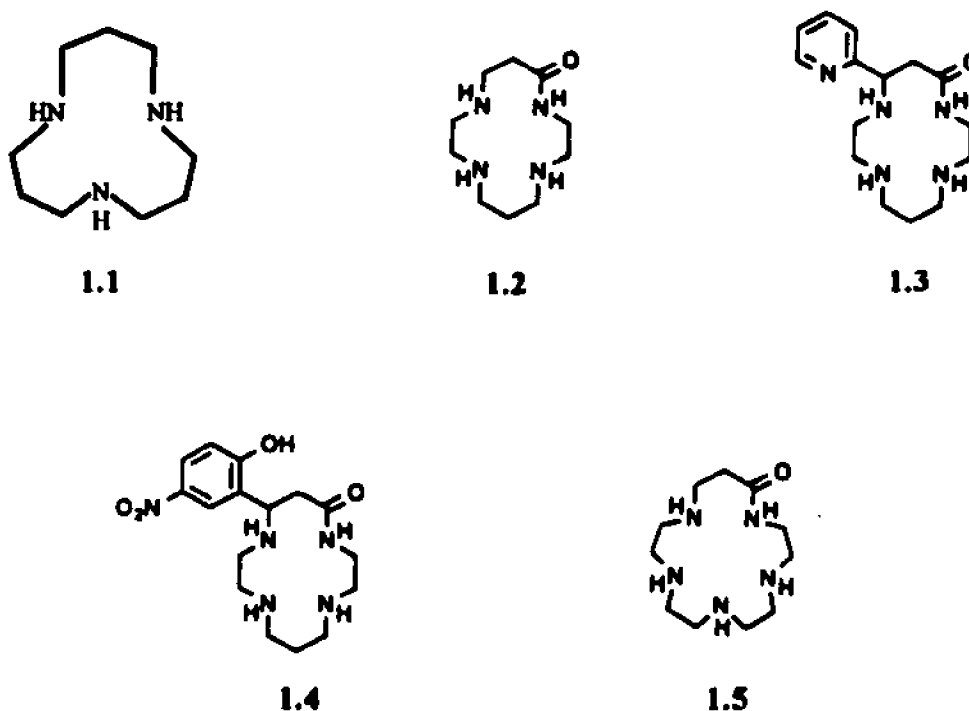
Figure 1.5. Ligands used to model Zn^{2+} containing enzymes.[45-48]

Kimura's tridentate, macrocyclic triamine 1.1 (see **Figure 1.5**),[46-47] yields a stable and structurally well-defined Zn^{2+} complex (see **Figure 1.6**), which by forming a Zn-OH⁻ species at physiological pH catalyzes ester hydrolysis and aldehyde hydration reactions. Because the Zn^{2+} ion (d^{10}) has no specially distorted or directional ligand field, Kimura

decided to use 4-5 coordinating ligands in order to determine the effects a fourth NH

would have on the Zn^{2+} acidity.[48]
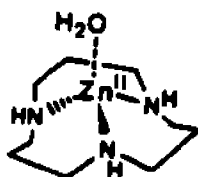
Figure 1.6. Zn^{2+} complex of ligand 1.1 (seen in **Figure 1.5**).

What he found was that ligands 1.2-1.5 can be used to distinguish Zn^{2+} from Cd^{2+} and

their inherent acid properties. The most significant finding for the larger macrocycle 1.5

is that the Zn^{2+} (1.6) and Cd^{2+} (1.7) complex stability orders reverse upon deprotonation

of the amid (see **Figure 1.7**).[48] The Zn^{2+} deprotonated complex is more stable than the

corresponding Cd^{2+} complex.
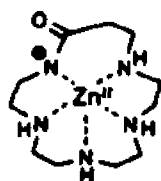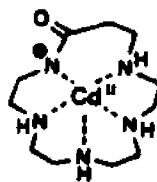
1.6   1.7

Figure 1.7. Zn^{2+} and Cd^{2+} complexes of deprotonated ligand 1.5.[48]

Breslow et. al. have found that the Zn^{2+} complex shown in **Figure 1.8** catalyzes

the hydrolysis of diphenyl p-nitrophenyl phosphate (DPPNPP) in a base-promoted

reaction.[49] He has gone one step further than Kimura by making his macrocycle soluble

in organic media. This was done by attaching long alkyl chains to 1.8. In micelles, 1.9 is

a particularly good catalyst for DPPNPP hydrolysis.

1.8 R = H   DPPNPP
1.9 R = $C_{16}H_{33}$
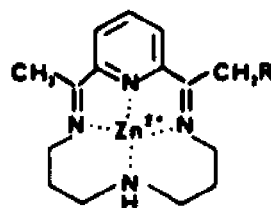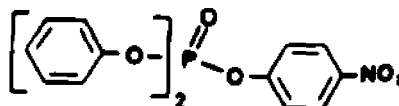
Figure 1.8. Breslow's Zn^{2+} complex and the DPPNPP substrate with which it
reacts.[49]

Kimura and Breslow have shown that in order to be effective catalysts, their

complexes must invoke a bifunctional system, with both Lewis acid and nucleophilic

components. Our cofacial bimetallic bis(β-diketones) allow for the incorporation of both

of these features. Kimura and Breslow's complexes are great for modeling enzymes such

as carbonic anhydrase which has one metal ion at the active site, but they fall one metal

ion short of giving an accurate picture of the active site of alkaline phosphatase.

Karlin et. al. have synthesized a ligand (1.10) capable of binding two metal Cu^{2+} ions as seen at the active site of the enzymes hemocyanin and tyrosinase.[50] The Cu^{2+} complex of this ligand is like hemocyanin in that it binds O_2 (1.11). The complex resembles tyrosinase in that upon reaction with O_2, there is an insertion of an oxygen atom between a C-H bond (1.12) which results in the formation of a phenol (1.13) (see Equation 1.3). Complex 1.14 can be synthesized from a methanol solution of 1.13 by adding NaOH and $[Cu(CH_3CN)_4]PF_6$. In a dichloromethane solution, complex 1.14 was found to reversibly bind O_2.[50]

| 1.10 | 1.11 | 1.12 | 1.13 |
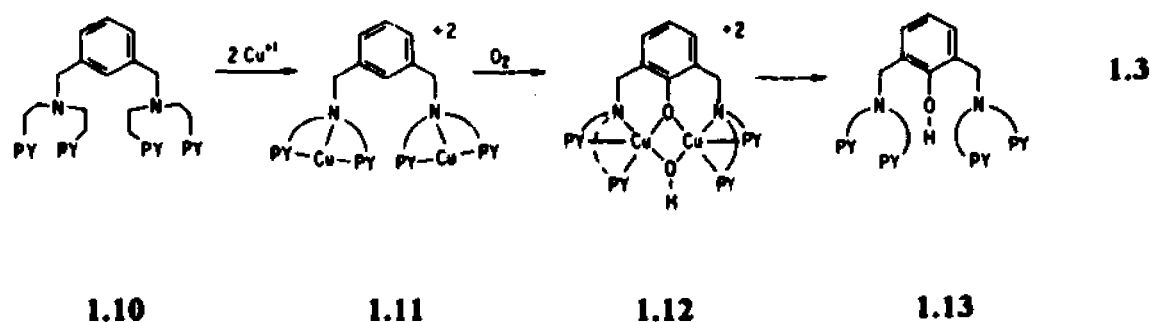
Another dicopper(II) complex of Karlin's which reversible binds O_2 is 1.15 (see Equation 1.4).[51] Complex 1.16 possesses both the spectroscopic and reactivity properties which allow it to be considered as the best possible model, thus far, for mimicking the O_2-binding properties of oxy-hemocyanin and O_2-activating properties of oxy-tyrosinase.[51]
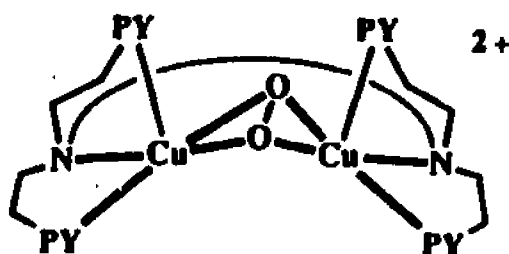
1.15
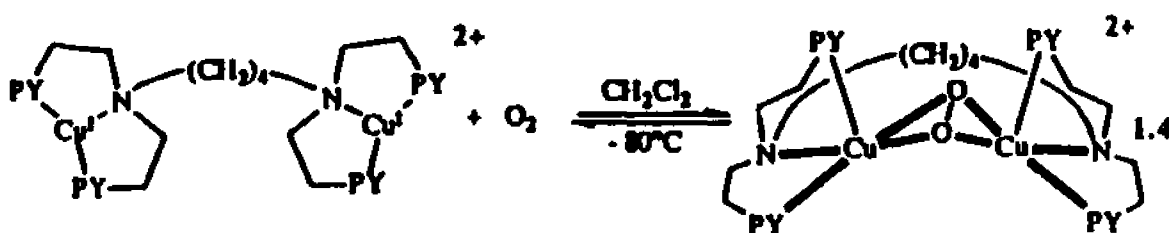
1.16

Karlin's models are useful for studying O_2 binding, but the short Cu---Cu distance of 3.4-3.6 Å limits this complex to binding molecules no larger than O_2.[50-52] The aromatic groups bridging the metal atoms of our cofacial binuclear bis(β-diketone) complexes can be varied in size in order to decrease or increase the Cu---Cu distance so that a range of different sized guests can fit inside. The bridging aromatic rings also provide places for the attachment of substituents, a feature lacking from Karlin's models.

1.4 History of Our Cofacial Bimetallic Complexes

The first attempt at synthesizing a bis(β-diketone) ligand capable of binding two metal atoms in a cofacial orientation resulted in *m*-XBAH$_2$[36] (3,3'-[1,3-phenylenebis(methylene)]bis(2,4-
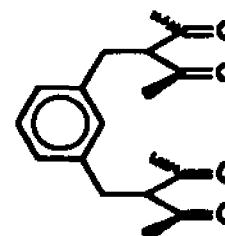
1.17

pentanedione)) (1.17). The procedure for alkylation of the acetylacetonate(acac⁻) ion with organic dihalides was developed by Martin and coworkers[40] for α,ω-alkylene and *p*-xylylenebis(acetylacetone). Although the complexes formed from the *para*-substituted ligand frequently were polymeric,[33] the *meta*-substituted ligand could be used to connect two copper atoms cofacially at a distance of 4.91 Å in the olive green Cu$_2$(XBA)$_2$ (1.18).

This cavity could provide enough room to accommodate a diatomic guest such as O$_2$. Attempts to bind O$_2$ to Cu$_2$(XBA)$_2$ were not successful, but the host was found to interact with nitrogenous bases such as
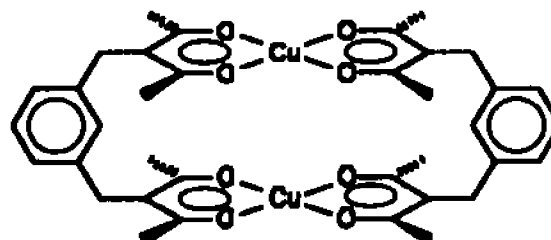
1.18

pyridine. Being too large to fit in the cavity, the pyridine had to be binding externally (**Figure 1.9**). The most likely mode of binding for this nitrogenous base was axially to the Lewis-acid metal atoms. Since the ultimate goal of these complexes was to have interaction between these substituents and an internal guest molecule, it was decided that the possibility of internally binding a guest might be increased if the size of the bridging ligand was increased.

Empty   Internal   External
Complex   Binding   Binding
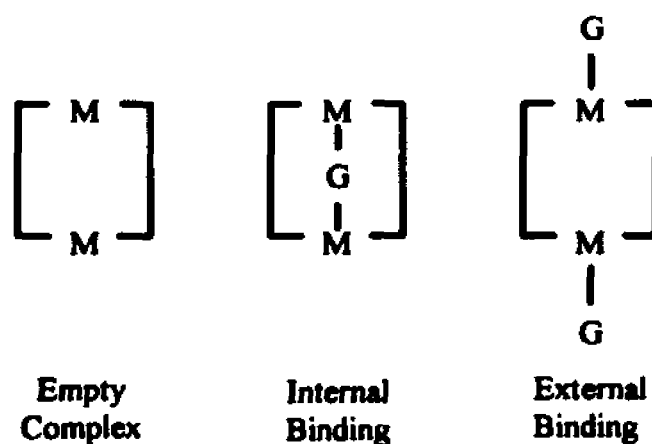
Figure 1.9. Internal and external binding of guest molecule.

A second bis(β-diketone) ligand, NBAH$_2$ (3,3'-(2,7-naphthalenediyl-bis-

(methylene))bis(2,4-pentanedione) (1.19)[37], was synthesized with the larger 2,7-

naphthalenediylbis(methylene) bridge. The distance between the copper atoms in the

resulting complex (Cu$_2$(NBA)$_2$), 7.349 Å (1.20)[38], provided more room in the cavity for

larger guest molecules, such as (aliphatic and aromatic) heterocyclic amines.
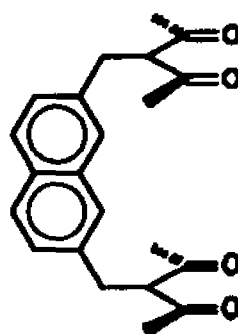
1.19
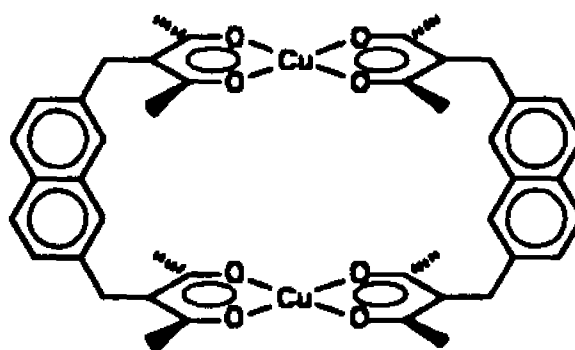
1.20

Diamines such as Dabco and various pyrazines bind to (Cu$_2$(NBA)$_2$) in an endo (intramolecular) fashion as seen in **1.21**. Pyridine and quinuclidine bind to the Cu atoms via their one nitrogen atom in an exo manner (**1.22**).
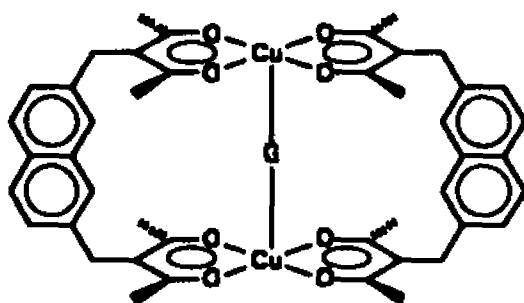
1.21
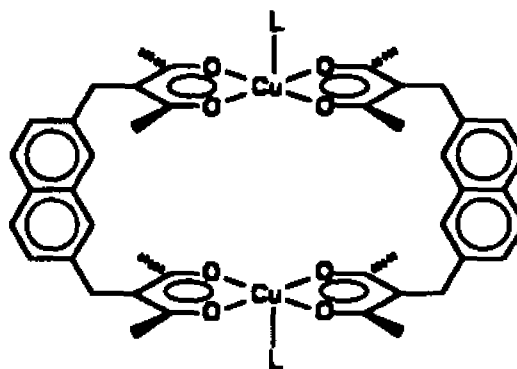
1.22

The endo coordination (**1.21**) has been demonstrated in the structures solved for the turquoise crystals of the Cu$_2$(NBA)$_2$(μ-Dabco)[37] and the Cu$_2$(NBA)$_2$(μ-2,5-dimethylpyrazine)[38] complexes. The Cu atoms of these host-guest complexes are in square pyramidal coordination environments, displaced slightly toward each other (and away from the planes of O atoms); the Cu-Cu distances are 7.4-7.6 Å.

We have also synthesized colorless $Zn_2(NBA)_2$ complexes which bind Dabco, pyrazine, and piperazine. Unlike the $Cu_2(NBA)_2$ complexes, these are diamagnetic and can be studied using NMR spectroscopy. The host-guest interactions were, therefore, examined using NMR spectroscopy techniques. These compounds were also found to emit measurable luminescence which will be presented along with the NMR data.

When I joined this research group, internally functionalized bis(β-diketones), ($NBAH_2$-X), and their metal complexes were being synthesized. We have prepared the ligands with X = Br and CN (1.23), as seen in **Figure 1.10**, and the corresponding cofacial binuclear Cu complexes as seen in **Equation 1.5**.
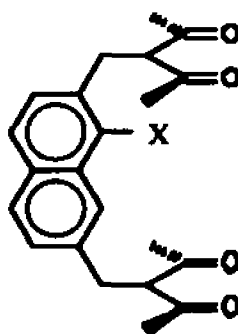
1.23. X=H, Br, CN

Upon addition of the nitrogenous bases to $CHCl_3$ solutions of these derivatized complexes, the familiar turquoise color was observed. The binding constants of these new complexes could then be measured. The data from these experiments will be presented.
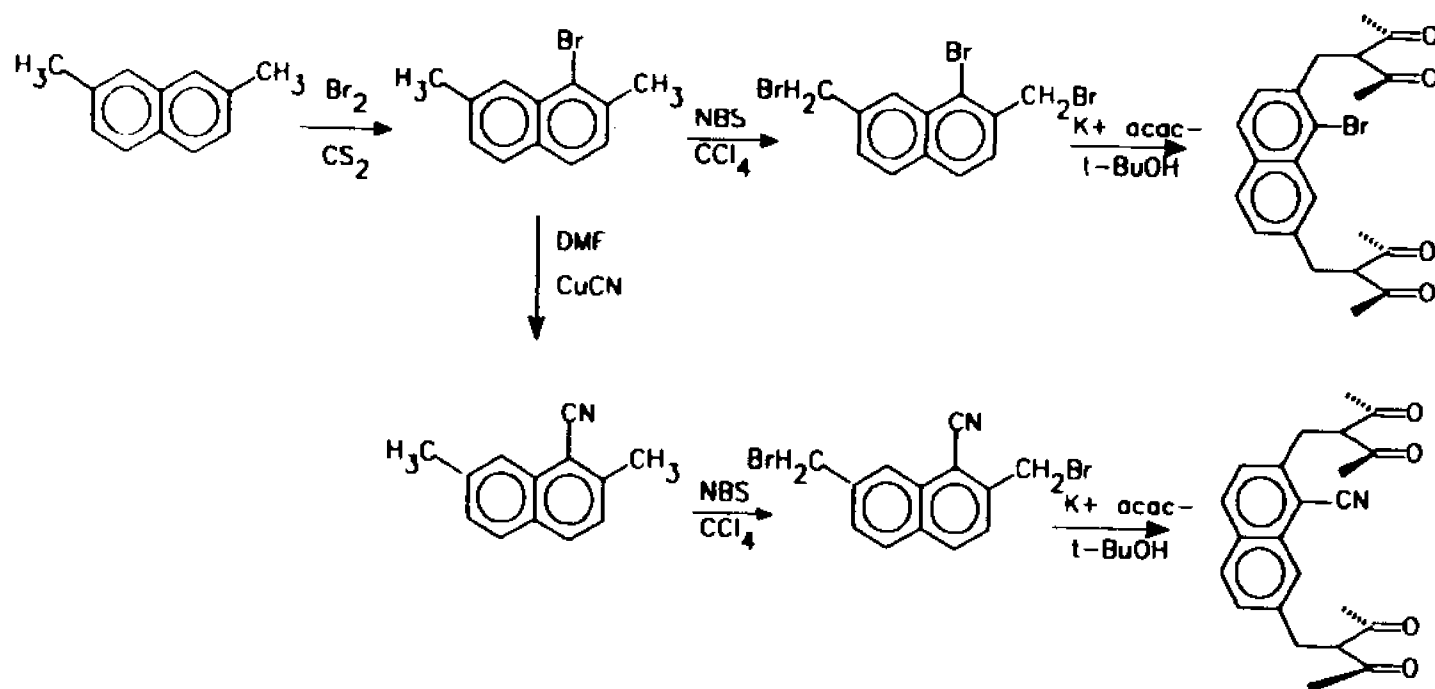
Figure 1.10. Synthesis scheme for substituted bis(β-diketone) ligands.

Chapter 2. Synthesis, Crystal Structure, and Luminescence of 2,7-Dimethylnaphthalene-1-carbonitrile

2.1 Introduction

We have been synthesizing cofacial binuclear copper(II) bis(β-diketone) host complexes (see $Cu_2(NBA)_2$, **2.1**) in order to develop new catalysts based on the recognition of guest molecules G (G = a nitrogenous base).[36-38] We have also prepared internally functionalized derivatives such as $Cu_2(NBA\text{-}CN)_2$ (see **2.2**). In order to prepare $Cu_2(NBA\text{-}CN)_2$, pure 2,7-dimethylnaphthalene-1-carbonitrile (1-CN-2,7-$(CH_3)_2C_{10}H_5$, **2.3**) was required.
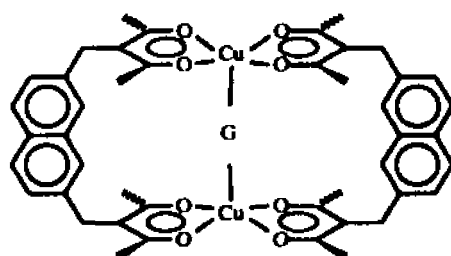
2.1
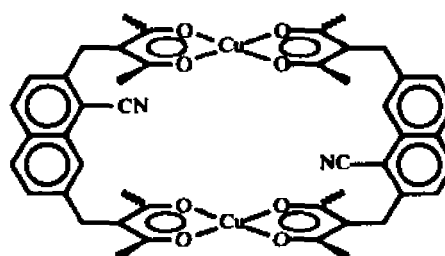
2.2
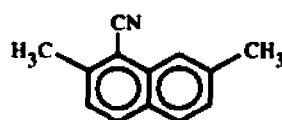
2.3

Our synthesis of **2.3** gave an intensely luminescent product. This intense luminescence was found to be due to an impurity, the majority of which could be separated from **2.3** via column chromatography. The GC-MS data suggests that the impurity is a bromo-2,7-dimethylnaphthalene-1-carbonitrile compound. In the course of purifying **2.3**, we also identified its monomer and excimer fluorescence, which are comparable to that previously observed for naphthalene-1-carbonitrile (1-

17

cyanonaphthalene).[54] These results, and the X-ray crystal structure analysis of 2.3, are presented in this chapter.

2.2 Experimental Section

2.2.1. Materials and Procedures.
Materials were reagent or spectrophotometric grade and were used as received. Solutions used in fluorescence studies were deoxygenated by bubbling with N_2.

The ^{1}H-^{13}C correlation experiment was performed on a Bruker AC250 spectrometer using the DISB91 software, and the NOE and 2D COSY experiments were done on a Bruker ARX300 spectrometer. (These techniques were used to assign the ^{1}H and ^{13}C NMR spectra for 1-CN-2,7-$(CH_3)_2C_{10}H_5$; the resulting ^{1}H assignments, except for minor chemical shift differences, differ from those of Gore and Siddiquei[55] only at H-4 and H-5.) Electronic absorption spectra were recorded on an Aviv Model 14DS absorption spectrophotometer. Luminescence spectra were recorded using a Spex Industries Fluorolog 2 Model F112X emission spectrophotometer (with a Hamamatsu R636 PMT and an ESCO UG11 colored-glass excitation filter to reduce stray light) and were corrected as previously described[56] for variations in detector sensitivity with wavelength.

2.2.2. Synthesis of 2,7-Dimethylnaphthalene-1-carbonitrile, 1-CN-2,7-$(CH_3)_2C_{10}H_5$ (2.3).
2,7-Dimethylnaphthalene-1-carbonitrile was prepared by a nucleophilic substitution method similar to that used in the synthesis of naphthalene-1-carbonitrile.[57] 1-Bromo-2,7-dimethylnaphthalene (7.6 g, 0.032 mol; prepared by the literature method[58,59]) was dissolved in 70 mL of dimethylformamide (DMF), a 20%

excess of CuCN (3.5 g, 0.039 mol) added, and the mixture refluxed for 4.5 h. The

heat source was removed and the dark green reaction mixture was allowed to cool to

65 °C. Then a solution of $FeCl_3 \cdot 6H_2O$ (16 g) in conc. HCl (4 mL) and H_2O (24 mL)

was added, and the mixture was stirred for 20 min to oxidize any remaining Cu(I).

The two layers were separated and the aqueous layer was washed twice with 50 mL

CH_2Cl_2. The organic layers were combined, washed successively with 100 mL each

of 6 M HCl, 10 % NaOH, and H_2O, dried over $MgSO_4$, and evaporated. If the

residue was an oil, then DMF was still present. 50 mL of H_2O was added,

precipitating the compound, which was then taken up by addition of 50 mL of

CH_2Cl_2. The CH_2Cl_2 layer was dried over $MgSO_4$ and the solvent evaporated. This

sequence of precipitating, extracting, and drying was repeated, as many as six times,

until a cream-colored solid was produced. Yield 5.7 g, 0.031 mol (96 %), m.p. 93.1-

93.3 °C. ^{1}H NMR ($CDCl_3$): δ 2.57 (s, 7-CH_3), 2.73 (s, 2-CH_3), 7.32 (d, J=8.4 Hz, H-

3), 7.38 (dd, J=1.56, 8.34, H-6), 7.76 (d, J=8.3, H-5), 7.90 (d, J=8.44, H-4), 7.96 (m,

H-8). ^{13}C NMR ($CDCl_3$): δ 21.27 (2-CH_3), 21.91 (7-CH_3), 108.46 (C1), 117.28

(C11), 123.93 (C8), 126.69 (C3), 128.12 (C5), 128.79 (C6), 129.44 (C10), 132.27

(C4), 133.04 (C9), 138.85 (C7), 142.83 (C2). Intensely fluorescing needle-like crystals

could be obtained by partial evaporation of a CH_2Cl_2-hexane (2:3 v/v) solution. These

crystals were used for X-ray analysis. The compound was purified for fluorescence

measurements via column chromatography (200-400 mesh, 70 Å silica gel; hexane-

CH_2Cl_2, 1:1 v/v) and recrystallization from 1:1 hexane:CH_2Cl_2.

2.2.3. ^{1}H and ^{13}C NMR of 2,7-Dimethylnaphthalene-1-carbonitrile, 1-CN-

2,7-$(CH_3)_2C_{10}H_5$, (2.3). The ^{1}H assignments (see Experimental section) differ from

those previously reported by Gore and Siddiquei[55] in the assignments of H-4 and H-5.

A 2-D COSY experiment shows H-4 (7.90 ppm) to be coupled to H-3 (7.32 ppm) and

H-5 (7.76 ppm) to be coupled to H-6 (7.38 ppm). This coupling would not be

possible based on the earlier chemical shift assignments of H-4 and H-5, in which the

doublet labeled H-5 was farther downfield than the corresponding H-4 doublet. The 2-

D COSY experiment also revealed a small amount of coupling between H-4 and H-5,

as well as between H-6 and H-8.

A ^{1}H NOE experiment (irradiating 7-CH_3 at δ 2.57 or 2-CH_3 at δ 2.73)

allowed us to distinguish between the methyl protons. The results were as expected

with the methyl resonance at 2.73 ppm being located on the more substituted ring.

The ^{13}C assignments were made based on a ^{1}H-^{13}C correlation experiment.

2.2.4. X-ray Methods. Diffraction data were collected on an Enraf-Nonius

CAD4 diffractometer fitted with $CuK\alpha$ source and graphite monochromator, using the

θ-2θ scan method within the limits $2° < \theta < 75°$. The sample crystal was a needle

fragment of dimensions 0.22 x 0.23 x 0.45 mm, and was mounted in a capillary. Final

unit cell constants were determined from the orientations of twenty-five centered high-

angle reflections. The intensities were corrected for absorption using ψ scan data for

five reflections and the minimum relative transmission coefficient was 92.9 %. The

MolEN set of programs for structure solution and refinement were used.[60] The 1544

data having $I > 1\sigma(I)$ were used in the refinement, and H atoms were refined

isotropically. Details of data collection and structure refinement are given in **Table**

2.1. The ORTEP drawing can be seen in **Figure 2.1.**

Table 2.1.   Crystal data for 2,7-dimethylnaphthalene-1-carbonitrile.[a]

chemical formula	$C_{13}H_{11}N$	space group	$P2_1/c$
fw	181.2	temp/°C	22
$a/Å$	7.119(1)	$\lambda/Å$	1.54184 (Cu$K\alpha$)
$b/Å$	18.389(4)	$D_c/g\ cm^{-3}$	1.217
$c/Å$	7.538(6)	$\mu(CuK\alpha)/cm^{-1}$	5.1
β/deg	91.661(7)	$R(F_o)$	0.069
$V/Å^3$	986.4(5)	$R_w(F_o)$	0.061
Z	4		

[a]Values in parentheses in **Tables 2.1-2.5** are estimated standard deviations of the last digit.
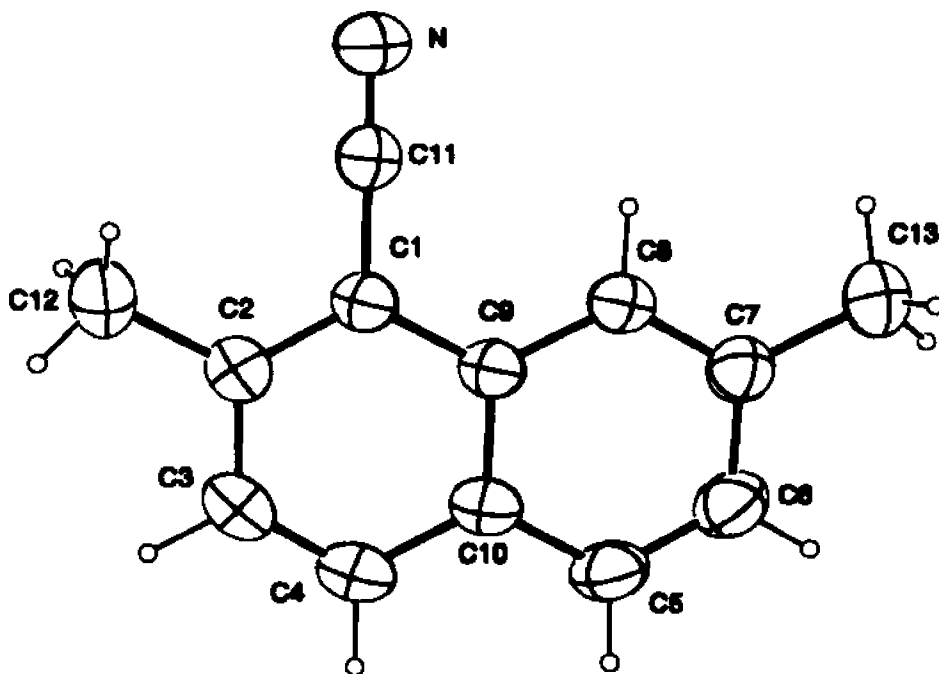
Figure 2.1. ORTEP drawing of 2,7-Dimethylnaphthalene-1-carbonitrile.

2.2.5. Lifetime Measurements. A Nd:YAG laser (using the 355 nm third

harmonic) was used to excite a solid sample containing the expected

bromonaphthalene impurities (4-bromo-2,7-dimethylnaphthalene-1-carbonitrile, 5-

bromo-2,7-dimethylnaphthalene-1-carbonitrile, 2,7-dimethylnaphthalene-1,4-

dicarbonitrile, and dimethylnaphthalene-1,5-dicarbonitrile) present in unpurified 2.3.

The resulting fluorescence signal and its decay was detected by a photomultiplier tube

and displayed of one channel of a Tektronix oscilloscope as a function of time.

Displayed on the second channel was a simulated decay-time curve from a photo

diode, standardized with the laser pulse prior to fluorescence lifetime measurements.

The ln of the decay curve could be plotted against time. From this plot the lifetime of

the excited state could be determined.

2.3 Results and Discussion

    2.3.1. X-ray Analysis of 1-CN-2,7-(CH$_3$)$_2$C$_{10}$H$_5$ (2.3). The bond lengths in

1-CN-2,7-(CH$_3$)$_2$C$_{10}$H$_5$ differ by no more than 0.019 Å from those of naphthalene.[61]

The greatest difference in bond angle is found at C1-C2-C3, which is 2.5° smaller than

the corresponding angle in naphthalene. Atomic parameters are given in **Tables 2.2**

and **2.3**. Bond lengths and angles are listed in **Table 2.4.**

Table 2.2. Fractional atomic coordinates and equivalent isotropic displacement
      parameters.

Atom	x	y	z	B_{eq}(Å^2)
N	0.5242(2)	0.36009(8)	0.2599(2)	5.95(4)
C1	0.2350(2)	0.28281(8)	0.1648(2)	3.99(3)
C2	0.0705(2)	0.31690(9)	0.1110(2)	4.37(3)
C3	−0.0812(2)	0.27309(9)	0.0531(2)	4.98(4)
C4	−0.0692(2)	0.1997(1)	0.0497(2)	5.02(4)

                                            (table *con'd.*)

C5	0.1139(2)	0.08683(9)	0.1090(3)	5.25(4)
C6	0.2756(2)	0.05410(9)	0.1657(3)	5.45(4)
C7	0.4321(2)	0.09488(9)	0.2260(2)	4.77(4)
C8	0.4182(2)	0.16943(9)	0.2253(2)	4.39(3)
C9	0.2534(2)	0.20542(8)	0.1672(2)	3.99(3)
C10	0.0963(2)	0.16346(9)	0.1082(2)	4.37(3)
C11	0.3955(2)	0.32604(9)	0.2195(2)	4.52(4)
C12	0.0514(3)	0.39816(9)	0.1118(3)	5.98(4)
C13	0.6080(2)	0.0572(1)	0.2893(3)	6.62(5)

Table 2.3. Coordinates and isotropic displacement parameters for hydrogen atoms.

Atom	x	y	z	$B_{iso}(\text{Å}^2)$
H3	-0.195(2)	0.2977(9)	0.010(2)	7.1(4)
H4	-0.177(2)	0.1703(9)	0.015(2)	5.7(4)
H5	0.010(2)	0.0575(8)	0.077(2)	6.4(4)
H6	0.283(2)	0.0035(9)	0.166(2)	6.5(4)
H8	0.530(2)	0.1962(9)	0.260(2)	5.4(4)
H12a	-0.079(3)	0.409(1)	0.120(3)	11.2(7)
H12b	0.089(3)	0.417(1)	-0.001(3)	13.8(8)
H12c	0.111(3)	0.419(1)	0.200(3)	12.4(7)
H13a	0.615(3)	0.014(1)	0.236(3)	12.8(7)
H13b	0.601(3)	0.042(1)	0.411(4)	13.8(8)
H13c	0.719(2)	0.088(1)	0.283(3)	8.7(5)

Table 2.4. Bond distances (Å) and bond angles (°).

Atoms	Distance	Angle	Atoms	Distance	Angle
N C11	1.144(2)		C5 C6	1.357(2)	
C1 C2	1.379(2)		C5 C10	1.415(2)	
C1 C9	1.429(2)		C6 C7	1.408(2)	
C1 C11	1.442(2)		C7 C8	1.374(2)	
C2 C3	1.406(2)		C7 C13	1.497(2)	
C2 C12	1.501(2)		C8 C9	1.406(2)	
C3 C4	1.352(2)		C9 C10	1.419(2)	
C4 C10	1.413(2)				
C2 C1 C9		122.2(1)	C6 C7 C13		120.2(2)
C2 C1 C11		119.5(1)	C8 C7 C13		121.5(1)
C9 C1 C11		118.3(1)	C7 C8 C9		122.0(1)
C1 C2 C3		118.0(1)	C1 C9 C8		123.2(1)
C1 C2 C12		121.8(1)	C1 C9 C10		117.8(1)
C3 C2 C12		120.2(1)	C8 C9 C10		119.0(1)
C2 C3 C4		121.9(1)	C4 C10 C5		123.0(1)

(table *con'd.*)

C3 C4 C10	121.2(1)	C4 C10 C9	118.9(1)
C6 C5 C10	121.2(1)	C5 C10 C9	118.1(1)
C5 C6 C7	121.5(2)	N C11 C1	178.7(2)
C6 C7 C8	118.3(1)		

The naphthalene portion of the molecule is planar within ±0.014(2) Å. The substituents deviate from this plane by 0.058(2) Å (C11), 0.118(2) Å (N), −0.025(2) Å (C12), and −0.025(2) Å (C13). The closest intermolecular contact is 3.494(2) Å between C2 and C4' at x, ½−y, ½+z (i.e. between C2 and C4 of two adjacent molecules related by the c glide plane). The close contacts (<4.0 Å) between these symmetry-related molecules are listed in **Table 2.5**. The approximately parallel molecules are separated by ca. 3.55 Å. The majority of the intermolecular contacts are between 4 and 6 Å apart.

Table 2.5. Intermolecular distances <4 Å (e.s.d.'s in parentheses).

	x, ½−y, ½+z	Distance(Å)	x, ½−y, −½+z	Distance(Å)
N	C6	3.911(2)	C13	3.921(3)
N	C7	3.687(2)		
N	C8	3.650(2)		
N	C9	3.865(2)		
C1	C1	3.958(2)	C1	3.958(2)
C1	C3	3.883(2)	C8	3.701(2)
C1	C4	3.685(2)	C9	3.763(2)
C1	C9	3.792(2)		
C1	C10	3.649(2)		
C2	C3	3.901(2)	C8	3.882(2)
C2	C4	3.494(2)	C9	3.648(2)
C2	C10	3.764(2)	C10	3.818(2)
C3	C3	3.864(2)	C3	3.864(2)
C3	C4	3.776(2)	C4	3.831(2)
C3	C9	3.834(2)		
C3	C10	3.802(2)		
C4	C12	3.878(3)		
C5	C12	3.839(3)	C11	3.943(2)
C5	C12	3.771(3)		

(table con'd)

C6	C12	3.865(3)		
C8	C11	3.735(2)	C11	3.812(2)
C9	C11	3.598(2)		
C10	C12	3.984(3)	C11	3.677(2)
C10	C12	3.914(3)		

2.3.2. Solution Fluorescence of 2,7-Dimethylnaphthalene-1-carbonitrile, 1-CN-2,7-$(CH_3)_2C_{10}H_5$, (2.3). The corrected emission spectra of 1-CN-2,7-$(CH_3)_2C_{10}H_5$ (see **Figure 2.2**) in CH_2Cl_2 comprise a structured band at 350 nm and a broad band at 421 nm, in varying proportions depending on concentration. The transition at 421 nm meets the general criteria[54] for excimer fluorescence: it is broad, it is red-shifted with respect to the monomer fluorescence, and it appears only at high concentrations of **2.3**, with no corresponding concentration-dependent band in the absorption spectrum.

It can be seen from the spectra in **Figure 2.2** that as the concentration decreases the relative intensity of the excimer fluorescence does also. The excimer emission is no longer apparent as a distinct band at 6×10^{-4} M or 2.2×10^{-3} M. A concentrated solution of **2.3** allows for the required intermolecular overlap to produce a dimer species as seen in the solid phase of molecules having the B type stacking (see solid-state fluorescence).[62] The monomer emission continues to increase as the excimer emission decreases until a concentration of approximately 1.25×10^{-4} M is reached. Further dilution at this point results in a decrease in the intensity of the monomer emission.

2.3.3. Solid-state Fluorescence of 2,7-Dimethylnaphthalene-1-carbonitrile, 1-CN-2,7-$(CH_3)_2C_{10}H_5$ (2.3). Under varying conditions, three different emission

Monomer & Excimer Fluorescence of
2,7-Dimethylnaphthalene-1-carbonitrile
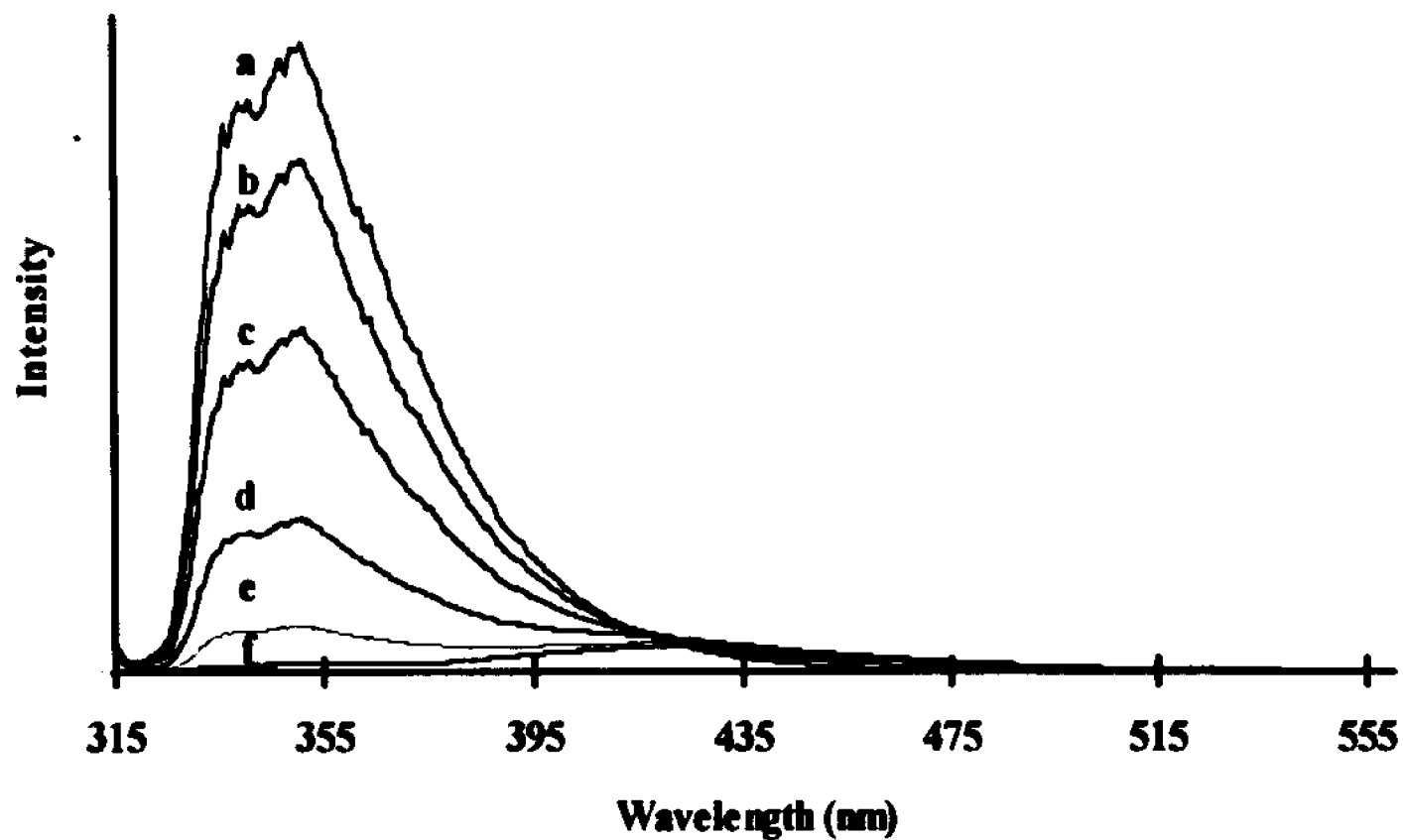
Figure 2.2. Corrected fluorescence spectra for 2,7-dimethylnaphthalene-1-carbonitrile solutions in CH₂Cl₂, showing monomer (~350 nm) and excimer (~420 nm) emission: a. 0.0006 M; b. 0.0022 M; c. 0.0089 M; d. 0.0356 M; e. 0.1422 M; f. 1.1378 M.

Absorption & Monomer Emission of 2,7-Dimethylnaphthalene-1-carbonitrile
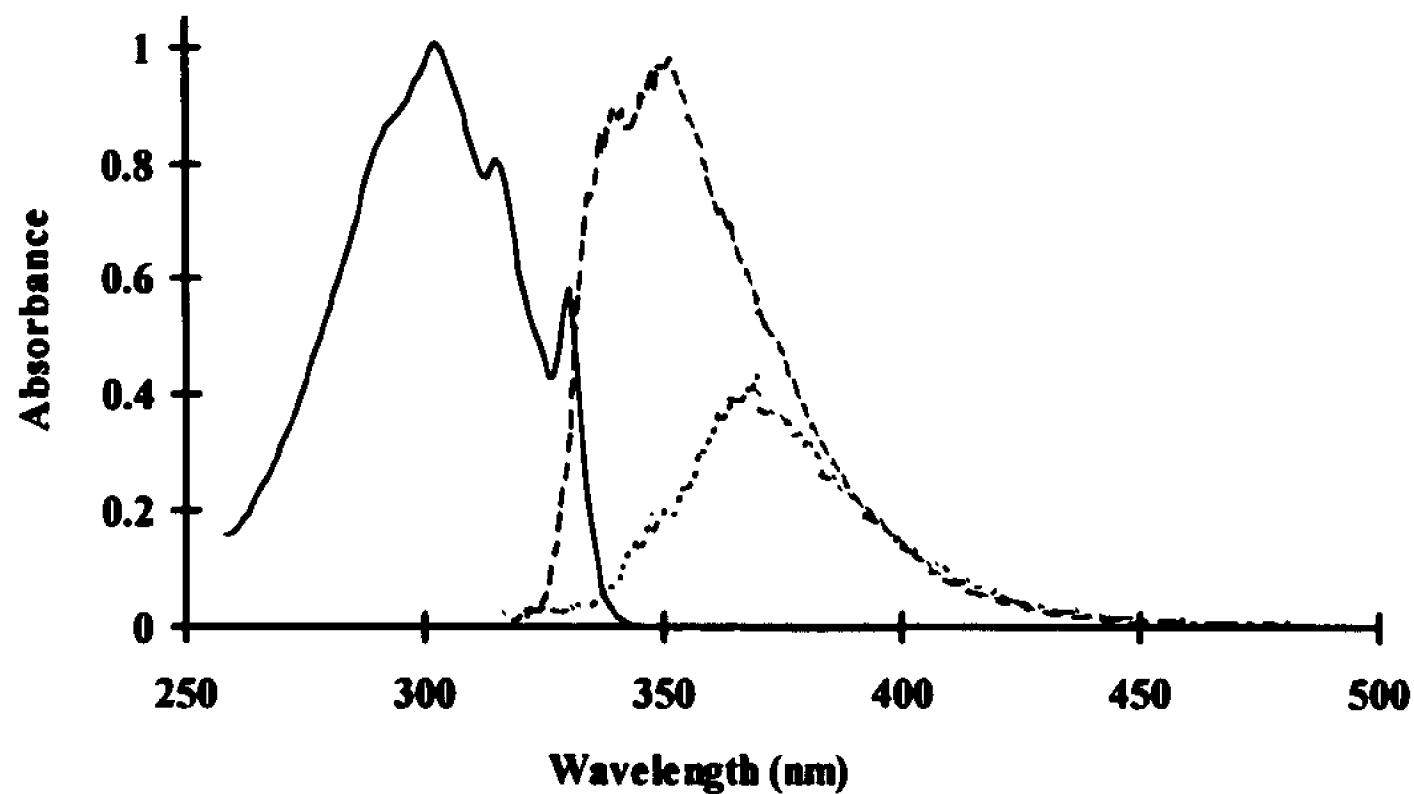
Figure 2.3. Absorption and corrected fluorescence spectra for 2,7-dimethylnaphthalene-1-carbonitrile. ——— Absorption (1.245 x 10⁻⁴ M); − − Solution fluorescence (6.0 x 10⁻⁴ M); ····· Crystal fluorescence.

bands have been observed from crystalline 1-CN-2,7-$(CH_3)_2C_{10}H_5$: 370, 490, and 465 nm. We were initially intrigued by the readily apparent 490 nm luminescence in some samples of 2.3, but found it absent in carefully purified samples.

Crystalline aromatic compounds show monomer or excimer fluorescence depending or crystal packing. **Figure 2.3** shows the absorption and corrected emission spectra of a dilute CH_2Cl_2 solution (6 x 10^{-4} M) and a crystal of purified 2.3 at room temperature. The transition at 350 nm is due to monomer emission as seen in dilute CH_2Cl_2 solutions (see solution fluorescence). In the crystal of 2.3, the large number of intermolecular contacts >4 Å limit the π-orbital overlap of adjacent parallel molecules as is common with crystals possessing the A type crystalline stacking.[63] This intermolecular π-orbital overlap, in the proper orientation, appears to be necessary for excimer formation as crystals of 2.3, not having good π-orbital overlap, do not emit excimer fluorescence.

Molecules achieving the A type lattice, such as naphthalene, phenanthrene, anthracene, and chrysene, have an interplanar separation >4 Å.[62] The crystalline lattice of 2.3 is similar to the A type in that there are 125 intermolecular contacts separating one molecule 4 to 6 Å from the molecules at x, ½–y, –½+z and x, ½–y, ½+z directly above and below it. The aromatic plane of 2.3 is also like those seen in A type molecules in that the π-orbital overlap of adjacent molecules is not very good. The stacking within the crystal structure of 2.3 differs from the A type in that the molecules related by the c glide plane are all very nearly parallel, forming a dihedral angle of 3.1(3)°, while adjacent molecules in an A type lattice are at approximately

90° to each other. This allows for a greater π-overlap of adjacent molecules, an interaction severely restricted in the classical A type lattice in which the large angle of inclination of the molecular planes to the symmetry plane of the crystal limits the π-orbital overlap.

The other type of stacking commonly observed in crystal structures of multi-ring aromatic compounds is the B type (B_1 and B_2) possessed by pyrene, perylene, coronene, and ovalene; all having interplanar distances below 3.5 Å.[62] In the B type stacking, the molecules are grouped in parallel sandwich-like pairs allowing for π-orbital overlap. The intermolecular distances in 2.3, shorter than 4 Å, are listed in Table 2.5. Molecules possessing a B_2 type lattice in the monoclinic form almost completely overlap at a similar interplanar distance by stacking in columns with their planes at 45 ° to the symmetry plane.[62] As previously implied, stacked molecules of 2.3 do not overlap completely and the molecular plane is approximately 90 ° to the symmetry plane.

The projection down the crystallographic b axis, shown in Figure 2.4 (a), shows that the molecules are approximately parallel in stacks along the c axis. (The average separation between adjacent molecular planes, determined as half of the distance between molecules one unit-cell-length apart along c, is ca. 3.55 Å.) This arrangement appears to be similar to that in the B_2-type crystals, which often show excimer fluorescence in the solid state. However, adjacent molecules are related by a glide plane (i.e. reflection + translation) rather than by a simple translation. Figure 2.4 (b) illustrates the relationship of the molecules to the glide plane. The result of

the glide-plane relationship, as shown in **Figure 2.4** (c), is that the π systems of two adjacent molecules actually overlap rather poorly. Therefore, it is not surprising that solid $C_{10}H_5$-2,7-$(CH_3)_2$-1-CN shows only monomer fluorescence in the solid state.

Figures 2.4 and **2.5** reveal that the molecular stacking within the crystalline lattice of **2.3** is not of the classical A and B types. **2.3** does have certain characteristics similar to the molecules in both categories. Even though there are some short contacts in **2.3**, there are not enough or not the right orientation to make excimers so the fluorescence of **2.3** is like that of the A type crystals.

Excimer emission is not observed from crystalline **2.3**, instead upon going from a dilute solution of **2.3** to that of the crystal a slight red-shift of the emission to 370 nm is observed (see **Figure 2.3**). We believe this shift is due to auto-absorption of the short wave portion of the fluorescence. A red-shift is also observed in the emission of the previously mentioned molecules, such as naphthalene, possessing the A type stacking.[62] Although the fluorescence of crystalline **2.3** is red-shifted as is the fluorescence of solid naphthalene, the fine structure is not as apparent as it is in the emission band representing the fluorescence of naphthalene.[62] This absence of fine structure in the solid state fluorescence was also observed in the case of solid 3,4-benzpyrene having the A type crystal structure.[62] Both A and B type lattice arrangements have been observed for 3,4-benzpyrene, with the shortest intermolecular contacts <3.5 Å in the B type ca. 3.49 Å.[64] This is shorter than the 3.55 Å
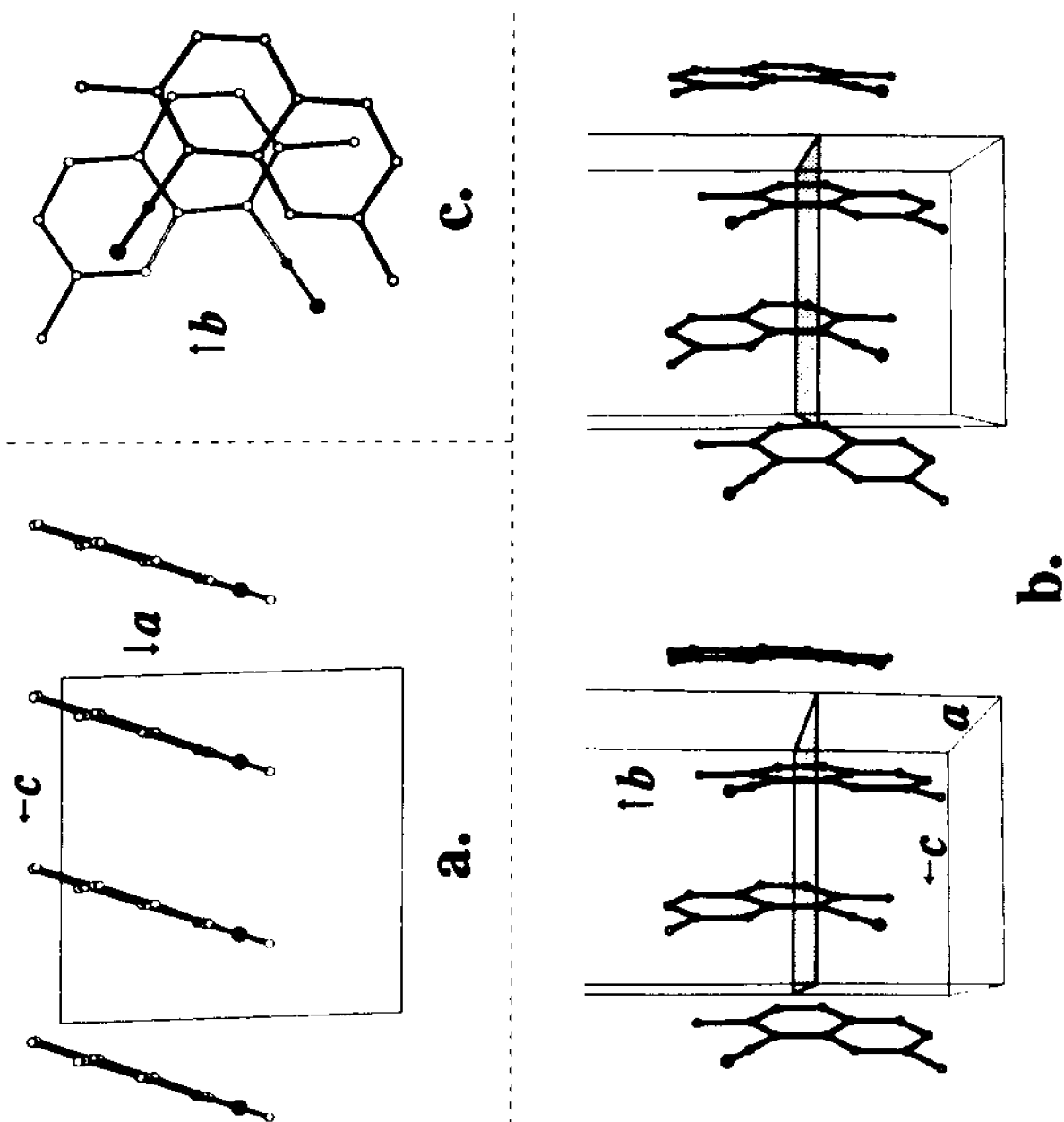
Figure 2.4. Views of the packing of molecules in crystalline $C_{10}H_5$-2,7-$(CH_3)_2$-1-CN. Atoms in CN groups are filled (solid black) for clarity. (a) View down crystallographic b axis, showing approximately parallel molecules stacked along c. (b) Stereo view approximately down a axis, showing relationship of molecules to glide plane (shaded). (c) View of one molecule (heavy lines) approximately perpendicular to its molecular plane, showing the poor overlap with its nearest neighbor.
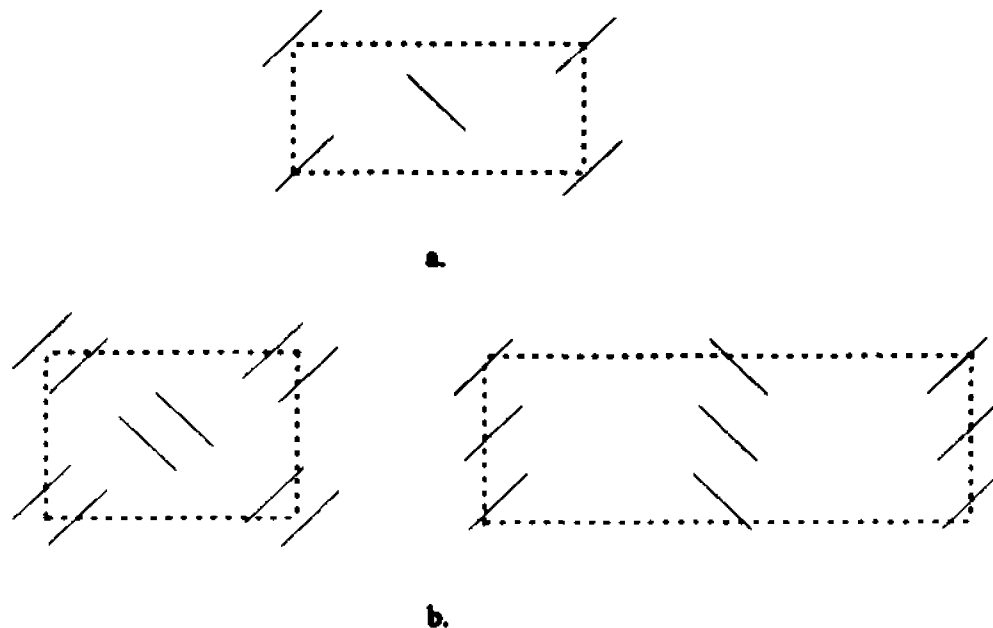
Figure 2.5. Molecular stacking of a. A type lattices; b. B type, B_1 and B_2, lattices.

intermolecular distance observed for **2.3**. The solid 3,4-benzpyrene exhibits excimer emission as do solids having the B type crystal lattice.

The resemblance of absorption and fluorescence for both the dilute solution and the crystal of **2.3** suggests that the emitting species is the monomer in each case as would be expected from a crystal possessing an A type lattice. The A type molecules, though, do not produce excimer emission at the concentrations observed for **2.3**.

As mentioned previously, our initial interest in the fluorescence properties of 1-$CN-2,7-(CH_3)_2C_{10}H_5$ was due to the observation of its intense fluorescence at 490 nm, later found to be caused by an impurity. The following compounds were observed, via GC-MS, to be present in small amounts in the unpurified crystalline sample of **2.3** showing emission at 490 nm: two bromo-2,7-dimethylnaphthalenecarbonitriles (m/e 259,261) and two 2,7-dimethylnaphthalenedicarbonitriles (m/e 206) (typical

electrophilic aromatic substitution patterns suggest 4-bromo-2,7-dimethylnaphthalene-1-carbonitrile (c.), 5-bromo-2,7-dimethylnaphthalene-1-carbonitrile (d.), 2,7-dimethylnaphthalene-1,4-dicarbonitrile (e.), and 2,7-dimethylnaphthalene-1,5-dicarbonitrile (f.) are the isomers present; see **Figure 2.6**). These reaction by-products (c.-f.) are a result of 1,4-dibromo-2,7-dimethylnaphthalene (a.) and 1,5-dibromo-2,7-dimethylnaphthalene (b.) undergoing substitution of a Br for a CN in the reaction responsible for the synthesis of **2.3**. These impurities (a. and b.) were synthesized in the reaction preceding the synthesis of **2.3**. Although the impurities c. - f. comprised less than 5 % of an average sample of **2.3**, their presence distorted the luminescence properties of **2.3**.

The lifetime of the excited state of a solid sample containing only the reaction impurities, which could not be separated, was found to be ~6 μsec (λ_{max} 490 nm). The average excited state lifetime of a phosphorescing molecule is 10 μsec.[65] The phosphorescence is likely to be due to one or more of the brominated compounds. 1-Bromonaphthalene is known to phosphoresce to a greater extent than it fluoresces as a result of the presence of the Br.[65] The heavy atom substituent produces spin-orbit coupling which favors intersystem crossing to the triplet state. The GC-MS data indicated an absence of these impurities in the samples used for fluorescence measurements. After 30 min. of irradiation at 300 nm, the solid sample produces a second emission peak at 465 nm which grows in intensity with continued irradiation. GC-MS of the irradiated solid does not indicate the presence of a decomposition product. Dissolving the irradiated solid in $CHCl_3$ and allowing the solvent to

evaporate, produces a solid which again emits at 370 nm and can be irradiated to produce the same emission at 465 nm. This new peak could be the result of a dimeric defect at the crystal surface acting as an exciton trap.
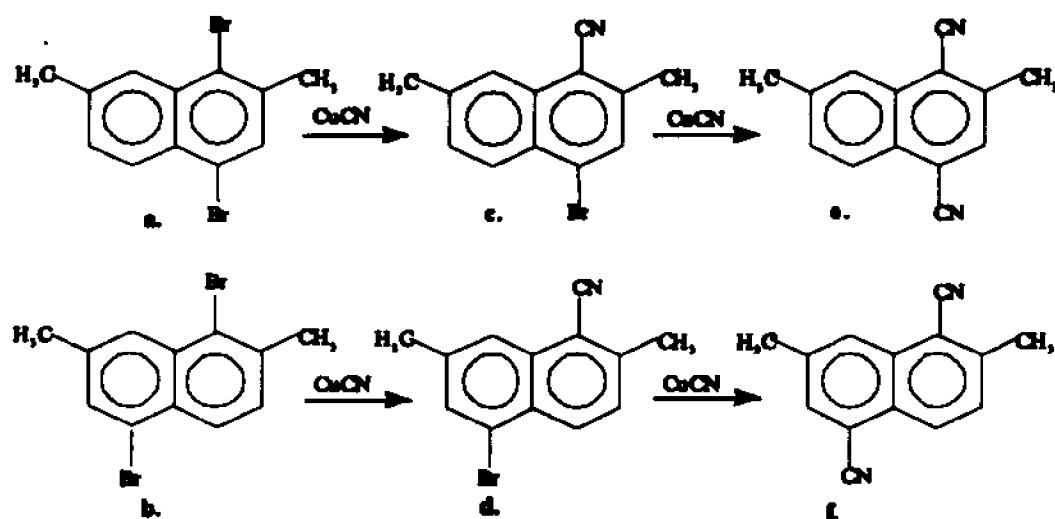
Figure 2.6. Scheme for the synthesis of luminescent impurities in a sample of **2.3**: **a.** 1,4-dibromo-2,7-dimethylnaphthalene, **b.** 1,5-dibromo-2,7-dimethylnaphthalene, **c.** 4-bromo-2,7-dimethylnaphthalene-1-carbonitrile, **d.** 5-bromo-2,7-dimethylnaphthalene-1-carbonitrile, **e.** 2,7-dimethylnaphthalene-1,4-dicarbonitrile, and **f.** 2,7-dimethylnaphthalene-1,5-dicarbonitrile.

2.4 Conclusions

Partially purified crystalline 2,7-dimethylnaphthalene-1-carbonitrile (1-cyano-2,7-dimethylnaphthalene, **2.3**) showed intense blue-green luminescence (λmax = 490 nm). Further purification of **2.3** showed that the 490 nm emission was due to an impurity. The luminescence of purified **2.3**, determined to be fluorescence based on studies done on 1-cyanonaphthalene[54], was found to vary from solution to solid phase. Dilute CH_2Cl_2 solutions (<4 x 10^{-3} M) of **2.3** fluoresced only at 350 nm. Excimer

emission (421 nm) was observed in more concentrated solutions. Solid **2.3** luminesced at 370 nm. The single-crystal X-ray structure of **2.3** has also been determined.

The fluorescence properties of 2,7-dimethylnaphthalene-1-carbonitrile may prove to be useful in studying the host-guest interactions of our cofacial binuclear bis(β-diketone) complexes. We have successfully synthesized colorless $Zn_2(NBA)_2(\mu$-G) complexes which do luminesce (see **Chapter 5**), and the $Zn_2(NBA-CN)_2(\mu$-G) complexes might show luminescence connected with the 2,7-dimethylnaphthalene-1-carbonitrile moieties that would be sensitive to the binding and exchanging of G.

Chapter 3. Synthesis of Functionalized Bis(β-diketones) from Bis(bromomethyl)naphthalene Derivatives

3.1 Introduction

We have prepared cofacial binuclear bis(β-diketonate) complexes (Cu$_2$(NBA-X)$_2$ bearing internal functional groups X (X = CN and Br, **3.1**), with the goal of mimicking the high selectivity observed during enzymatic catalysis. We have used 2,7-bis(bromomethyl)naphthalenes to synthesize the bis(β-diketone) ligands (**3.2**). These ligands provide rigid bridging groups forming a cavity of well-defined size and shape into which nitrogenous bases (G) can bind via the Cu atoms (**3.3**).
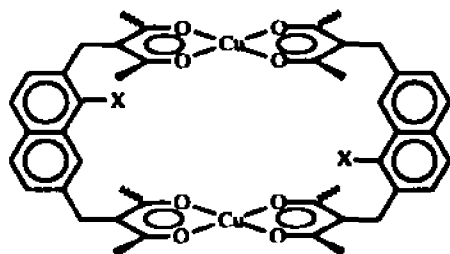
3.1 X = CN, Br
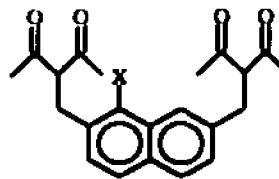
3.2 X = CN, Br
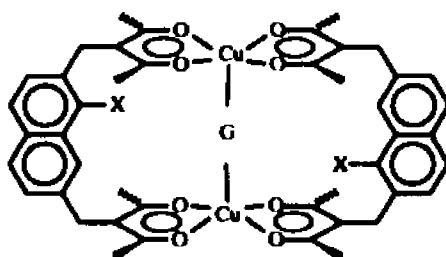
3.3

The chelating NBA-X ligands are formed by the substitution of acetylacetonate for the Br groups of 2,7-bis(bromomethyl)naphthalene-1-X which is synthesized via a free radical bromination as seen in **Figure 3.1**. The bromination of 2,7-dimethylnaphthalene-1-carbonitrile (1-CN-2,7-(CH$_3$)$_2$C$_{10}$H$_5$, **3.4**) is more sensitive to

reaction conditions than that of 1-bromo-2,7-dimethylnaphthalene. Bromination of the nitrile often results in the formation of di- and tribrominated side products. The effects of these

conditions on bromination of 3.4 will be presented in this chapter. The synthesis of
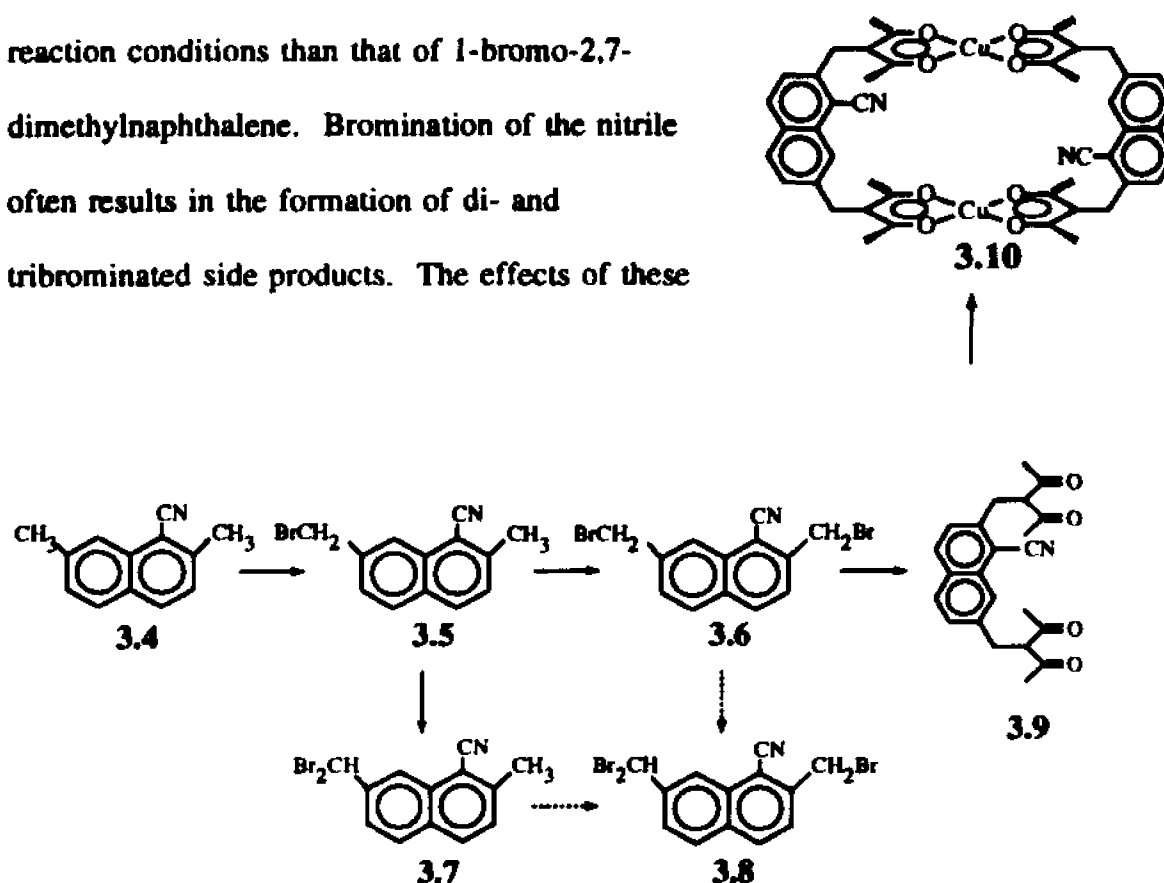
Figure 3.1. Synthesis of $Cu_2(NBA-CN)_2$ (**3.10**) from $1-CN-2,7-(CH_3)_2C_{10}H_5$ (**3.4**).

conditions on bromination of **3.4** will be presented in this chapter. The synthesis of

compounds **3.6, 3.9, 3.10**, and the corresponding 1-Br compounds will be outlined and

the mechanism of bromination of **3.6** will be described using ^1H NMR data.

The methyl groups of 2,7-dimethylnaphthalene-1-carbonitrile have been

successfully monobrominated via a free radical bromination reaction which passes

through a monobrominated intermediate (**3.5**) resulting in the desired 2,7-

bis(bromomethyl)naphthalene-1-carbonitrile $(2,7-(BrCH_2)_2-1-CNC_{10}H_5$, **3.6**) and di-

and tribrominated side products 7-(dibromomethyl)-2-methylnaphthalene-1-carbonitrile

$(1-CN-7-(Br_2CH)-2-(CH_3)-C_{10}H_5$, **3.7**) and 2-(bromomethyl)-7-

(dibromomethyl)naphthalene-1-carbonitrile (1-CN-2-(BrCH$_2$)-7-(Br$_2$CH)-C$_{10}$H$_5$, **3.8**), respectively. When the free radical side-chain bromination of 1-CN-2,7-(CH$_3$)$_2$C$_{10}$H$_5$ (**3.4**) was carried out with excess N-bromosuccinimide (NBS), the ratio of the di- and tribrominated side products (**3.7** & **3.8**) to the desired bis(bromomethyl) compound (**3.6**) increased. Procedural changes made in order to insure monobromination of each side-chain are described here, as well as single-crystal analyses of 1-CN-7-(Br$_2$CH)-2-CH$_3$C$_{10}$H$_5$ (**3.7**) and 1-CN-2-(BrCH$_2$)-7-(Br$_2$CH)-C$_{10}$H$_5$ (**3.8**).

3.2 Experimental Section

3.2.1. Materials and Procedures.
1-CN-2,7-(CH$_3$)$_2$C$_{10}$H$_5$ (**3.4**) and 1-Br-2,7-(CH$_3$)$_2$C$_{10}$H$_5$ were synthesized as described in **Chapter 2 and reference 59**, respectively. NBS (Aldrich) and benzoyl peroxide (Matheson Coleman & Bell) were used as received. Spectrophotometric grade solvents used were purchased from Mallinckrodt.

The NMR experiments were done on Bruker AC250 and ARX300 spectrometers. Electronic absorption spectra were recorded on an Aviv Model 14DS absorption spectrophotometer.

3.2.2. Synthesis of 2,7-Bis(bromomethyl)naphthalene-1-carbonitrile, (2,7-(BrCH$_2$)$_2$-1-CNC$_{10}$H$_5$) (**3.6**).
A solution of 1-CN-2,7-(CH$_3$)$_2$C$_{10}$H$_5$ (5.5 g; 0.030 mol) in 150 ml of CCl$_4$ was brought to reflux. NBS was added in small portions (0.6-0.7 g) to the refluxing mixture every 15 min for 4 hrs. After the first addition of NBS, 0.1 g of benzoyl peroxide was added. A total of 10.8 g (0.060 mol) of NBS was added. Refluxing was continued for a total of 12 h, at which point succinimide could be seen

floating in the solution. The mixture was allowed to cool to room temperature, whereupon further precipitation occurred. The mixture was filtered, and the filtrate (see below) was saved. The collected solid, an off-white powder, was washed twice with 100 mL of 1.5 M NaOH in order to remove succinimide. The solid residue, crude 3.6, was dissolved in CH_2Cl_2 and then dried over $MgSO_4$ and evaporated to give 3.4 g of product (34%). EI-MS m/e (%) 337, 339, 341 (M^+, 16); 258, 260 (M^+ − Br, 100); 179 (M^+ − 2Br, 87). Crystallization from t-BuOH gave needle-like crystals, m.p. 152-155 °C. ^1H NMR ($CDCl_3$): δ 4.68 (s, 7-CH_2), 4.82 (s, 2-CH_2), 7.62 (d, J = 8.52 Hz, H3), 7.67 (dd, J = 1.92, H6), 7.91 (d, J = 8.25, H5), 8.05 (d, J = 8.52, H4), 8.21 (s, H8). ^{13}C NMR ($CDCl_3$): δ 29.801 (2-CH_2), 32.602 (7-CH_2), 109.622 (C1), 115.531 (C11), 125.222 (C8), 127.340 (C3), 129.102 (C6), 129.370 (C5), 132.012 (C10), 132.430 (C9), 133.255 (C4), 138.964 (C7), 142.066 (C2).

3.2.3. Isolation of 7-(Dibromomethyl)-2-methylnaphthalene-1-carbonitrile ($1\text{-}CN\text{-}7\text{-}(Br_2CH)\text{-}2\text{-}CH_3C_{10}H_5$) (3.7) & 2-(Bromomethyl)-7-(dibromomethyl)naphthalene-1-carbonitrile ($1\text{-}CN\text{-}2\text{-}(BrCH_2)\text{-}7\text{-}(Br_2CH)\text{-}C_{10}H_5$) (3.8).

Compounds 3.7 and 3.8 were isolated from the CCl_4 filtrate in the 2,7-$(BrCH_2)_2$-1-$CNC_{10}H_5$ synthesis (see above). The solvent was removed leaving a yellow residue, from which 3.7 and 3.8 were isolated by column chromatography (70-230 mesh, 60 Å silica gel; hexane-CH_2Cl_2; 1:1, v/v). Colorless needle-like crystals of 3.7 and rectangular crystalline plates of 3.8 were obtained after solvent evaporation. 1-CN-7-(Br_2CH)-2-$CH_3C_{10}H_5$ (3.7), m.p. 155-157 °C; EI-MS m/e (%) 337, 339, 341 (M^+, 16); 258, 260 (M^+ − Br, 100); 179 (M^+ − 2Br, 87). ^1H NMR ($CDCl_3$): δ 6.85

(s, 7-CH), 2.76 (s, 2-CH$_3$), 7.46 (d, H3), 7.98 (s, H6), 7.93 (d, H5), 7.92 (d, H4), 8.15

(s, H8). 1-CN-2-BrCH$_2$-7-Br$_2$CHC$_{10}$H$_5$ (3.8), 134-137 °C; EI-MS m/e (%) 415, 417,

419, 421 (M$^+$, 5); 336, 338, 340 (M$^+$ − Br, 100); 257, 259 (M$^+$ − 2Br, 51); 178 (M$^+$ −

3Br, 15). ^{1}H NMR (CDCl$_3$): δ 6.85 (s, 7-CH), 4.82 (s, 2-CH$_2$), 7.67 (d, H3), 7.99 (s,

H6), 7.99 (s, H5), 8.08 (d, H4), 8.21 (s, H8).

3.2.4. X-ray Methods. Diffraction data were collected on an Enraf-Nonius

CAD4 diffractometers. The diffractometer on which the data for compound 3.7 was

collected was fitted with MoKα and graphite monochromator while the one on which

the data for 3.8 was fitted with CuKα source. The θ-2θ scan method was used within

the limits 2<θ<75° for 3.8 and 1<θ<30° for 3.7. The sample crystal of 3.7 was a

colorless needle fragment of dimensions 0.17 x 0.28 x 0.40 mm, and was mounted in

a capillary. The sample crystal of 3.8 was a colorless plate of dimensions 0.32 x 0.25

x 0.08 mm, and was also mounted in a capillary. Final unit cell constants were

determined from the orientations of twenty-five centered high-angle reflections. The

intensities were corrected for absorption using Ψ scan data for five reflections and a

minimum relative transmission coefficient for 3.7 of 59.15 % and 32.9 % for 3.8. The

MolEN set of programs for structure solution and refinement was used.[60] The 1120

data having I>1σ(I) were used in the refinement of 3.7, and its H atoms were refined

isotropically. The 1817 data having I>3σ(I) were used in the refinement of 3.8, and

its H atoms were not refined. Details of data collection and structure refinement on

3.7 and 3.8 are given in **Tables 3.1** and **3.2**, respectively. The ORTEP drawings can

be seen in **Figures 3.2** and **3.3**, respectively.

Table 3.1. Crystal data for 7-(dibromomethyl)-2-methylnaphthalene-1-carbonitrile (3.7).[a]

chemical formula	$C_{13}H_9NBr_2$	space group	$P2_1/m$
fw	339.0	temp/°C	24
a/Å	9.0939(6)	λ/Å	0.71073 (MoKα)
b/Å	7.0840(3)	D_c/g cm⁻³	1.798
c/Å	9.8738(7)	μ(MoKα)/cm⁻¹	63.8
β/deg	100.303(6)	$R(F_o)$	0.046
V/Å³	625.8(1)	$R_w(F_o)$	0.039
Z	2		

[a]Values in parentheses in **Tables 3.1-3.8** are estimated standard deviations of the last digit.

Table 3.2. Crystal data for 2-(bromomethyl)-7-(dibromomethyl)naphthalene-1-carbonitrile (3.8).

chemical formula	$C_{13}H_8NBr_3$	space group	$P\bar{1}$
fw	417.9	temp/°C	23
a/Å	8.0509(8)	λ/Å	1.5418 (CuKα)
b/Å	8.1060(9)	D_c/g cm⁻³	2.086
c/Å	10.395(1)	μ(MoKα)/cm⁻¹	111.8
β/deg	80.41(1)	$R(F_o)$	0.093
V/Å³	665.5(2)	$R_w(F_o)$	0.106
Z	2		

Figure 3.2. ORTEP of 7-(dibromomethyl)-2-methylnaphthalene-1-carbonitrile (3.7).
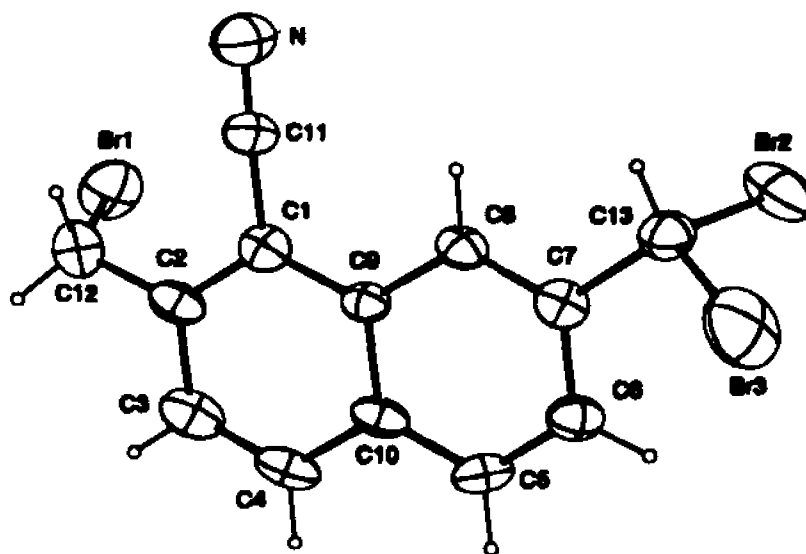
Figure 3.3. ORTEP of 2-(bromomethyl)-7-(dibromomethyl)naphthalene-1-carbonitrile (**3.8**).

3.2.5. Synthesis of NBAH$_2$-1-CN (3,3'-(1-cyanonaphthalene-2,7-diylbis(methylene))bis(2,4-pentanedione)) (3.9) and NBAH$_2$-1-Br (3,3'-(1-bromonaphthalene-2,7-diylbis(methylene))bis(2,4-pentanedione)). These NBAH$_2$-X ligands were prepared by the methods outlined by Martin and coworkers for the synthesis of (RCO)(R'CO)CH-Y-CH(COR)(COR') type compounds.[40]

Dried t-butyl alcohol (45 ml) was placed in an oven-dried two-neck flask (100 mL), purged with N$_2$, and brought to reflux temperature. Potassium metal (0.018 g, 4.60 x 10^{-4} mol) was added and the mixture stirred until all of the potassium had dissolved. Distilled acetylacetone (acacH; 0.069 g, 6.89 x 10^{-4} mol) was then added dropwise. The mixture was stirred 35 min. before the bis(bromomethyl)naphthalene-X

compound (X = CN 0.078 g or X = Br 0.090 g, 2.30 x 10^{-4} mol) was added. Small

portions of the brominated reactant were added over a period of 5 min. The mixture

became cloudy during the following hour. KI (0.005 g, 3.0 x 10^{-5} mol) was added

and the reaction was continued 4 more hrs. Distilled H_2O (50 ml) was added to the

mixture to dissolve any or all of the following: KI, KBr, KacacH, and/or acac.

CH_2Cl_2 (50 ml) was added to extract the ligand. The CH_2Cl_2 layer was dried over

$MgSO_4$, filtered, and the solvent evaporated resulting in a cloudy oil. The product

could be precipitated from concentrated CH_2Cl_2 solutions by adding large volumes of

hexane. $NBAH_2$-1-CN yield 40 %, m.p. 118-121 °C. EI-MS m/e (%) 335 (M^+ –

$COCH_3$, 2), 292 (M^+ – $2COCH_3$, 42), 43 ($COCH_3$, 100), PDMS m/e (%) 378 (M^+ +

H, 12), 335 (M^+ – $COCH_3$, 100), 292 (M^+ – $2COCH_3$, 30). $NBAH_2$-1-CN ^1H NMR

(C_6D_6) of enol form: δ 1.62 (s, 7'-CH_3), 1.71 (s, 2'-CH_3), 3.27 (s, 7-CH_2), 3.64 (s, 2-

CH_2), 6.83 (d, H_3), 7.02 (dd, H6), 7.39 (d, H5), 7.42 (d, H4), 8.19 (m, H8), 17.54 (s,

7'-OH), 17.56 (s, 2'-OH). $NBAH_2$-1-Br yield 45 %, m.p. 115-119 °C. $NBAH_2$-1-Br

was not isolated in the pure enol or keto form. The NMR data is, therefore, that of a

mixture of the two. $NBAH_2$-1-Br ^1H NMR ($CDCl_3$) of keto-enol mixture: A. keto

resonances: δ 2.13 (s, 7'-CH_3), 2.18 (s, 2'-CH_3), 3.37 (d, 2'-CH_2), 3.39 (d, 2'-CH_2),

3.47 (d, 7'-CH_2), 4.13 (t, 2'-CH), 4.16 (t, 2'-CH), 4.26 (t, 7'-CH); B. enol resonances:

δ 2.05 (s, 7'-CH_3), 2.14 (s, 2'-CH_3), 3.86 (s, 2'-CH_2), 3.87 (s, 2'-CH_2), 3.92 (s, 7'-

CH_2), 16.89 (s, 7'-OH), 16.90 (s, 2'-OH). The spectrum is further complicated by the

fact that the two acac groups are different, due to the presence of the Br group. The

doublet and triplet resonances characteristic of the keto form of $NBAH_2$ (see **Chapter**

5) are present. We are not sure why certain resonances are doubled, but the same

trend is observed from the 1H NMR data of a mixture of the keto and enol forms. If

the Br restricts the free rotation of the adjacent Ar-CH$_2$ bond, then the spectrum could

be complicated.

3.2.6. Synthesis of Cu$_2$(NBA-1-X)$_2$ (X = CN and Br) (3.1). The metal atoms

were attached to the ligand by shaking a CHCl$_3$ solution of the ligand with an aqueous

solution containing a 10-fold excess of Cu(NH$_3$)$_4$$^{2+}$. During this procedure, the CHCl$_3$

layer turned green, indicating the formation of Cu$_2$(NBA-1-X)$_2$. The organic layer

containing the complex was separated from the aqueous layer and dried using MgSO$_4$.

Precipitation of the gray-green Cu$_2$(NBA-1-Br)$_2$ and yellow-green Cu$_2$(NBA-1-CN)$_2$

complexes could then be induced by mixing minimal amounts of the CHCl$_3$ solution

with a large excess of hexane. Anal. Calcd for Cu$_2$(NBA-1-CN)$_2$ (C$_{46}$H$_{42}$O$_8$N$_2$Cu$_2$):

C, 62.93; H, 4.82; N, 3.19. Found: C, 63.16; H, 4.68; N, 3.55; Absorbance max. 510

and 645 nm. Calcd. for Cu$_2$(NBA-1-Br)$_2$ (C$_{44}$H$_{42}$O$_8$Br$_2$Cu$_2$): C, 53.61; H, 4.29; Br,

16.21. Found: C, 58.14; H, 4.57; Br, 17.20; Absorbance max. 500 and 635 nm.

Crystals of Cu$_2$(NBA-1-CN)$_2$ could be grown by layering CHCl$_3$ solutions of the

metal complex with CH$_3$CN. Because the crystals were too small, they were not x-ray

quality.

3.3 Results and Discussion

3.3.1. X-ray Analysis of 7-(Dibromomethyl)-2-methylnaphthalene-1-

carbonitrile (3.7) and 2-(Bromomethyl)-7-(dibromomethyl)naphthalene-1-

carbonitrile (3.8). ORTEP drawings of 3.7 and 3.8 are seen in Figures 3.2 and 3.3,

respectively. The atomic coordinates obtained for the two structures are given in

Tables 3.3-3.6; bond distances and angles Tables 3.7 and 3.8.

Table 3.3. Fractional atomic coordinates and equivalent isotropic temperature parameters for 1-CN-7-Br$_2$CH-2-CH$_3$-C$_{10}$H$_6$ (3.7).

Atom	x	y	z	$B_{eq}(Å^2)$
Br	0.76695(5)	0.47149(7)	0.54760(4)	6.08(1)
N	0.0982(5)	1/4	0.1596(6)	7.4(2)
C1	0.3132(5)	1/4	0.0213(5)	3.4(1)
C2	0.2836(6)	1/4	-0.1202(6)	3.9(1)
C3	0.4070(6)	1/4	-0.1886(5)	4.5(1)
C4	0.5489(6)	1/4	-0.1189(5)	3.8(1)
C5	0.7292(5)	1/4	0.1021(5)	3.6(1)
C6	0.7558(5)	1/4	0.2416(5)	3.5(1)
C7	0.6367(5)	1/4	0.3134(5)	3.3(1)
C8	0.4942(5)	1/4	0.2428(5)	3.4(1)
C9	0.4621(5)	1/4	0.0984(5)	2.9(1)
C10	0.5823(5)	1/4	0.0252(5)	3.2(1)
C11	0.1922(6)	1/4	0.0979(6)	4.7(1)
C12	0.1279(6)	1/4	-0.2015(6)	5.5(2)
C13	0.6617(6)	1/4	0.4667(5)	4.2(1)

Table 3.4. Coordinates and isotropic thermal parameters for hydrogen atoms for 1-CN-7-Br$_2$CH-2-CH$_3$-C$_{10}$H$_6$ (3.7).

Atom	x	y	z	$B_{iso}(Å^2)$
H3	0.388(4)	1/4	-0.285(4)	2.7(9)
H4	0.623(4)	1/4	-0.164(4)	3(1)
H5	0.799(4)	1/4	0.064(4)	3(1)
H6	0.854(4)	1/4	0.284(4)	2.5(9)
H8	0.425(4)	1/4	0.283(4)	2.4(9)
H12a	0.121(5)	1/4	-0.291(5)	5(1)
H12b	0.073(3)	0.176(5)	-0.168(3)	6(1)
H13	0.582(5)	1/4	0.496(4)	3(1)

Table 3.5. Fractional atomic coordinates and equivalent isotropic temperature parameters for 1-CN-2-BrCH$_2$-7-Br$_2$CH-C$_{10}$H$_6$ (3.8).

Atom	x	y	z	$B_{eq}(Å^2)$
Br1	0.5433(2)	0.2668(2)	0.0368(1)	7.20(4)
Br2	-0.0838(2)	0.5124(2)	0.7592(2)	7.73(5)

(table con'd.)

Br3	0.0383(3)	0.2278(3)	0.9620(2)	9.81(6)
N	0.148(1)	0.047(2)	0.297(1)	6.7(3)
C1	0.403(1)	0.154(1)	0.377(1)	4.2(2)
C2	0.561(1)	0.148(1)	0.296(1)	4.3(2)
C3	0.698(1)	0.207(2)	0.343(1)	5.3(3)
C4	0.677(1)	0.272(2)	0.461(1)	5.0(3)
C5	0.496(1)	0.349(2)	0.665(1)	4.7(3)
C6	0.337(1)	0.356(2)	0.742(1)	4.5(3)
C7	0.201(1)	0.290(1)	0.700(1)	4.2(2)
C8	0.219(1)	0.226(1)	0.584(1)	3.9(2)
C9	0.379(1)	0.216(1)	0.500(1)	3.4(2)
C10	0.517(1)	0.281(1)	0.545(1)	4.2(2)
C11	0.263(1)	0.092(2)	0.331(1)	4.6(3)
C12	0.586(2)	0.087(2)	0.169(1)	5.5(3)
C13	0.023(1)	0.296(2)	0.782(1)	5.2(3)

Table 3.6. Coordinates and isotropic thermal parameters for hydrogen atoms for 1-CN-2-BrCH$_2$-7-Br$_2$CH-C$_{10}$H$_5$ (3.8).

Atom	x	y	z	B$_{iso}$(Å^2)
H3	0.8069	0.2024	0.2917	6
H4	0.7716	0.3116	0.4896	6
H5	0.5894	0.3896	0.6952	6
H6	0.3209	0.4055	0.8224	5
H8	0.1228	0.1856	0.5568	5
H12a	0.6995	0.0444	0.1482	7
H12b	0.5114	0.0014	0.1685	7
H13	-0.0460	0.2211	0.7533	6

Table 3.7. Bond distances (Å) and bond angles (°) for 1-CN-7-Br$_2$CH-2-CH$_3$-C$_{10}$H$_5$ (3.7).

Atoms		Distance	Angle	Atoms		Distance	Angle
N	C11	1.135(8)		C7	C8	1.357(6)	
C1	C2	1.375(7)		C7	C13	1.490(7)	
C1	C9	1.430(6)		C8	C7	1.357(6)	
C1	C11	1.442(8)		C8	C9	1.403(7)	
C2	C1	1.375(7)		C9	C1	1.430(6)	
C2	C3	1.410(8)		C9	C8	1.403(7)	
C2	C12	1.497(7)		C9	C10	1.414(7)	
C3	C2	1.410(8)		C10	C4	1.401(7)	
C3	C4	1.349(7)		C10	C5	1.413(6)	
C4	C3	1.349(7)		C10	C9	1.414(7)	

(table *con'd.*)

Atoms		Distance		Atoms		Distance	
C4	C10	1.401(7)		C11	N	1.135(8)	
C5	C6	1.355(7)		C11	C1	1.442(8)	
C5	C10	1.413(6)		C12	C2	1.497(7)	
C6	C5	1.355(7)		C13	Br	1.935(3)	
C6	C7	1.397(7)		C13	C7	1.490(7)	
C7	C6	1.397(7)					

Atoms			Angle	Atoms			Angle
C2	C1	C9	122.4(5)	C6	C7	C13	121.6(4)
C2	C1	C11	120.2(4)	C8	C7	C13	118.7(5)
C9	C1	C11	117.4(4)	C7	C8	C9	121.9(5)
C1	C2	C3	117.3(4)	C1	C9	C8	123.1(4)
C1	C2	C12	122.7(5)	C1	C9	C10	118.2(4)
C3	C2	C12	120.0(5)	C8	C9	C10	118.7(4)
C2	C3	C4	121.7(5)	C4	C10	C5	123.9(5)
C3	C4	C10	122.2(5)	C4	C10	C9	118.1(4)
C6	C5	C10	121.7(5)	C5	C10	C9	117.9(4)
C5	C6	C7	120.1(4)	N	C11	C1	179.2(6)
C6	C7	C8	119.7(4)	Br	C13	C7	113.2(2)
Br	C13	Br'	108.4(2)				

Table 3.8. Bond distances (Å) and bond angles (°) for 1-CN-2-BrCH$_2$-7-Br$_3$CH-C$_{10}$H$_5$ (3.8).

Atoms		Distance	Angle	Atoms		Distance	Angle
C1	C2	1.41(1)		C7	C13	1.54(1)	
C1	C9	1.39(2)		C8	C7	1.33(2)	
C1	C11	1.43(2)		C8	C9	1.43(1)	
C2	C1	1.41(1)		C9	C1	1.39(2)	
C2	C3	1.41(2)		C9	C8	1.43(1)	
C2	C12	1.43(2)		C9	C10	1.42(2)	
C3	C2	1.41(2)		C10	C4	1.42(1)	
C3	C4	1.36(2)		C10	C5	1.39(2)	
C4	C3	1.36(2)		C10	C9	1.42(2)	
C4	C10	1.42(1)		C11	N	1.14(2)	
C5	C6	1.39(1)		C11	C1	1.43(2)	
C5	C10	1.39(2)		C12	Br1	1.97(1)	
C6	C5	1.39(1)		C12	C2	1.43(2)	
C6	C7	1.40(2)		C13	Br2	1.92(1)	
C7	C6	1.40(2)		C13	Br3	1.92(1)	
C7	C8	1.33(2)		C13	C7	1.54(1)	
C2	C1	C9	123(1)	C7	C8 C9		122(1)
C2	C1	C11	118(1)	C1	C9 C8		124(1)
C9	C1	C11	119.5(9)	C1	C9 C10		119.5(9)
C1	C2	C3	117(1)	C8	C9 C10		117(1)

(table con'd.)

C1 C2 C12	123(1)	C4 C10 C5	122(1)
C3 C2 C12	120(1)	C4 C10 C9	117(1)
C2 C3 C4	121(1)	C5 C10 C9	120.8(9)
C3 C4 C10	123(1)	N C11 C1	177(1)
C6 C5 C10	120(1)	Br1 C12 C2	110.1(9)
C5 C6 C7	120(1)	Br2 C13 Br3	113.2(6)
C6 C7 C8	121.4(9)	Br2 C13 C7	110.3(8)
C6 C7 C13	121(1)	Br3 C13 C7	109.5(8)
C8 C7 C13	117(1)		

There are no major differences between the geometries of **3.7** and **3.8**. All non-H atoms in **3.7** except Br lie on a crystallographic mirror; the Br atoms are anti to H8, which is also the case for **3.8**. The largest changes in bond lengths upon addition of a Br to C12 are the C2-C12 and C7-C13 distances. The C7-C13 bond distance increases by 0.05(1) Å while the C2-C12 distance decreases by 0.07(2) Å. On comparing the distance between C7 and C13 of **3.4** with C7-C13 of **3.8** and **3.9**, it is unusual that when 2Br's were added to C13 no difference was observed. Upon addition of a third Br to the molecule, Br2-C13-C7 and Br3-C13-C7 decrease by 2.9(8) and 3.7(8) °, respectively, as well as Br2-C13-Br3 which increases by 4.8(6) °. These differences are of marginal statistical significance.

Table 3.9 compares angles C2-C1-C9 and C1-C2-C3 of naphthalene to those of the substituted naphthalenes we have synthesized. A consistent trend of an increase in C2-C1-C9 and a decrease in C1-C2-C3 is observed upon substitution at the first and second positions of naphthalene. The opposite trend is observed for another series of substituted naphthalenes (see **Table 3.10**).[66-68]

Table 3.9. A comparison of C2-C2-C9 and C1-C2-C3 of naphthalene[61] with C2-C1-C9 and C1-C2-C3 of our trisubstituted naphthalenes.

	Naphthalene[24]	1-Br,2,7-$(CH_3)_2$[18]	3.4	3.7	3.8
C2-C1-C9	120.3(3)	123.5(3)	122.2(1)	122.4(5)	123(1)
C1-C2-C3	120.5(2)	116.2(3)	118.0(1)	117.3(4)	117(1)
Δ from naphthalene C2-C1-C9		3.2(4)	1.9(3)	2.1(6)	2.7(1)
Δ from naphthalene C1-C2-C3		−4.3(4)	−2.5(2)	−3.2(4)	−3.5(1)

Table 3.10. A comparison of C2-C1-C9 and C1-C2-C3 of naphthalene[61] with C2-C1-C9 and C1-C2-C3 of three trisubstituted naphthalenes.[66-68]

	Naphthalene[61]	1-Ac,2,7-OCH_3[66]	1-CCl=CH_2, 2,7-OCH_3[67]	1-Ac, 2-OH, 7-OCH_3[68]
C2-C1-C9	120.3(3)	120.1(1)	120.3(1)	118.3(2)
C1-C2-C3	120.5(2)	121.2(1)	121.0(1)	121.9(3)
Δ from naphthalene C2-C1-C9		−0.2(3)	0.0(3)	−2.0(4)
Δ from naphthalene C1-C2-C3		0.7(2)	0.5(2)	1.4(4)

The three naphthalene derivatives in Table 3.10 differ from ours in that the bulky substituent is located at the 1 position of the naphthalene. The methyl and substituted methyl groups at the 2 position of our compounds are bulkier than the CN or Br at the

1 position. The more bulky group is pushed out away from the naphthalene, decreasing the respective angle.

A unit cell of 3.7 contains two molecules stacked so that the rings containing the CN groups overlap, but the respective CN groups do not. The adjacent CN's are instead oriented 180° from one another. Although both rings of adjacent molecules in a unit cell of 3.8 overlap, the CN groups are still alternating as seen in the stacking of 3.7. A different arrangement is found for two overlapping molecules in a unit cell of 1-CN-2,7-$(CH_3)_2C_{10}H_5$ (3.4) (see Chapter 2): adjacent molecules are rotated by only approximately 90°.

3.3.2. Synthesis of 2,7-Bis(bromomethyl)naphthalene-1-carbonitrile (2,7-$(BrCH_2)_2$-1-$CNC_{10}H_5$) (3.6).

Free-radical bromination of 3.4 is much more sensitive to experimental conditions than bromination of 2,7-dimethylnaphthalene. The reaction conditions presented in the experimental section under the synthesis of 3.6 are those used to obtain the highest yield of 3.6 and the least amounts of 3.7 and 3.8. Certain procedural variations in the bromination of 3.4 resulted in little or no of 3.6 being formed. The yield of 3.6 decreased to less than 10% when the NBS was added all at the start of the reaction instead of at intervals. Under these conditions, the yield of 3.6 (estimated by GC-MS) was so low that it did not precipitate with the succinimide; this made purification very difficult. If the quantity of CCl_4 was decreased to 50 mL or if an excess of NBS was added, in order to insure reaction completion, the yield of 3.6 was again very low.

The progress of the bromination reaction was monitored by ^{1}H NMR. The starting material, 3.4, shows resonances at 2.73 (2-CH$_3$) and 2.57 ppm (7-CH$_3$) (see Table 3.11 and Chapter 2). After 1.5 h of refluxing, there was a noticeable decrease in intensity of the peak at 2.57 ppm, when compared to the peak at 2.73 ppm, and a new resonance appeared at 4.68 ppm which we attribute to the bromomethyl protons at position 7 of compound 3.5. The fact that, under the proper conditions, 3.4 can be brominated twice at position 7, as seen by the existance of 3.7, before bromination at position 2 occurs further supports the proposed 3.5 over the formation of 2-CH$_2$Br-7-CH$_3$. The 2-CH$_3$ is also more sterically hindered to attack, due to the presence of the 1-Br, than the 7-CH$_3$. When the reaction time reached 2 h a resonance at 4.82 ppm was observed. At this point, the desired product, 3.6, was forming. After 2.5 h a small peak could be observed at 6.85 ppm. It appeared as if the methyl group at position 7 was then being brominated a second time. At the completion of the reaction the only resonance peak below 4 ppm was at 2.77 ppm, indicative of succinimide. After removal of the succinimide a peak which was previously masked, was observed at 2.76 ppm. The resonance at 2.76 ppm can be assigned to the unbrominated methyl at position 2 of compound 3.7.

The chemical shifts for the methyl resonances obtained from ^{1}H NMR studies done on CDCl$_3$ solutions of the crystals are summarized in Table 3.11.

Table 3.11. ^{1}H NMR Chemical Shifts (ppm) for 3.4, 3.5, 3.6, 3.7, and 3.8.

	3.4	3.5^a	3.6	3.7	3.8
H2	2.73	2.76	4.82	2.76	4.82
H7	2.57	4.68	4.68	6.85	6.85

^{a}Chemical shifts for proposed intermediate compound 3.5.

3.4 Conclusion

The yield for the free radical side-chain bromination of 3.4 to give 2,7-bis(bromomethyl)naphthalene-1-carbonitrile (3.6) can be maximized first, by carrying out the reaction in dilute CCl_4 solutions of; second, by adding the brominating agent (NBS) in small quantities over a four hour period; and third, by not adding an excess of NBS. The major side products in this reaction are 7-(dibromomethyl)-2-methylnaphthalene-1-carbonitrile (3.7) and 2-(bromomethyl)-7-(dibromomethyl)naphthalene-1-carbonitrile (3.8), both of which have been characterized by X-ray crystallography.

The bis(brominated)dimethylnaphthalene derivatives can be used to successfully synthesize the functionalized bis(β-diketones) 3.2 from which the cofacial bimetallic copper(II) complexes 3.1 can be synthesized.

Chapter 4. Host-Guest Chemistry of Internally Functionalized Binuclear Copper(II) Complexes

4.1 Introduction

We are synthesizing cofacial binuclear transition-metal complexes in order to develop new catalysts that use structural and functional features of multi-metal enzyme active sites. Our complexes utilize readily synthesized bis(β-diketone) ligands as shown in **Figure 4.1**. The acetylacetonate (acac⁻) ends of the ligand bind to the copper(II) atoms holding them cofacial, or parallel, to one another.
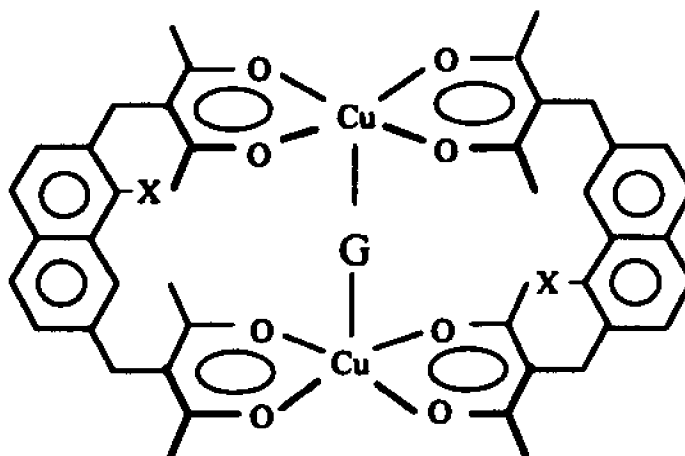

Figure 4.1. Cu$_2$(NBA-X)$_2$ (X=H, Br, or CN) host complex with guest (G = Dabco, pyrazine, aminopyrazine, or piperazine).

The cofacial structure of the complexes lends itself to intramolecular binding of small nitrogenous bases. We have now added internal functional groups (X in **Figure 4.1**) to the previously synthesized NBAH$_2$ (3,3'-[2,7-naphthalenediylbis(methylene)]bis(2,4-pentanedione))[37] ligand. Br and CN groups have been added to the bridging naphthyl rings at position 1. By varying the substituents (X = Br, CN) on the naphthyl rings, we

possibility of intramolecular interactions. The synthesis of these host complexes and UV-Vis spectroscopic studies of the host-guest interactions of these complexes with small nitrogenous bases will be presented in this chapter.

There are several characteristics of both the host and the guest molecules that determine the extent of the interactions between the two. The size of the cavity at the binding site of the host can determine how well the guest will bind. The basicity, size, and shape of the guest can influence its binding to the host. The features of our host complexes ($Cu_2(NBA-X)_2$, X=H, Br, or CN) and the guest molecules (G = Dabco (1,4-diazabicyclo[2.2.2]octane), pyrazine, aminopyrazine, and piperazine) which influence binding will be described and how well the guests bind is reported quantitatively as binding constants.

4.2 Experimental Section

4.2.1. Materials. The nitrogenous bases, other than Dabco (1,4-diazabicyclo[2.2.2]octane), were purchased from the Aldrich Chemical Co. and were used without further purification. Dabco was obtained from Air Products and Chemicals and was sublimed before use. The *tert*-butyl alcohol (Mallinckrodt) was purified by distillation or drying over molecular sieves. All other materials were reagent, HPLC, or spectrophotometric grade and were used as received.

4.2.2. $Cu_2(NBA-X)_2$ (X = H, Br, CN). The $NBAH_2$ derivatives and their Cu^{2+} complexes were prepared as outlined in Chapter 3. This material was used for binding constant measurements.

Attempts to grow X-ray-quality crystals of the functionalized complexes and their host-guest adducts failed. Crystals of $Cu_2(NBA)_2$ [37] and $Cu_2(NBA-CN)_2$ were grown by layering a $CHCl_3$ solution of the complexes with CH_3CN. X-ray quality crystals of the $Cu_2(NBA)_2(\mu\text{-piperazine})$ complex have been grown by the same layering procedure by placing piperazine in the CH_3CN layer. The $Cu_2(NBA-Br)_2(\mu\text{-piperazine})$ complex could be crystallized using the same method. After 24-48 h, turquoise parallelepipeds had formed. These crystals become opaque immediately upon exposure to the air suggesting that they contained solvent.

4.2.3. Adducts of $Cu_2(NBA-X)_2$ with Lewis Bases. $CHCl_3$ solutions of $Cu_2(NBA-X)_2$ turned various shades of blue-green upon addition of the nitrogenous bases (Dabco, piperazine, pyrazine, or aminopyrazine). Higher binding constants were measured for the more blue solutions, suggesting that the better the binding, the bluer the solution. While most of the complexes eventually reached a turquoise shade of blue at the highest guest concentrations, the $CHCl_3$ solution of $Cu_2(NBA-Br)_2(\mu\text{-NH}_2\text{pyz})$ was predominantly green. The $Cu_2(NBA-CN)_2(\mu\text{-piperazine})$ complex readily precipitated, even in dilute solutions, limiting the range of usable concentrations for binding constant measurements. The crystal structure of $Cu_2(NBA)_2(\mu\text{-piperazine})$ provides information on how piperazine binds to these host complexes.

4.2.4. X-ray Methods. Diffraction data were collected on an Enraf-Nonius CAD4 diffractometer fitted with Cu $K\alpha$ source and graphite monochromator, using the θ-2θ scan method. Final unit cell constants were determined from the orientations of 25 centered high-angle reflections. The intensities were corrected for absorption using ψ-

scan data for five reflections (transmission coefficient of 65.26 %). Details of data

collection and structure refinement are given in **Table 4.1**. The ORTEP drawing can be

seen in **Figure 4.2**.

Table 4.1.   Crystal data for Cu₂(NBA)₂(μ-piperazine)·4CHCl₃·2CH₃CN.ª

chemical formula	$Cu_2C_{56}H_{44}N_4O_8Cl_{12}$	space group	P $\overline{1}$
fw	1473.7	λ/Å	1.5418(CuKα)
a/Å	10.5929(6)	temp/°C	24
b/Å	11.4581(8)	D_c/g cm⁻³	1.474
c/Å	14.1552(10)	μ(Cu Kα)/cm⁻¹	57.7
α/deg	90.256(6)	$R(F_o)$	0.067
β/deg	104.321(5)	$R_w(F_o)$	0.061
γ/deg	94.249(5)	Z	1
V/Å³	1659.7(4)		

ªValues in parentheses in **Tables 4.1-4.4** are estimated standard deviations of the last
digit.
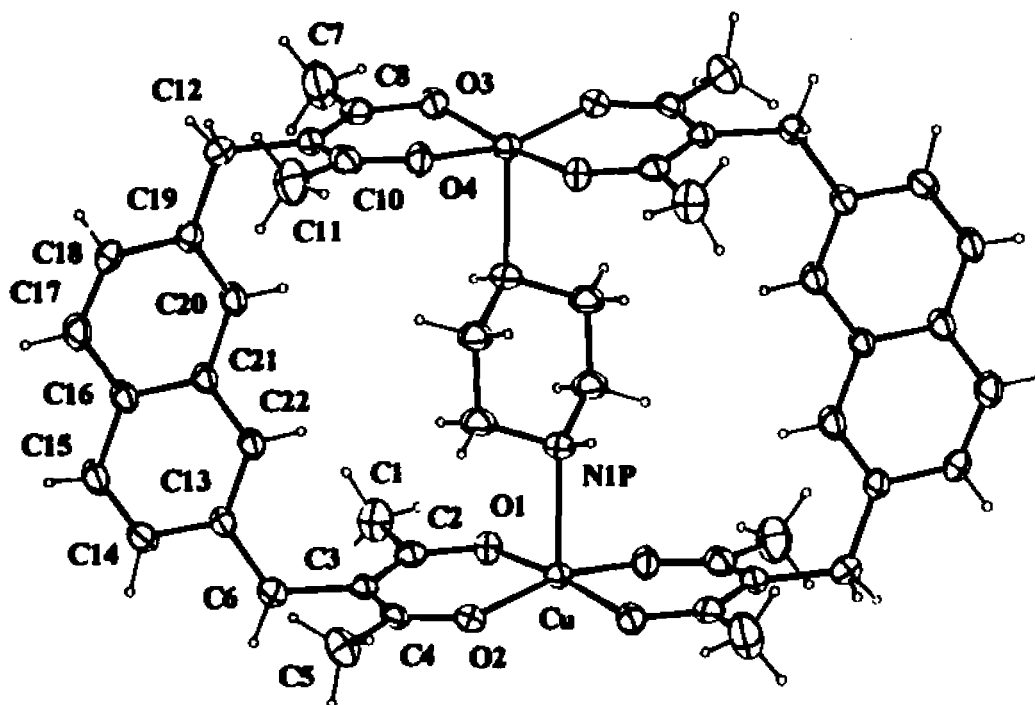
Figure 4.2. ORTEP drawing of Cu₂(NBA)₂(μ-piperazine)·4CHCl₃·2CH₃CN. P used to
denote atom belonging to piperazine.

4.2.5. Molecular Modeling. The molecular modeling was done using the SYBYL (version 6.01) molecular modeling program. Since SYBYL has little or no metal modeling capabilities, we made use of the default average force field parameters present in the Tripos Force Field to do our modeling. A new metal atom type modeled after the existing Cl atom type was created using the Parameter Add Atom_Def command. The name M1 was used for a generic first-row transition metal for this new atom type. The crystal structure for the existing $Cu_2(NBA)_2$(m-piperazine) complex was loaded into SYBYL and used as a starting point for the modeling. The copper atoms (read in as dummy atoms) were changed to the M1 first-row transition metal atom type. To do this several of the metal-ligand bonds had to be deleted since the program will not allow atom type changes when there are more than the expected number of bonds present. Once the atom type is changed, however, the program allows one to add as many bonds to M1 as you like, so the deleted bonds were re-added.

The ligand was then modified to produce the syn- & anti-Br and CN ligand substitutions. The structure was then minimized. SYBYL, not recognizing the M1-ligand bonds, used internal default force field parameters that use the existing metal-ligand bond lengths and angles as the equilibrium values. The bond stretching parameter is a rather strong, 600 $kcal/Å^2$, while the bond angle and torsional parameters are relatively weak (0.02 $kcal/deg^2$ and 0.2 kcal/cos(3*theta)). This locks in the crystallographic metal-ligand bond distances, but allows steric factors to distort the metal ligand angles and torsions. Dr. George Stanley has used this technique to model a variety of transition metal mono-

and bimetallic complexes with good results (coordination geometry bond angles

typically within 3° of the experimental values, except when electronic factors are present;

torsional values involving M typically within 10° of the experimental value).[69]

Once the minimization procedure was finished, we did conformational searching

and relaxing of the structure to find the global (or good local) minimum conformation.

This was accomplished by simulated annealing molecular dynamics runs. A typical

dynamics run started at 1000-1200 K for a run length of several thousand femtoseconds.

The temperature was then dropped by 200-300 K increments to a final temperature of 0

K. A dynamics run at 0 K is very similar to a straight minimization run. Since these

annealing dynamics runs are not guaranteed to find the global minimum, one typically

should run 4 to 8 dynamics runs with different temperatures and run times, to allow more

extensive searching of conformational space. For these rather constrained bimetallic host-

guest complexes, however, only one dynamics run was needed to illustrate an appropriate

low energy model structure. The energies (without electrostatic contributions) of the

various structures from the dynamics runs are: anti-$Cu_2(NBA-Br)_2(\mu$-piperazine) 15.2

kcal/mol; syn-$Cu_2(NBA-Br)_2(\mu$-piperazine) 16.1 kcal/mol; anti-$Cu_2(NBA-CN)_2(\mu$-

piperazine) 21.9 kcal/mol; syn-$Cu_2(NBA-CN)_2(\mu$-piperazine) 22.8 kcal/mol.

4.2.6. Instruments and Procedures. Electronic absorption spectra were

recorded on an Aviv 14DS absorption spectrophotometer. Binding constants were

determined by using ca. 2.5 x 10^{-3} M $Cu_2(NBA)_2$, $Cu_2(NBA-Br)_2$, and $Cu_2(NBA-CN)_2$

$CHCl_3$ solutions, with maximum concentrations of added guest (G) chosen so as to cause

90% conversion to $Cu_2(NBA)_2 \cdot L$ where solubility permitted. Equilibrium constants

were calculated by applying the method of Rose and Drago[70] to the electronic spectra

recorded using solutions in which the concentration of G was varied.

4.3 Results and Discussion

4.3.1. X-ray Analysis of $Cu_2(NBA)_2(\mu\text{-piperazine}) \cdot 4CHCl_3 \cdot 2CH_3CN$. The

$Cu_2(NBA)_2(\mu\text{-piperazine})$ complex was crystallized from $CHCl_3$ by layering with a

solution of piperazine in CH_3CN. Because the crystals contained solvent, they could not

be removed from the mother liquor for more than 30 sec without becoming opaque. A

turquoise plate of dimensions 0.28 x 0.18 x 0.05 mm was transferred to a glass capillary

along with the mother liquor, and the capillary was then flame sealed. The atomic

coordinates for $Cu_2(NBA)_2(\mu\text{-piperazine}) \cdot 4CHCl_3 \cdot 2CH_3CN$ can be seen in Table 4.2.

Table 4.2. Fractional atomic coordinates and equivalent isotropic temperature parameters for $Cu_2(NBA)_2(\mu\text{-piperazine}) \cdot 4CHCl_3 \cdot 2CH_3CN$.

atom	x	y	z	$B_{eq}/\text{Å}^2$
Cu	0.22376(7)	0.60820(7)	0.32181(6)	3.03(2)
O1	0.1651(3)	0.4452(3)	0.3030(3)	3.35(9)
O2	0.2999(3)	0.6038(3)	0.2111(3)	3.30(9)
O3	0.7410(4)	0.2239(3)	0.6712(3)	3.61(9)
O4	0.8947(3)	0.3814(3)	0.5952(3)	3.46(9)
C1	0.1323(6)	0.2500(6)	0.2516(5)	5.0(2)
C2	0.1867(5)	0.3735(5)	0.2399(4)	3.1(1)
C3	0.2539(5)	0.4011(5)	0.1690(4)	3.0(1)
C4	0.3086(5)	0.5142(5)	0.1586(4)	3.3(1)
C5	0.3860(6)	0.5404(6)	0.0854(4)	5.0(2)
C6	0.2694(5)	0.3057(5)	0.0978(4)	3.6(1)
C7	0.7011(8)	0.0334(6)	0.6092(5)	6.6(2)
C8	0.7627(5)	0.1530(5)	0.6064(4)	3.8(1)
C9	0.8352(5)	0.1837(5)	0.5389(4)	3.4(1)
C10	0.9023(5)	0.2953(5)	0.5409(4)	3.7(1)
C11	0.9935(6)	0.3187(6)	0.4750(5)	5.5(2)

(table con'd.)

C12	0.8498(5)	0.0927(5)	0.4635(4)	4.0(1)
C13	0.3955(5)	0.2443(5)	0.1246(4)	3.0(1)
C14	0.4427(6)	0.1969(5)	0.0490(4)	3.8(1)
C15	0.5538(5)	0.1403(5)	0.0684(4)	4.0(1)
C16	0.6259(5)	0.1257(5)	0.1644(4)	3.4(1)
C17	0.7433(5)	0.0680(6)	0.1885(4)	4.1(1)
C18	0.8110(5)	0.0593(5)	0.2824(4)	3.9(1)
C19	0.7688(5)	0.1057(5)	0.3613(4)	3.4(1)
C20	0.6539(5)	0.1582(5)	0.3385(4)	3.7(1)
C21	0.5800(5)	0.1710(5)	0.2421(4)	3.0(1)
C22	0.4643(5)	0.2303(5)	0.2189(4)	3.2(1)
N1P	0.4093(4)	0.5769(4)	0.4397(3)	3.6(1)
C1P	0.4980(5)	0.5071(6)	0.4000(4)	4.1(2)
C2P	0.3802(5)	0.5200(6)	0.5242(4)	4.1(2)
Cl1S[b]	0.2462(2)	0.9715(2)	0.1060(1)	6.47(5)
Cl2S	0.1113(2)	0.7636(2)	0.0042(1)	6.88(6)
Cl3S	−0.0048(2)	0.8893(2)	0.1315(2)	9.72(7)
Cl4S	0.9324(2)	0.5511(2)	0.1276(2)	9.15(7)
Cl5S	0.7699(3)	0.3986(2)	0.2099(2)	12.14(9)
Cl6S	0.7880(3)	0.6413(3)	0.2500(3)	15.9(1)
C1S	0.1399(6)	0.8488(6)	0.1106(4)	4.5(2)
C2S	0.8690(6)	0.5260(6)	0.2284(5)	5.4(2)
N1S	0.3572(8)	0.1982(6)	0.5596(6)	10.6(3)
C3S	0.4004(8)	0.1853(6)	0.6382(6)	7.2(2)
C4S	0.4616(7)	0.1658(7)	0.7395(7)	7.6(3)

[a] The equivalent isotropic thermal parameter B_{eq} is defined as $(8\pi^2/3)\Sigma_i\Sigma_j U_{ij}a_i^*a_j^*a_i\cdot a_j$.
[b] S used to denote an atom belonging to a solvent molecule.

Table 4.3. Coordinates and isotropic thermal parameters for hydrogen atoms for Cu$_2$(NBA)$_2$(μ-piperazine)·4CHCl$_3$·2CH$_3$CN.

atom	x	y	z	$B_{iso}/Å^2$[a]
H1NP	0.455(5)	0.644(4)	0.463(4)	5(1)
H1aP	0.536(4)	0.551(4)	0.354(3)	3(1)
H1bP	0.445(5)	0.425(4)	0.377(4)	6(1)
H2aP	0.328(5)	0.447(4)	0.502(4)	5(1)
H2bP	0.318(5)	0.566(5)	0.551(4)	8(2)
H6a	0.267(4)	0.343(4)	0.034(3)	5(1)
H6b	0.199(4)	0.243(4)	0.093(3)	3(1)
H12a	0.819(4)	0.025(4)	0.484(3)	4(1)
H12b	0.946(4)	0.085(4)	0.465(3)	5(1)
H14	0.403(4)	0.220(4)	−0.012(3)	4(1)

(table con'd.)

H15	0.583(5)	0.110(4)	0.027(4)	6(1)
H17	0.767(4)	0.037(4)	0.136(3)	3(1)
H18	0.881(4)	0.020(4)	0.298(3)	4(1)
H20	0.629(4)	0.189(4)	0.386(3)	3(1)
H22	0.430(4)	0.253(4)	0.268(3)	4(1)
H1a	0.0806	0.2504	0.2977	6
H1b	0.2022	0.2016	0.2738	6
H1c	0.0797	0.2204	0.1905	6
H5a	0.3287	0.5581	0.0249	6
H5b	0.4311	0.4740	0.0766	6
H5c	0.4472	0.6054	0.1077	6
H7a	0.7669	−0.0204	0.6235	8
H7b	0.6431	0.0133	0.5476	8
H7c	0.6538	0.0304	0.6581	8
H11a	0.9463	0.3049	0.4090	7
H11b	1.0623	0.2680	0.4908	7
H11c	1.0289	0.3977	0.4837	7
H1S	0.1803	0.8028	0.1636	5
H2S	0.9383	0.5178	0.2845	7
H4aS	0.3971	0.1624	0.7758	9
H4bS	0.5256	0.2281	0.7642	9
H4cS	0.5019	0.0939	0.7448	9

Table 4.4. Bond distances (Å) and bond angles (°) for Cu₂(NBA)₂(μ-piperazine)·4CHCl₃·2CH₃CN.

Atoms		Distance	Angle	Atoms		Distance	Angle
Cu	Cu'ᵃ	7.315(1)		C13	C14	1.410(8)	
Cu	O1	1.920(4)		C13	C22	1.370(7)	
Cu	O2	1.934(4)		C14	C15	1.355(8)	
Cu	O3'	1.930(4)		C15	C16	1.401(7)	
Cu	O4'	1.929(4)		C16	C17	1.420(8)	
Cu	N1P	2.294(4)		C16	C21	1.418(8)	
O1	C2	1.284(7)		C17	C18	1.353(7)	
O2	C4	1.285(7)		C18	C19	1.416(9)	
O3	C4	1.296(7)		C19	C20	1.365(8)	
O4	C10	1.267(7)		C20	C21	1.409(7)	
C1	C2	1.514(9)		C21	C22	1.413(8)	
C2	C3	1.392(8)		N1P	C1P	1.485(8)	
C3	C4	1.404(8)		N1P	C2P	1.452(8)	
C3	C6	1.529(8)		C1P	C2P'	1.514(7)	
C4	C5	1.492(9)		C11S	C1S	1.747(7)	

(table con'd.)

C6	C13	1.521(8)		C12S	C1S	1.741(6)	
C7	C8	1.479(9)		C13S	C1S	1.727(7)	
C8	C9	1.398(9)		C14S	C2S	1.737(8)	
C9	C10	1.412(8)		C15S	C2S	1.713(7)	
C9	C12	1.531(8)		C16S	C2S	1.694(8)	
C10	C11	1.512(9)		N1S	C3S	1.11(1)	
C12	C19	1.503(7)		C3S	C4S	1.45(1)	
O1	Cu	O2	91.2(2)	C3	C4	C5	121.9(5)
O1	Cu	O3'	171.9(1)	C3	C6	C13	116.5(4)
O1	Cu	O4'	87.2(2)	O3	C8	C7	113.2(6)
O1	Cu	N1P	94.4(2)	O3	C8	C9	124.9(5)
O2	Cu	O3'	88.9(2)	C7	C8	C9	121.9(6)
O2	Cu	O4'	164.3(1)	C8	C9	C10	121.9(5)
O2	Cu	N1P	97.2(2)	C8	C9	C12	119.8(5)
O3'	Cu	O4'	90.6(2)	C10	C9	C12	118.2(5)
O3'	Cu	N1P	93.6(2)	O4	C10	C9	125.7(6)
O4'	Cu	N1P	98.5(2)	O4	C10	C11	114.6(5)
Cu	O1	C2	127.3(4)	C9	C10	C11	119.7(6)
Cu	O2	C4	127.9(4)	C9	C12	C19	116.0(5)
Cu	O3'	C8'	126.6(4)	C6	C13	C14	118.6(4)
Cu	O4'	C10'	126.9(4)	C6	C13	C22	123.3(5)
O1	C2	C1	112.1(5)	C14	C13	C22	118.1(5)
O1	C2	C3	126.0(5)	C13	C14	C15	121.3(5)
C1	C2	C3	121.9(5)	C14	C15	C16	121.3(6)
C2	C3	C4	122.9(5	C15	C16	C17	123.5(5)
C2	C3	C6	119.6(5)	C15	C16	C21	118.7(5)
C4	C3	C6	117.4(5)	C17	C16	C21	117.8(5)
O2	C4	C3	124.4(5)	C16	C17	C18	121.0(6)
O2	C4	C5	113.6(5)	C17	C18	C19	122.4(5)

* Prime denotes an atom related by the inversion center.

4.3.2. Structure of Cu₂(NBA)₂(μ-piperazine)·4CHCl₃·2CH₃CN. X-ray analysis

of this compound demonstrates that piperazine coordinates intramolecularly to

Cu₂(NBA)₂. The Cu atoms, O1, O1', O3, O3', and the piperazine N atoms all lie

approximately on a plane containing the inversion center.

The top view of the complex in **Figure 4.3** illustrates the chair conformation of the

piperazine, whose N atoms are almost eclipsed by the Cu atoms to which they are

attached. The Cu atoms are themselves

offset 0.685 Å (d) from the vector, parallel to

the Cu-N1P bonds (see right), that contains

the inversion center. The torsion angle
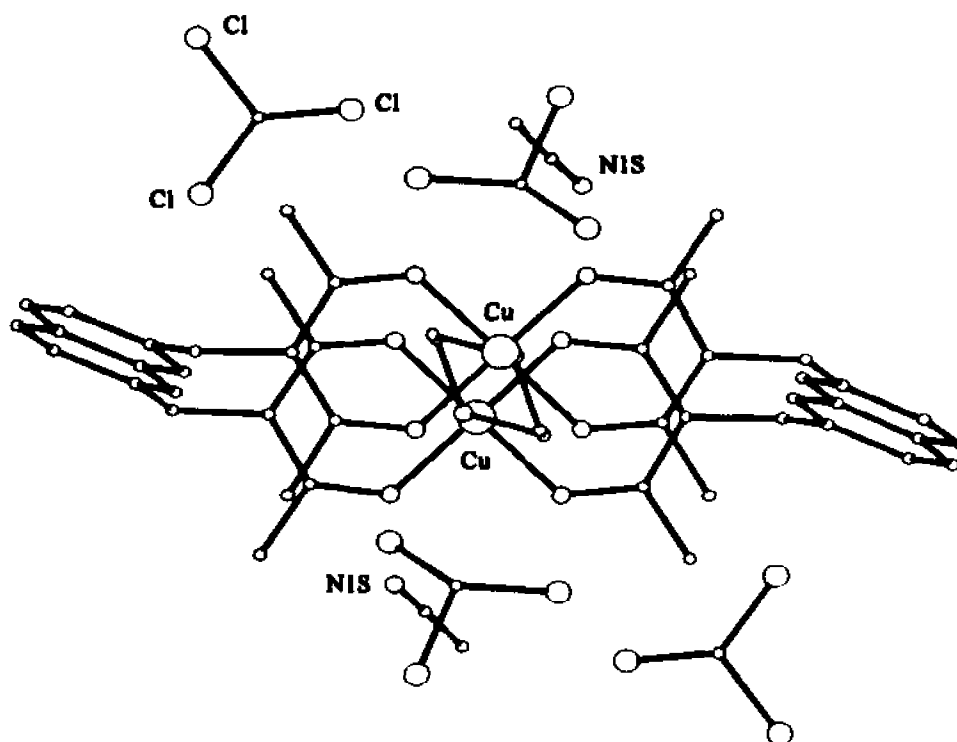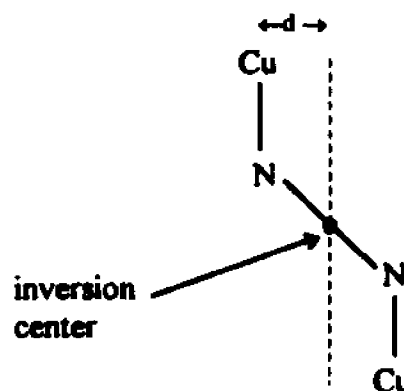
O1-Cu-N1P-N1P' is 4.0(4)°.

Figure 4.3. PLUTO drawing of a top view of Cu₂(NBA)₂(μ-
piperazine)·4CHCl₃·2CH₃CN showing chair conformation of the piperazine
guest and the shifting of the Cu atoms away from each other to accommodate
piperazine.

The contacts between piperazine and the CH_3CN molecule suggest a close approach, which is strengthened by the enhanced acidity of NH and the polarity of CH_3CN. The N1P---N1S distance is 3.435(9) Å and the H1N1P---N1S distance is 2.67(5) Å. The N1P-H1N1P---N1S angle is 145(5)°. The acac O atoms do not appear to H-bond with piperazine as seen by the O3-H1N1P-N1P angle (90(3)°), although the O3---N1P distance of 3.089(6) Å suggests it is possible. The proposed O3---H1N1P bond distance of 2.96(5) Å is still longer than that of H1N1P---N1S.

4.3.3. Comparison of $Cu_2(NBA)_2(\mu$-piperazine) with Other Structures. Upon complexation of the host complex to the guest molecule, it is anticipated that the host complex will undergo minor structural changes in order to accommodate the guest molecule. There are certain structural changes to $Cu_2(NBA)_2$ when piperazine binds that we did not expect. The Cu---Cu distance in the present structure (7.315(1) Å) is shorter than those in $Cu_2(NBA)_2$ (7.349(1) Å), $Cu_2(NBA)_2(\mu$-Dabco) (7.401(4) Å),[38] and $Cu_2(NBA)_2$-(μ-2,5-Me$_2$pyrazine) (7.559(2) and 7.596(2) Å).[38] The N---N distance in piperazine is 2.9 Å, in Dabco it is 2.6 Å, and in pyrazine it is 2.8 Å. Thus, we were surprised to find that the Cu---Cu distance in $Cu_2(NBA)_2(\mu$-piperazine) is the shortest of the four. The distance from one N1P containing plane to the other is only 2.7 Å. The piperazine is bound in the chair conformation which allows for the shorter N---N distance, but also does not allow for the N1P atoms to be situated one on top of the other, or eclipsed, which is possible in the other two complexes. Therefore, the Cu atoms in $Cu_2(NBA)_2(\mu$-piperazine) are not eclipsing each other and are displaced from the planes formed by the O atoms (deviation from the best plane is 0.064 A).

The environment about the Cu atoms in $Cu_2(NBA)_2(\mu$-piperazine) is square

pyramidal, with the Cu atoms displaced 0.199 Å out of the acac planes toward the axial

NIP atoms. This displacement is larger than observed in other Cu complexes formed

using NBA: $Cu_2(NBA)_2(\mu$-2,5-Me$_2$pyrazine) (0.141(2) and 0.155(2) Å)[35] and

$Cu_2(NBA)_2(\mu$-Dabco) (0.175(2) Å),[37] and comparable to those in other five-coordinate

adducts of bis(β-diketonato) Cu complexes: $[Cu(hfac)_2]_2(\mu$-pyrazine) (0.24(1) Å) and

$[Cu(hfac)_2]_2(\mu$-Dabco) (0.251(4), 0.271(4), and 0.240(4) Å).[38]

When binding piperazine, the Cu atoms appear to be shifted more than would be

expected on the basis of the naphthalene-CH_2-acac bond angles (116.0(5) and 116.5(4)°),

which are very similar to those of $Cu_2(NBA)_2$ (116.0(3) and 116.3(3)°)[36], $Cu_2(NBA)_2(\mu$-

Dabco) (117(2) and 118(1)°), and only marginally smaller than those of $Cu_2(NBA)_2(\mu$-

2,5-Me$_2$pyrazine) (117.8(5) and 118.4(4)°).[38]

4.3.4. Binding of Lewis Bases. The electronic absorption spectra of $Cu_2(NBA)_2$,

$Cu_2(NBA$-Br$)_2$, and $Cu_2(NBA$-CN$)_2$ (see **Figure 4.4**) are very similar with each having

two recognizable bands in the 450-800 nm region due to d-d transitions. Each Cu^{2+}

contains 9 electrons in its five d orbitals (d_{z^2}, $d_{x^2-y^2}$, d_{xz}, d_{yz}, and d_{xy}). The orbital energy

levels are split or made nondegenerate by the presence of a ligand field around the metal.

When the d-orbitals are equally occupied and ligands are not present, the d orbitals

are degenerate. In an octahedral complex, the d_{z^2} and $d_{x^2-y^2}$ orbitals ("e_g*") are directed

toward the ligands. The repulsion of the ligands raises the energy of these orbitals relative

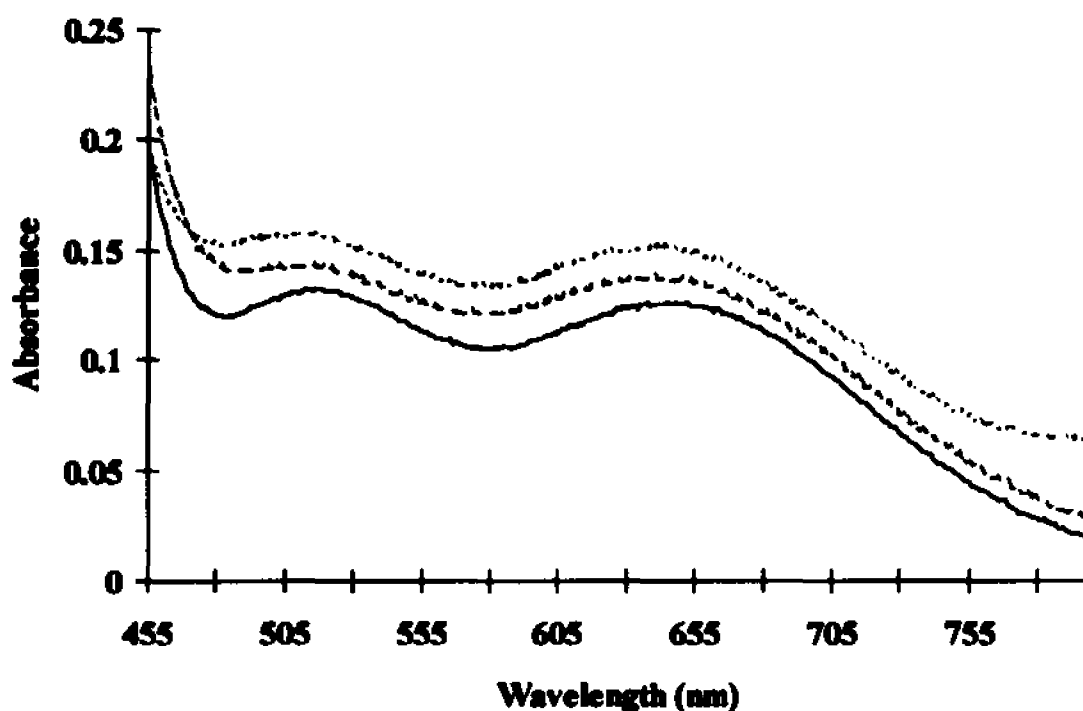to the d_{xz}, d_{yz}, and d_{xy} orbitals ("t_{2g}") (see **Figure 4.5**).

Cu₂(NBA-X)₂ (X = H, CN, Br)

Figure 4.4. Electronic absorption spectra of Cu₂(NBA-X)₂ (X = H, CN, Br)
(2.5 x 10⁻³ M) in CHCl₃ at room temperature: ——X = H; − − −X =
CN; · · · · ·X = Br.

Depending on the ligand field, the metal d-orbitals can be further distorted in order to gain

additional stabilization (see **Figure 4.5**). Our NBA²⁻ ligands provide a square planar

environment around the metal center. The singly occupied $d_{x^2-y^2}$ orbital is highest in

energy. From the orbital energy level scheme for a square planar complex in **Figure 4.5**, it

can be seen that three transitions are possible (from d_{xz} or d_{yz}, d_{z^2}, and d_{xy} to $d_{x^2-y^2}$).

When another ligand, the guest molecule (G), is added to our host complex; it

binds directing lone pair electron density toward the metal d_{z^2} orbital. This results in

destabilization of the metal d_{z^2} orbital. This interaction can be detected by the color

No ligands   Octahedral complex   Planar complex

e_g^* $d_{x^2-y^2}$

d_{xy}

t_{2g} d_{z^2}

d_{xz}, d_{yz}
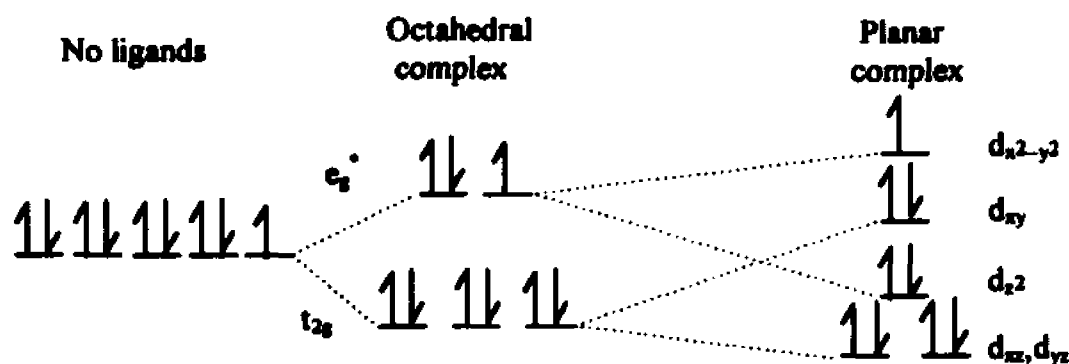
Figure 4.5. Splitting of orbital energy levels for a Cu^{2+} square planar complex.

change seen upon addition of the guest. The olive green $CHCl_3$ solutions of $Cu_2(NBA)_2$, $Cu_2(NBA-Br)_2$, and $Cu_2(NBA-CN)_2$ turn turquoise on addition of $CHCl_3$ solutions of the nitrogenous bases (Dabco, pyrazine, aminopyrazine, and piperazine). Spectra measured in a typical experiment, involving $Cu_2(NBA-Br)_2$ and increasing amounts of Dabco, are illustrated in **Figure 4.6.** We used these electronic spectral changes to calculate the binding constants listed in **Tables 4.5-4.8.** The wavelengths at which the largest changes occurred upon addition of the guest were used in the calculations. For the $Cu_2(NBA)_2$ complex, 500 and 620 nm were used; 500 and 635 nm were used for the $Cu_2(NBA-Br)_2$ complex; and 510 and 645 nm, for the $Cu_2(NBA-CN)_2$ complex.

The Lewis bases chosen for these experiments (Dabco, pyrazine, aminopyrazine, and piperazine) are the appropriate size to fit into the cavity made by the host molecule. Each base also contains two nitrogen heteroatoms whose lone pairs are capable of bonding in an endo (intramolecular) manner.
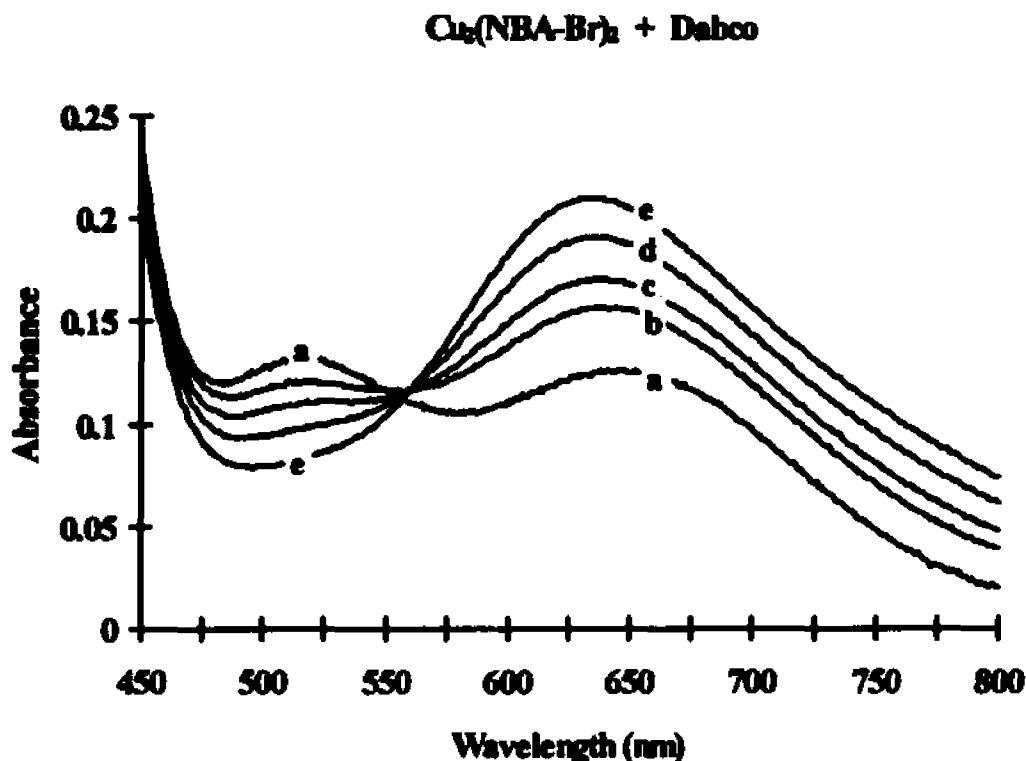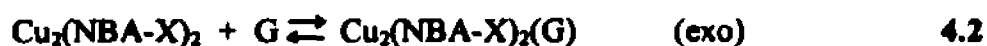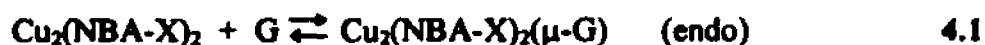
Cu₂(NBA-Br)₂ + Dabco

Figure 4.6. Electronic absorption spectra of Cu₂(NBA-Br)₂ (2.5 x 10⁻³
M) in CHCl₃ at room temperature, with the following
concentrations of added Dabco: trace a, 0 M; trace b, 2.3 x 10⁻²
M; trace c, 4.6 x 10⁻² M; trace d, 9.3 x 10⁻² M; trace e, 0.186
M.

If the guest does not cause strain in the Cu₂(NBA-X)₂ (X-H, Br, or CN) complexes, ΔH

for endo coordination of G (Equation 4.1) should be approximately twice as great as that

for the exo coordination (Equation 4.2).

$$Cu_2(NBA-X)_2 + G \rightleftharpoons Cu_2(NBA-X)_2(\mu\text{-}G) \qquad (endo) \qquad 4.1$$

$$Cu_2(NBA-X)_2 + G \rightleftharpoons Cu_2(NBA-X)_2(G) \qquad (exo) \qquad 4.2$$

In both the endo and exo binding situations we have two molecules coming together to form one complex, so ΔS for Equations 4.1 and 4.2 should be similar. Therefore, ΔG_1, and the corresponding binding constant K_1, can be substantially more favorable.

4.3.5. Calculation of Equilibrium Constants (K). The equilibrium constants were obtained by a graphical method outlined by Rose and Drago[70] in which Equation 4.3 was solved simultaneously for varying concentrations of guest molecule.

$$K^{-1} = [M_o][G_o]\Delta\epsilon/\Delta A - ([M_o] + [G_o]) + \Delta A/\Delta\epsilon \qquad 4.3$$

M_o and G_o are the total concentrations of the host metal complex and the guest molecule, respectively. The changes in molar extinction coefficient and absorbance between M and M·G (with G assumed to be colorless) are represented, respectively, by $\Delta\epsilon$ and ΔA. M_o was kept constant and a plot of K^{-1} vs. $\Delta\epsilon$ was obtained for each concentration of G_o over a range of $\Delta\epsilon$ values. The resulting curves should all intersect at one point indicating one value for $\Delta\epsilon$ and one value for K^{-1}. In practice, if the data are good, deviations from intersection in a single point will be small.

The K values describing the interactions between four guest molecules (Dabco, pyrazine, aminopyrazine, and piperazine) and the $Cu_2(NBA-X)_2$ (X=H, Br, or CN) complexes over a range of temperatures are presented in Tables 4.5-4.7.

4.3.6. Calculation of Enthalpy (ΔH) and Entropy (ΔS) for Host-Guest Complexes. The free energy change (ΔG) between the product ($Cu_2(NBA-X)_2(\mu-G)$) and the reactants ($Cu_2(NBA-X)_2$ and G) was calculated from the equilibrium constant (K) using Equation 4.3.

Table 4.5. Binding constants (K) for Cu₂(NBA)₂(μ-piperazine) measured in CHCl₃.

Temp. °C	μ-piperazine, K M^{-1}
0	65.2 ± 0.4
5	56.3 ± 0.4
10	48.8 ± 0.3
15	42.2 ± 0.3
20	36.8 ± 0.2
25	32.3 ± 0.3
30	28.4 ± 0.1

Table 4.6. Binding constants (K) for Cu₂(NBA-Br)₂(μ-G) measured in CHCl₃.

Temp. °C	μ-Dabco, K M^{-1}	μ-pyrazine, K M^{-1}	μ-aminopyrazine, K M^{-1}	μ-piperazine, K M^{-1}
0	24 ± 35	1.1 ± 0.8	10 ± 3	10.4 ± 0.5
5	21 ± 11	0.9 ± 0.8	12 ± 6	8 ± 2
10	21 ± 11	0.8 ± 0.6	10 ± 5	7 ± 2
15	19 ± 5	0.7 ± 0.6	7 ± 3	6 ± 2
20	13 ± 3	0.5 ± 0.4	5 ± 4	5 ± 2
25	12 ± 4	0.6 ± 0.3	0.7 ± 0.2	5 ± 2
30	11 ± 3	0.5 ± 0.2	*	4 ± 2

*Binding not great enough to calculate K.

Table 4.7. Binding constants (K) for Cu₂(NBA-CN)₂(μ-G) measured in CHCl₃.

Temp.	μ-Dabco, K	μ-pyrazine, K	μ-aminopyrazine, K	μ-piperazine, K
°C	M⁻¹	M⁻¹	M⁻¹	M⁻¹
0	12 ± 1	1.92 ± 0.04	9	290 ± 100*
5	10 ± 6	1.64 ± 0.07	8	1170 ± 100*
10	9 ± 1	1.48 ± 0.02	8	850 ± 100*
15	8 ± 1	1.35 ± 0.01	8	700 ± 100*
20	7 ± 1	1.2 ± 0.1	9	480 ± 100*
25	6 ± 1	1.0 ± 0.1	9	250 ± 100*
30	4 ± 1	1.0 ± 0.2	11	150 ± 100*

*Approximately 100.

$$\Delta G = -RT \ln K \qquad 4.3$$

R is the gas constant (8.314510 J/mol·K) and T is the temperature in Kelvin. The values obtained for ΔG were fit to Equation 4.4 to estimate ΔH and ΔS.

$$\Delta G = \Delta H - T\Delta S \qquad 4.4$$

The ΔH and ΔS values calculated for the three host complexes with four different guests can be viewed in Table 4.9.

4.3.7. Binding of Dabco. Dabco is one of the best binders to our host complexes (see Table 4.8). Dabco, which is shaped like a football, fits well into the Cu₂(NBA)₂ complex (K= 220 M⁻¹). The binding constants were lower for the internally substituted complexes. The Br and CN substituents protrude into the cavity. The CN (4.25 Å into

Table 4.8. Binding constants for $Cu_2(NBA-X)_2$ (X= H, Br, or CN) host complexes and nitrogenous base guests measured in $CHCl_3$ at 25 °C.
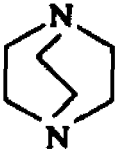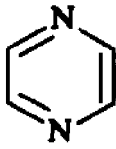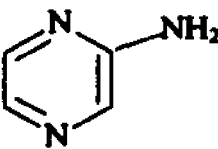
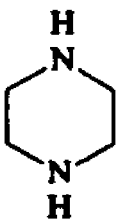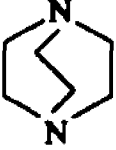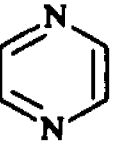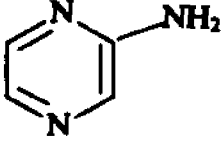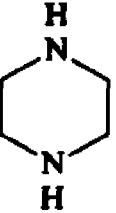|	$Cu_2(NBA)_2$	$Cu_2(NBA-Br)_2$	$Cu_2(NBA-CN)_2$
	K/M^{-1}	K/M^{-1}	K/M^{-1}
Dabco pK_b 5.3[71a]	220 ± 20 [3]	12 ± 4.0	6 ± 1
pyrazine pK_b 13.35[71b]	5 ± 1 [3]	0.6 ± 0.3	1.0 ± 0.1
aminopyrazine pK_b 10.93[71c]	93 ± 9 [3]	0.7 ± 0.2	9
piperazine pK_b 4.17[71b]	32.3 ± 0.3	5 ± 2	250 ± 100

Table 4.9. ΔH and ΔS values for binding of Cu₂(NBA-X)₂ (X = H, Br, or CN) host complexes to guest molecules.

	Cu₂(NBA)₂		Cu₂(NBA-Br)₂		Cu₂(NBA-CN)₂	
	ΔH kJ/mol	ΔS J/mol·K	ΔH kJ/mol	ΔS J/mol·K	ΔH kJ/mol	ΔS J/mol·K
Dabco	-30 ± 5^3	-50 ± 10^3	-20 ± 10	-50 ± 40	-24 ± 1	-65 ± 3
pyrazine	-28 ± 5^3	-80 ± 10^3	-25 ± 20	-90 ± 70	-12 ± 6	-40 ± 20
aminopyrazine	-29 ± 5^3	-60 ± 10^3	-10 ± 50	-20 ± 100	-0 ± 30	-15 ± 100
piperazine	-19 ± 2	-33 ± 8	-15 ± 30	-26 ± 13	-52 ± 25	-189 ± 150

cavity) occupies more space than the Br (3.75 Å into cavity) also seen by the fact that the

binding constant for Cu₂(NBA-CN)₂(μ-Dabco) is approximately one-half the binding

constant observed for Cu₂(NBA-Br)₂(μ-Dabco).

Table 4.6 shows that the reproducibility of the binding constants for Cu₂(NBA-

Br)₂(μ-Dabco) is poorer than that for the Cu₂(NBA-CN)₂(μ-Dabco) complex, measured at

the same temperatures. The derived ΔH and ΔS values (see Table 4.9) for $Cu_2(NBA-Br)_2$ are, therefore, not as accurate. The ΔH values for $Cu_2(NBA-X)_2(\mu-Dabco)$ (X = H, CN) are similar, as expected for two similar hosts binding the same guest. The difference in binding constants must therefore be a result of ΔS. Because the rotation of bound Dabco is more restricted when X = CN, its ΔS is more negative than when X = H.

4.3.8. Binding of Pyrazines. Pyrazine is the least basic of the guests used (see pK_b in Table 4.8). It is also one of the poorest binders. Because it is aromatic, pyrazine is flat and should slide into the cavity more easily than the football shaped Dabco, but the binding constants are much less for the pyrazine systems than the Dabco (see Table 4.6). This suggests that the degree to which pyrazine binds to the host complexes is influenced by its lower basicity to a greater extent than its size. Pyrazine is only a slightly poorer binder to the substituted hosts $(Cu_2(NBA-X)_2$ (X = Br or CN)) than the unsubstituted (X=H). Therefore, the decrease in the size of the host cavity is not detrimental to the overall binding of pyrazine.

Table 4.6 shows that the binding constants calculated for $Cu_2(NBA-Br)_2(\mu-pyrazine)$ also had a larger range of error than those calculated for $Cu_2(NBA-CN)_2(\mu-pyrazine)$. This explains the large range of ΔH and ΔS values calculated for $Cu_2(NBA-Br)_2(\mu-pyrazine)$. We cannot explain the lower ΔH for the $Cu_2(NBA-CN)_2(\mu-pyrazine)$ complex. We expected it to be similar to ΔH for $Cu_2(NBA)_2(\mu-pyrazine)$. We also expected a more negative ΔS when X = CN, due to the more restricted environment found in the cavity of the X = CN host, than when X = H.

2-Aminopyrazine, which is bulkier than the parent pyrazine, is nevertheless a better binder to the $Cu_2(NBA-X)_2$ (X = Br or CN) hosts. With the electron donating NH_2 group donating electron density to the π-ring system, it is slightly more basic than pyrazine. This increase in basicity could be responsible for the increase in binding. We believe the increase in binding is also a result of hydrogen bonding between the NH_2 group and the bis(β-diketone) O atoms.[38] Figure 4.7 shows one possible geometry (suggested by SYBYL molecular modeling) of $Cu_2(NBA)_2(\mu$-aminopyrazine), in which the (N)H---O distance (2.08 Å) is appropriate for hydrogen bonding. Molecular modeling still needs to be done on the $Cu_2(NBA-X)_2(\mu$-aminopyrazine) (X = Br or CN) complexes to determine whether or not the increase in binding upon going from pyrazine to aminopyrazine is also a result of hydrogen bonding.

Binding constant data for the $Cu_2(NBA-Br)_2(\mu$-aminopyrazine) complex was difficult to obtain. When the aminopyrazine concentration was > 0.1 M, the complex decomposed after 30 minutes. When the concentration was < 0.03 M there was not a large enough difference in the absorption spectra of the bound and unbound complexes to calculate a binding constant. Because we were limited on the range of concentrations, due to decomposition at high concentrations and poor binding at low concentrations, only two data points were obtained at each temperature. The accuracy of this data is questionable. Because the change in binding of aminopyrazine to $Cu_2(NBA-CN)_2$ was minimal as the temperature changed, the values calculated for ΔH and ΔS are not accurate.

4.3.9. Binding of Piperazine. Piperazine is more basic than the other guests. It binds to the host complexes better than the pyrazines except in the case of
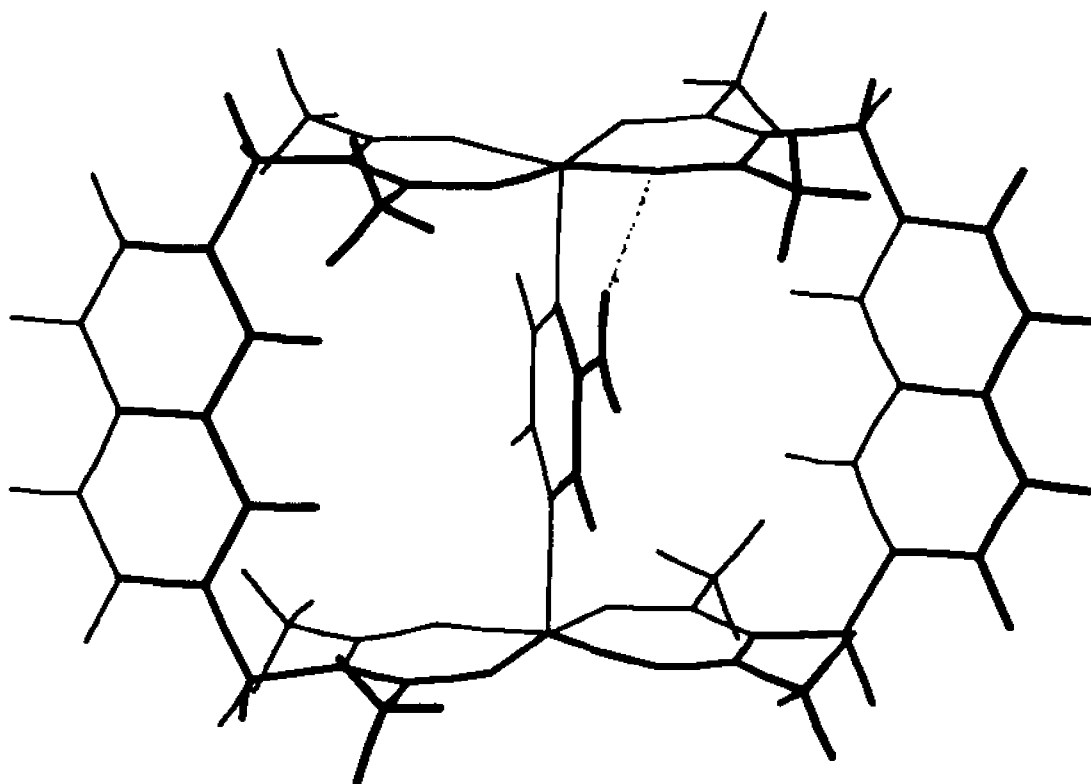
Figure 4.7. Proposed structure for Cu₂(NBA)₂(μ-aminopyrazine), with NH---O hydrogen bond indicated by thin dashed line.[72]

Cu₂(NBA)₂(aminopyrazine), where hydrogen bonding is suggested by the molecular models to be occurring between the NH₂ group and the bis(β-diketone) O atoms (see **Figure 4.7**). Dabco, which is slightly less basic, binds better than piperazine in all cases, except in the Cu₂(NBA-CN)₂ complex. Piperazine should be more flexible than the other guests and can achieve the low energy chair conformation when binding. This mode of binding, though, results in the Cu atoms being shifted so that they no longer lie one on top of the other (see **Figure 4.2**). This shift could be exerting strain on the host complex and reducing binding.

We performed molecular modeling experiments on the binding of piperazine to

the substituted hosts. The X-ray coordinates for the $Cu_2(NBA)_2(\mu$-piperazine) complex

were entered into the *SYBYL*[73] molecular modeling program and the substituents (Br or

CN) were used at the first position of the naphthalene in both the syn and anti isomers (see
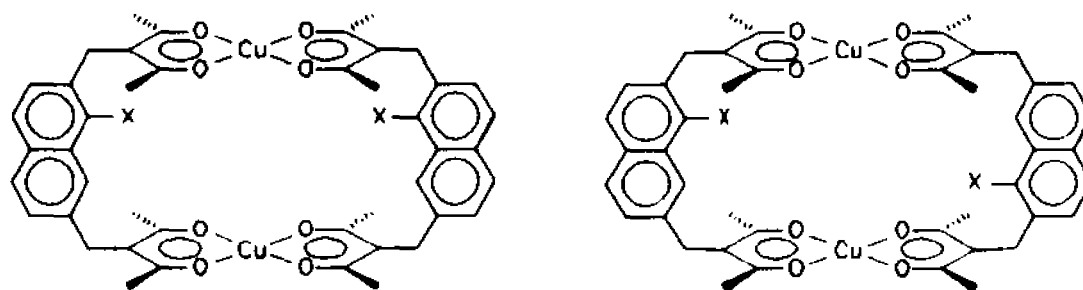
Figure 4.8).

Figure 4.8. Syn and anti isomers (X = Br, CN).

Minimization was then done in order to achieve the lowest energy structure. These

structures suggested that hydrogen bonding between the N of the CN group and the H of

the NH of piperazine was possible in both the syn and anti structures. We did not expect

the same of the $Cu_2(NBA$-$Br)_2(\mu$-piperazine) complex. The N1P---NC distances for the

syn complex were 2.491 and 2.549 Å; N1P-H1---NC bond angles were 133.4 and 138.6°.

The N1P---NC distances for the anti complex were even shorter at 2.460 and 2.472 Å;

N1P-H1---NC bond angles were 133.0 and 136.6°. The N1PH1---NC distances for the

syn complexes were 1.576 and 1.678 Å and 1.572 and 1.589 Å for the anti complex. As

Figure 4.10 indicates the naphthalene rings have even distorted themselves in order to

achieve the more stable hydrogen bonding conformation. Hydrogen bonds have been

known to stabilize host-guest complexes by 15-40 kJ mol^{-1} per hydrogen bond.[75]

Hydrogen bonding is also suggested by the ΔH and ΔS values calculated for the Cu$_2$(NBA-CN)$_2$(μ-piperazine) complex (see Table 4.10). The intramolecular contacts of the Cu$_2$(NBA-Br)$_2$(μ-piperazine) models do not suggest the possibility of hydrogen bonding (see Figure 4.9).

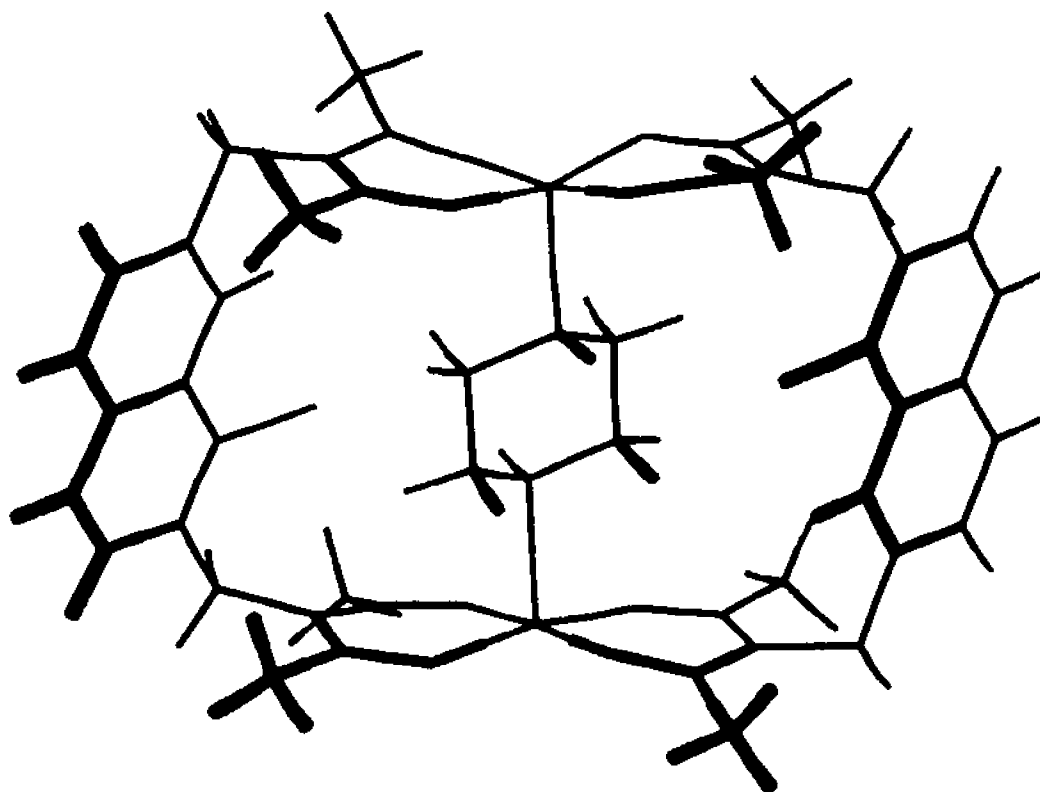**Figure 4.9.** Proposed anti conformer of Cu$_2$(NBA-Br)$_2$(μ-piperazine).[73]

4.4 Conclusions

As a first step towards new catalysts using cofacial binuclear transition metal complexes, we have synthesized functionalized bis(β-diketonate) copper(II) complexes which preferentially bind one guest over another due to intramolecular hydrogen bonding.
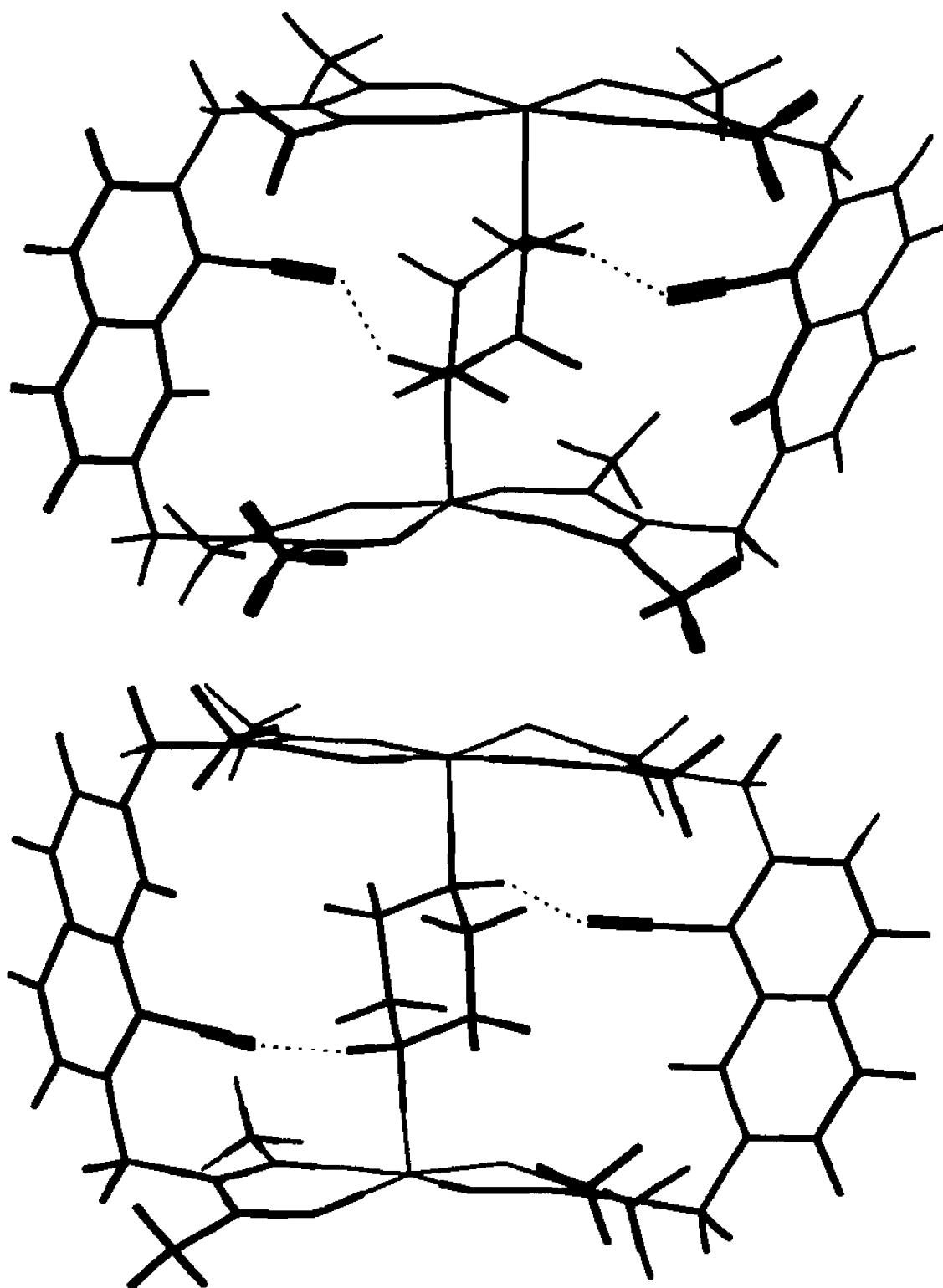
Figure 4.10. Proposed structures of syn and anti isomers of $Cu_2(NBA-CN)_2(\mu$-piperazine), with H1N1P---NC hydrogen bonds indicated by thin dashed line.[73]

In general, the binding constants decrease upon using bulkier substituents on the host complexes, larger guest molecules, or less basic guest molecules unless hydrogen bonding is possible as in the case of the following:

A. The O of $Cu_2(NBA)_2$ interacting with an NH_2 proton of aminopyrazine;

or

B. The N of $Cu_2(NBA-CN)_2$ interacting with the NH protons of piperazine.

Chapter 5. Cofacial Binuclear Zinc(II) Complexes of a Bis(β-diketone) Ligand

5.1 Introduction

The cofacial binuclear zinc(II) complex $Zn_2(NBA)_2$, capable of binding guest molecules (G = Dabco (1,4-diazabicyclo-[2.2.2]octane), piperazine, or pyrazine), was synthesized (Figure 5.1). This complex more closely resembles the enzyme alkaline phosphatase.[42,74]
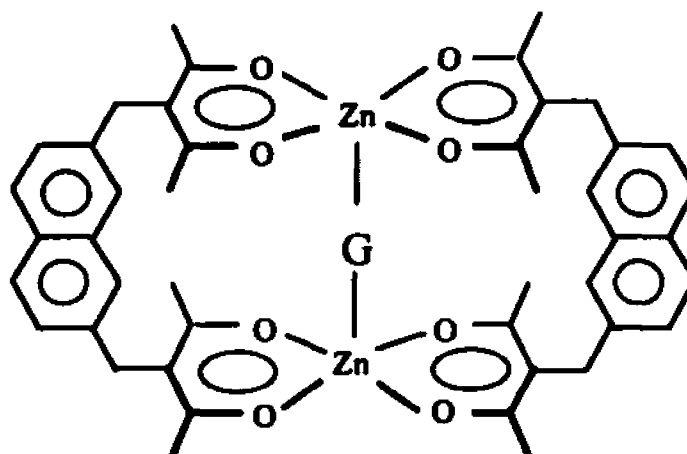

Figure 5.1. $Zn_2(NBA)_2(\mu\text{-}G)$ (G = Dabco, piperazine, or pyrazine.

As at the active site of alkaline phosphatase, there are two coordinated Zn^{2+} ions available for binding to the substrate or guest (G). The d^{10} Zn^{2+}, unlike d^9 Cu^{2+}, forms very few simple square-planar complexes;[75] instead, it is more stable in the five-coordinate geometry found in Figure 5.1. In fact, also unlike the copper(II) complexes, the zinc(II) complexes are synthesized in the presence of the guest. The binding constants for the $Zn_2(NBA)_2(\mu\text{-}G)$ complexes are greater than those measured for the analogous $Cu_2(NBA)_2(\mu\text{-}G)$ complexes.

The paramagnetism of the d^9 copper complexes makes them poor candidates for NMR spectroscopy studies. This is not the case for the $Zn_2(NBA)_2(\mu\text{-}G)$ complexes. ^1H NMR spectroscopy can be used to determine the binding constants of these molecules. The zinc complexes also differ from the copper in that they are colorless. While virtually no copper(II) complexes luminesce, our zinc(II) complexes do.

Within this chapter the synthesis of the $Zn_2(NBA)_2(\mu\text{-}G)$ complexes are described. Their ^1H NMR spectra and electronic absorption and emission data are discussed. The lifetime measurements of the complexes' excited states are presented.

5.2 Experimental Section

5.2.1. Materials. The $NBAH_2$ used in the synthesis of the zinc complexes was synthesized as outlined in reference 38. The $Zn(C_2H_3O_2)\cdot2H_2O$ was purchased from Mallinckrodt and the nitrogenous bases from Aldrich, except for Dabco which was obtained from Air Products and Chemicals.

5.2.2. Synthesis of $Zn_2(NBA)_2(\mu\text{-}Dabco)$. $NBAH_2$ (16.4 mg, 4.66 x 10^{-4} mol) was dissolved in 2 mL of DMF. $Zn(C_2H_3O_2)_2\cdot2H_2O$ (0.102 g, 4.66 x 10^{-4} mol) was dissolved in 1.5 mL of DMF and the solution was added to the $NBAH_2$ solution. Sublimed Dabco (0.209 g, 1.90 x 10^{-3} mol) was dissolved in 1.5 mL of DMF and added to the ligand-metal solution. The mixture was stirred at room temperature. A small amount of white precipitate had formed after 5 min. This precipitate was then removed by filtration and the filtrate was allowed to stir for 1hr. The filter cake was washed with 2 mL of methanol, to remove excess DMF, then 2 mL of hexane, to dry the while solid. ^1H NMR data from a $CDCl_3$ solution indicate that only 5 mg of the 80 mg collected were the

$Zn_2(NBA)_2(\mu\text{-Dabco})$ complex. After 1 hr of stirring, the filtrate contained a white

precipitate which was filtered and washed by the same procedure as the first filter cake.

^1H NMR data from $CDCl_3$ and CD_2Cl_2 solutions indicate that the majority of this filter

cake is the $Zn_2(NBA)_2(\mu\text{-Dabco})$ complex (80 mg). $Zn_2(NBA)_2(\mu\text{-Dabco})$ total yield 85

mg of white powder, 1.4×10^{-4} mol (39%). ^1H NMR ($CDCl_3$): δ 2.13 (s, CH_3, f), 3.90

(s, CH_2, d), 7.30 (H1, a), 7.38 (H3, b), 7.79 (d, H4, c), μ-Dabco 3.13 (s, CH_2, h). ^1H

NMR (CD_2Cl_2): δ 2.08 (s, CH_3, f), 3.90 (s, CH_2, d), 7.32 (m, H1, a), 7.38 (dd, H3, b),

7.79 (d, H4, c), 3.05 (s, μ-Dabco CH_2, h). Crystals of the metal complex could be grown

from a CH_2Cl_2 solution by layering it with methanol or by slow evaporation.

5.2.3. Synthesis of $Zn_2(NBA)_2(\mu\text{-piperazine})$. The piperazine complex can be

prepared by the same procedure used to synthesize the Dabco complex. 94.5 mg (2.68 x

10^{-4} mol) of $NBAH_2$, 59.1 mg (2.69×10^{-4} mol) of $Zn(C_2H_3O_2)_2 \cdot 2H_2O$, and 88.6 mg

(1.03×10^{-3} mol) of anhydrous piperazine yielded 34 mg of white powder (3.7×10^{-5} mol,

27 %) of $Zn_2(NBA)_2(\mu\text{-piperazine})$. ^1H NMR ($CDCl_3$): δ 2.11 (s, CH_3, f), 3.89 (s, CH_2,

d), 7.24 (s, H1, a), 7.37 (dd, H3, b), 7.80 (d, H4, c), 3.21 (s, μ-piperazine CH_2, h), 3.49

(d, μ-piperazine NH, h). ^1H NMR (CD_2Cl_2): δ 2.08 (s, CH_3, f), 3.90 (s, CH_2, d), 7.25 (s,

H1, a), 7.39 (dd, H3, b), 7.80 (d, H4, c), 3.15 (s, μ-piperazine CH_2, h). Crystals of the

metal complex could be grown from a CH_2Cl_2 solution by layering it with methanol or by

slow evaporation.

Alternatively, $Zn_2(NBA)_2(\mu\text{-piperazine})$ can also be prepared in crude from the

Dabco complex. Piperazine (31.9 mg, 3.7×10^{-4} mol) was dissolved in 3 mL of methanol.

The Zn$_2$(NBA)$_2$(μ-Dabco) complex (11.8 mg, 1.3 x 10^{-5} mol) was added to 1.5 mL of the piperazine solution and stirred for 30 min. The solid was filtered and the filter cake was washed with 1mL of methanol. The filter cake was then washed with the remaining 1.5 mL of piperazine solution followed by 1 ml of methanol to remove any excess piperazine. The white solid was air dried resulting in a yield of 7 mg of white powder, only 4.56 mg (giving a total yield of 40%) of which were Zn$_2$(NBA)$_2$(μ-piperazine) based on the ^{1}H NMR data. According to the ^{1}H NMR data, Zn$_2$(NBA)$_2$(μ-Dabco) was still present. Because separation of the Dabco and piperazine complexes was not possible, we determined the amount of the piperazine complex produced by comparing the areas of the methylene peaks of piperazine and Dabco in the ^{1}H NMR spectrum of the product.

5.2.4. Synthesis of Zn$_2$(NBA)$_2$(μ-pyrazine). The pyrazine complex was synthesized from NBAH$_2$ (21.5 mg, 6.10 x 10^{-5} mol), Zn(C$_2$H$_3$O$_2$)$_2$·2H$_2$O (26.8 mg, 6.10 x 10^{-5} mol), and pyrazine (27.1 mg, 3.38 x 10^{-4} mol) by the same procedure used to synthesize the Dabco complex, yielding 7.4 mg of white powder, 8.10 x 10^{-6} mol (27 %) Zn$_2$(NBA)$_2$(μ-pyrazine). ^{1}H NMR (CDCl$_3$): δ 2.12 (s, CH$_3$, f), 3.89 (s, CH$_2$, d), 6.90 (s, H1, a), 7.35 (dd, H3, b), 7.77 (d, H4, c), 8.63 (s, μ-pyrazine Ar-H, h). ^{1}H NMR (CD$_2$Cl$_2$): δ 2.06 (s, CH$_3$, f), 3.89 (s, CH$_2$, d), 6.90 (s, H1, a), 7.35 (dd, H3, b), 7.76 (d, H4, c), 8.63 (s, μ-pyrazine Ar-H, h). The pyrazine complex, like the piperazine complex, can be synthesized from the Dabco complex. Washing 13.8 mg of the Zn$_2$(NBA)$_2$(μ-Dabco) complex with a methanol solution of pyrazine (0.185 g, 2.31 x 10^{-3} mol), as was done with piperazine, resulted in 4.9 mg of white powder, 5.4 x 10^{-6} mol (37%) of

$Zn_2(NBA)_2(\mu$-pyrazine). 5.4 mg of the starting complex, $Zn_2(NBA)_2(\mu$-Dabco), remained according to the same ^{1}H NMR analysis used on the piperazine complex.

5.2.5. Synthesis of $Zn_2(NBA)_2(\mu$-piperazine-1,4-d_2). The imine groups of the piperazine were deuterated by dissolving approximately 0.1 g of piperazine in 1 mL of CD_3OD (ND:NH, ~10:1) in a dry box. This solution was stirred for 10 min before approximately 40 mg of $Zn_2(NBA)_2(\mu$-piperazine) were added. The CD_3OH which formed was allowed to evaporate in the inert atmosphere.

5.2.6. Instruments and Procedures. The ^{1}H NMR, NOE, and 2D COSY experiments were done on Bruker AC250 and ARX300 spectrometers. Electronic absorption spectra were recorded on an Aviv Model 14DS absorption spectrophotometer. Luminescence spectra were recorded using a Spex Industries Fluorolog 2 Model F112X emission spectrophotometer (with a Hamamatsu R928P PMT and the appropriate colored-glass filters to reduce stray light) and were corrected as previously described[56] for variations in detector sensitivity with wavelength.

5.2.7. Lifetime Measurements. A Nd:YAG laser (using the 355-nm third harmonic) was used to excite the $Zn_2(NBA)_2(\mu$-G) (G = Dabco, piperazine, or pyrazine) complexes in degassed CH_2Cl_2 solutions ranging in concentrations from 2×10^{-4} to 7×10^{-4} M. The resulting fluorescence signal and its decay was detected by a photomultiplier tube and displayed on one channel of a Tektronix oscilloscope as a function of time. The ln of the decay curve could be plotted against time. From a plot of the logarithm of the emission intensity vs. time, the lifetime of the excited state could be determined. The complexes could not be left in CH_2Cl_2 for more than 8 hrs. without decomposing.

5.3 Results and Discussion

5.3.1. ^{1}H NMR Data. The ^{1}H NMR spectra of the three Zn^{2+} complexes

(**Figure 5.1;** $Zn_2(NBA)_2(\mu$-Dabco), $Zn_2(NBA)_2(\mu$-piperazine), and $Zn_2(NBA)_2(\mu$-

pyrazine) have similar chemical shifts, but can be distinguished from one another and that

of the ligand ($NBAH_2$) by certain resonances. The ^{1}H NMR spectral data for the two

forms of the ligand (see **Figure 5.2**) have been tabulated in **Table 5.1** and the data for the
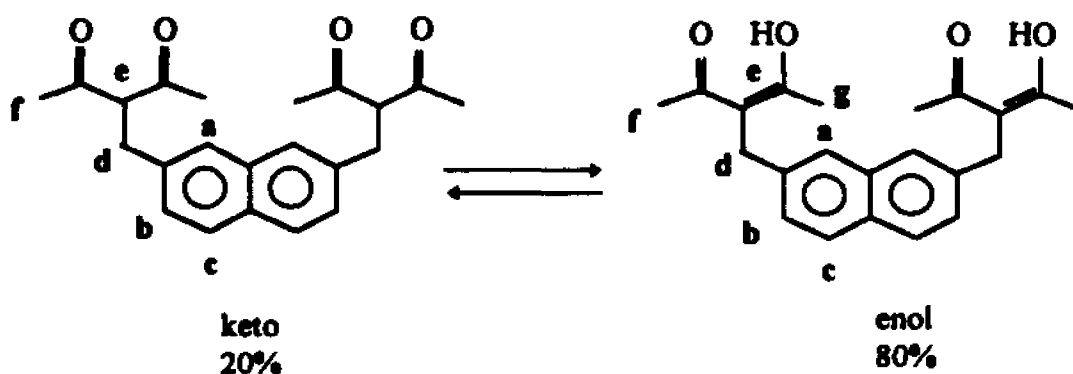
three complexes in **Table 5.2**.

keto
20%

enol
80%

Figure 5.2. Keto-enol tautomerism of $NBAH_2$ (approximate proportions of the two tautomers in $CDCl_3$ shown as %).

Table 5.1. ^{1}H NMR chemical shifts (ppm) of the keto and enol forms of $NBAH_2$ in $CDCl_3$.

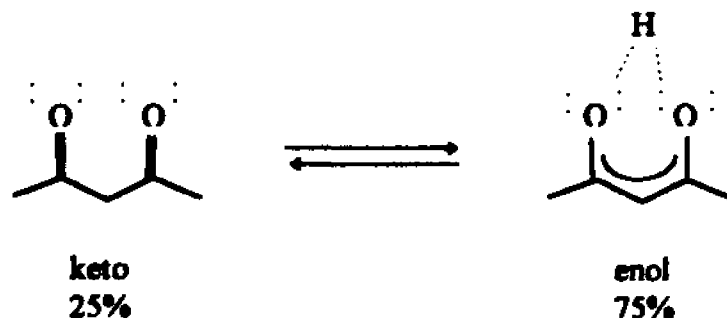|	NBAH₂	
	Keto form	*Enol form*
a	7.55 (s)	7.46 (s)
b	7.28 (d)	7.29 (d)
c	7.75 (d)	7.77 (d)
d	3.30 (d)	3.81 (s)
e	4.12 (t)	16.90 (s)
f, g	2.14 (s)	2.11 (s)

Figure 5.3. Keto-enol tautomerism of acac (approximate proportions of the two tautomers in CDCl₃ shown as %).

The NBAH₂ ligand (**Figure 5.2**) exists in a keto-enol tautomerism similar to that of acetylacetone (acacH). AcacH has been found to be in the keto form 25% of the time. The enol form is stabilized not only by conjugation but also by hydrogen bonding as the hydoxylic proton is shared between the two carbonyl oxygens (**Figure 5.3**). NBAH₂ experiences a similar stabilization of the enol form, which comprises 81% of the mixture as seen in the ^{1}H NMR spectrum. The ^{1}H resonances of NBAH₂ which allow for differentiation between the complexes are those of the methyl protons (f and g; see lettering in **Figure 5.2**), the methylene protons (d), and the protons at positions 1 and 8 on the aromatic rings (a).

When the enolic or the tertiary keto proton is removed upon treating the ligand with a basic solution containing Zn^{2+} ions, the carbonyl oxygens are available to chelate the Zn^{2+} ions to form the bimetallic complex (**Figure 5.4**). The resonances corresponding to the naphthyl protons (a) are shifted upfield to varying degrees depending on the identity of G (see **Table 5.2**).
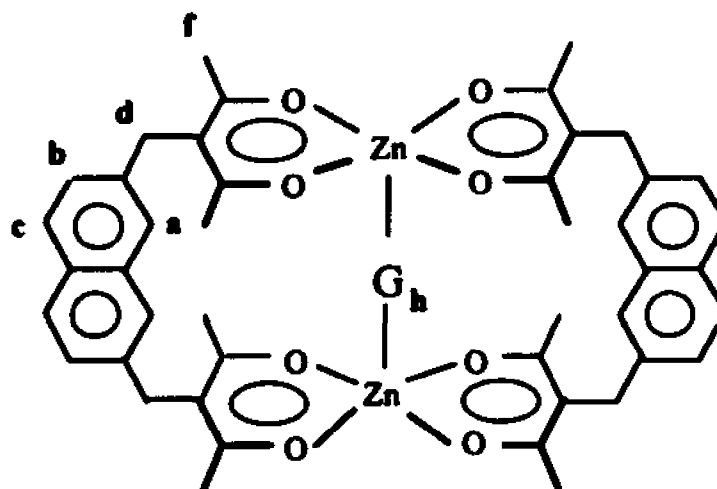
Figure 5.4. $Zn_2(NBA)_2(\mu-G)$ (G = Dabco, piperazine, or pyrazine) with H's labled.

Table 5.2. ^1H NMR chemical shifts (ppm) of Zn^{2+} complexes in $CDCl_3$ and CD_2Cl_2.

	$Zn_2(NBA)_2$ $(\mu$-Dabco)		$Zn_2(NBA)_2$ $(\mu$- piperazine)		$Zn_2(NBA)_2(\mu$- pyrazine)	
	CDCl₃	CD₂Cl₂	CDCl₃	CD₂Cl₂	CDCl₃	CD₂Cl₂
a	7.30 (s)	7.32 (s)	7.24 (s)	7.25 (s)	6.90 (s)	6.90 (s)
b	7.38 (dd)	7.38 (dd)	7.37 (dd)	7.39 (dd)	7.35 (d)	7.35 (d)
c	7.79 (d)	7.79 (d)	7.80 (d)	7.80 (d)	7.77(d)	7.76 (d)
d	3.90 (s)	3.90 (s)	3.89 (s)	3.90 (s)	3.89 (s)	3.89 (s)
f	2.13 (s)	2.08 (s)	2.11(s)	2.08 (s)	2.12 (s)	2.06 (s)
h	3.13 (s)	3.05 (s)	3.21 (s), 3.49 (d)	3.15 (s)	8.63 (s)	8.63 (s)

The complex containing a bridging pyrazine shows the greatest shift, 0.56 ppm upfield, for the resonance of a. The magnetic field of the ring current of pyrazine could be influencing the naphthyl protons at these positions. The methyl diphenyl bridge of a 1,3-

bis[[(6-aminopyrid-2-yl)amino]carbonyl]-5-nitrobenzene macrocycle had a similar effect

on the phenyl ring of its bound phosphate guest.[76] In this case the phenyl ring of the guest

was in a position to experience the magnetic field generated by the host's phenyl rings.

The end result was an upfield shift of ~ 0.5 ppm of the guest's phenyl protons.[76]

The other major change in the proton resonances of the ligand upon complexation

is the downfield shift of the methylene protons (d) from 3.81 to ~3.89 ppm. Now the

methylenes are experiencing some deshielding by the six membered rings formed from the

chelating acac's$^-$ and Zn^{2+} atoms. Being α to the Zn-acac system places the methylene

protons in the correct position to influence the ring current effect.

The resonances of the methylene and aromatic protons of the guest molecules all

experience a downfield shift upon binding to the host (see Table 5.3).

Table 5.3. ^{1}H NMR chemical shifts (ppm) for the methylene and aromatic protons
        of free and bound guests in a CDCl$_3$ at room temperature.

	Dabco CH$_2$ (ppm)	piperazine CH$_2$ (ppm)	pyrazine CH (ppm)
in complex	3.13 (s)	3.21 (s)	8.63 (s)
alone	2.80 (s)	2.81 (s)	8.59 (s)

The piperazine methylene peak is a broad singlet (3.21 ppm) showing no distinction

between bound and unbound methylene protons as seen for the Dabco complex in a

solution containing both bound and unbound Dabco. From the crystal stucture of

$Zn_2(NBA)_2(\mu\text{-piperazine})$,[77] it can be seen that the piperazine is in the chair comformation
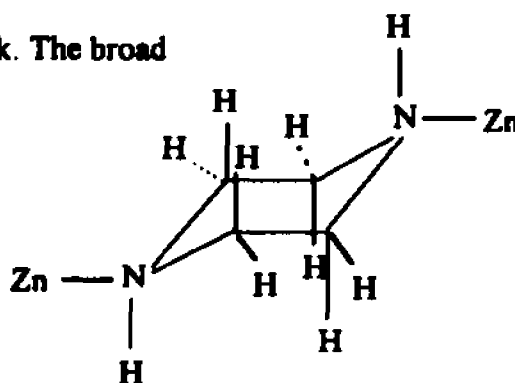
resulting in axial and equatorial methylene protons as seen to the right. This could

contribute to the increased width of the peak. The broad

peak could be masking a faintly visible

peak at 2.81 ppm representing unbound

piperazine. The peak representing the

aromatic protons of pyrazine is also broad

when it is bound to the complex. No distinction can be made here between the bound and

unbound pyrazine as in the case of piperazine.

We were also interested in the location of the piperazine NH resonance in the

complex, compared to the value for free piperazine (5.16 ppm). The resonances of the

NH protons of the piperazine move upfield upon binding. We were unable to locate the

NH protons in CD_2Cl_2. This result caused us to question our chemical shift assignments.

One way to identify the NH resonance is to prepare the corresponding deuterated

compound, and determine which peak(s) decrease in intensity. We prepared piperazine-

1,4-d_2 (see Experimental Section), and used it to prepare $Zn_2(NBA)_2(\mu$-piperazine).

This sample showed a much smaller resonance at 3.49 ppm; therefore, we assign this 3.49-

ppm resonance to N-H.

5.3.2. Binding Constant Measurements. The ^{1}H NMR data have proven to be

very useful in the calculation of relative binding constants. By knowing the initial

concentration of the complex in $CDCl_3$ and integrating the peaks representing the NBA

methylenes (3.80 or 3.89 ppm) and the methylenes for either piperazine or Dabco, the

following can be solved for the equilibrium constant:

$$K = [Zn_2(NBA)_2(\mu\text{-}G)]/([Zn_2(NBA)_2][G])$$

The calculations differ slightly for the two guests. When G is piperazine the ratio of host methylenes (3.89 ppm) to guest methylenes (3.21 ppm) is 1:1. Therefore, the excess area beneath the peak belonging to the resonating piperazine methylenes accounts for uncomplexed piperazine or the [piperazine] at equilibrium. When G is Dabco the [Dabco] can be determined by the recognizable peak (2.80 ppm) representing unbound Dabco. The [Zn_2(NBA)_2] is determined by the area of the peak at 3.80 ppm. We know from spin saturation experiments done in our lab that the Dabco moves in and out of the host complex in a $CDCl_3$ solution.[77] These experiments showed that the magnetization was being transferred from the free to the bound Dabco. When the Dabco moves out it gives an H_2O molecule a chance to take its place in the complex.

With each guest, the NMR spectra also showed small amounts of resonances as 3.80 and 7.45 ppm, which we attriibute to an "empty" complex (or $Zn_2(NBA)_2(H_2O)_2$). We used the ratio of these peaks to those for the host-guest peaks to estimate K. When calculated in this manner the binding constants of $Zn_2(NBA)_2(\mu\text{-piperazine})$ and $Zn_2(NBA)_2(\mu\text{-Dabco})$ differ by a factor of approximately 10: 1.5×10^4 M^{-1} and 3.7×10^5 M^{-1}, respectively. This factor of 10 difference in binding constants is similar to the difference found between the two upon binding to the $Cu_2(NBA)_2$ complex. The binding constant for pyrazine is on the order of 1000 times smaller than the piperazine complex and more difficult to report accurately, therefore, an approximate value for K of 50 M^{-1} for the pyrazine complex will be given at this time.

5.3.3. Luminescence Measurements. A molecule having a populated excited state can repopulate the ground state by three different methods.[65] The first method by which the molecule can move to a lower electronic energy level is by internal conversion. Internal conversion occurs when the vibrational levels of one excited state overlap (or are at thermal equilibrium) the vibrational levels of a lower electronic state so that the population shifts from one to the other. If the vibrational levels of adjacent electronic states do not overlap, another route of relaxation must be used. If the energy gap between electronic states is small, the molecule can relax to a lower electronic state by tunnelling. If the energy gap is large the third process, a radiative transition may be employed. More rigid molecules, such as those possessing aromatic systems, have fewer vibrational levels, so that the probability of overlap is less as is the probability of internal conversion. These molecules tend to relax by radiative processes such as fluorescence or phosphorescence.

When relaxing by a radiative process the molecule can move from an excited singlet state (the two electrons are opposite in spin) to the ground state (fluorescence), or it can be converted from a singlet state to a triplet state via intersystem crossing (changing the spin angular momentum) and then relax to the ground state (phosphorescence).

The first intense absorption and emission λ_{max} of the $Zn_2(NBA)_2(\mu\text{-}G)$ (G = Dabco, piperazine, or pyrazine) complexes and the ligand ($NBAH_2$) (in CH_2Cl_2 at room temperature) are given in Table 5.4. The absorption and emission λ_{max} for the complexes are very similar to those observed for the $NBAH_2$ ligand. This suggests that the origin of these electronic transitions is from within the ligand.

Table 5.4. Luminescence data on $Zn_2(NBA)_2(\mu-G)$ complexes and the $NBAH_2$ ligand in CH_2Cl_2 at room temperature.

	Absorption λ_{max} (nm)	Emission λ_{max} (nm)	Lifetime (nsec)
$Zn_2(NBA)_2(\mu-Dabco)$	285	530	400
$Zn_2(NBA)_2(\mu-piperazine)$	300	500	515
$Zn_2(NBA)_2(\mu-pyrazine)$	289	496	320
$NBAH_2$	300	428, 485	

These transitions are at slightly longer wavelengths due to the shift in electron density upon chelation to the Zn^{2+} atoms and binding to the various guests. Upon prolonged exposure to the excitation light, the complex solutions produce an emission peak at ~427 nm which is probably the ligand produced as a result of decomposition. The presence of H_2O in the samples increases the rate at which the intensity of the transition at 427 nm increases.

An examination of the lifetimes of these complexes can provide further information of the identity of these electronic transitions.

5.3.4. Lifetime Measurements. The distinction between fluorescence and phosphorescence can be made based upon whether or not the promoted electron changes spin. This can be determined quantitatively by the lifetime of the excited state. Once a molecule is excited, the time it takes to relax back to the ground state can be anywhere from 10^{-14} to several seconds[65] depending on the method of relaxation. For the mode of relaxation to be fluorescence, the energy gap between the lowest singlet vibrational state

and the highest ground vibrational state must be large enough to allow for a radiative transition as opposed to internal conversion.

The molecule can also relax from the first excited singlet state via radiationless intersystem crossing to the lowest triplet state. The process of relaxing from a triplet state to the ground state produces phosphorescence. Although the change in population of a singlet state to a triplet state requires a change in spin angular momentum, which is classically forbidden, it can occur. The triplet state, for a given molecule, usually lies lower in energy than the singlet state due to the fact that there is less electronic repulsion. The overlap of the excited singlet state lower vibrational levels with the triplet state higher vibrational levels is usually good so that the intersystem crossing process competes with fluorescence as a mode of relaxation.

From Table 5.4 it can be seen that the lifetimes of the $Zn_2(NBA)_2(\mu\text{-G})$ complexes fall within the range of 3.0×10^{-7} - 5.0×10^{-7} sec. The fluorescence lifetime of naphthalene in solution at 300 K is 1×10^{-7} sec.[78] This suggests that the radiative relaxation process for our complexes is phosphorescence.

5.4 Conclusions

By changing the metal atom of the cofacial binuclear bis(β-diketone) complexes from copper to zinc the electronic properties of the molecule have been altered creating a molecule having new spectroscopic properties. The ^1H NMR spectroscopy data as well as the luminescence of the $Zn_2(NBA)_2(\mu\text{-G})$ (G = Dabco, piperazine, or pyrazine) complexes have been measured.

The ^{1}H NMR data has been used to estimate binding constants which show the same trends as seen with the $Cu_2(NBA)_2(\mu\text{-}G)$ (G = Dabco, piperazine, or pyrazine) complexes. The greatest affinity for the host complex, or highest binding constant, is found for, Dabco. Pyrazine has the least affinity for the host complex, or lowest binding constant.

The colorless $Zn_2(NBA)_2(\mu\text{-}G)$ complexes exhibit luminescence similar to that of the NBAH$_2$ ligand. The luminescence of the ligand is characteristic of that exhibited by naphthalene and its derivatives. These transitions observed in the 496-530 nm region of the spectrum are where the $Cu_2(NBA)_2(\mu\text{-}G)$ complexes absorb light; therefore, it is not expected that luminescence would be observed for the copper complexes.

Chapter 6. Conclusions

6.1 Results

We have synthesized a variety of cofacial binuclear copper(II) and zinc(II) bis(β-diketone) complexes ($M_2(NBA)_2(\mu\text{-}G)$) (M = Cu^{2+} or Zn^{2+}) see Figure 6.1).
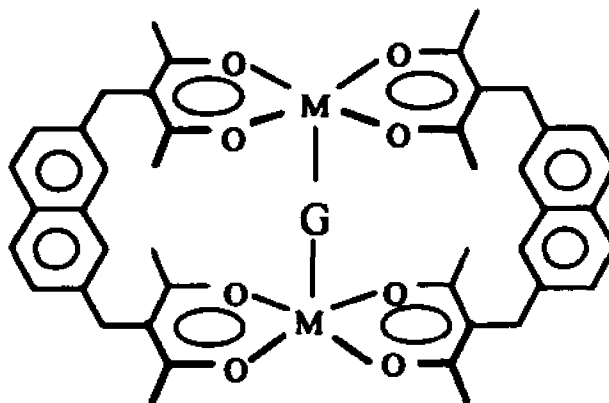

Figure 6.1. $M_2(NBA)_2$ (M = Cu^{2+} or Zn^{2+}) host complex with guest (G).

We have placed Br and CN substituents on the bridging naphthalenes of the $NBAH_2$ ligand and synthesized the cofacial bimetallic copper(II) complexes. These substituents result in preferential binding of one guest over another.
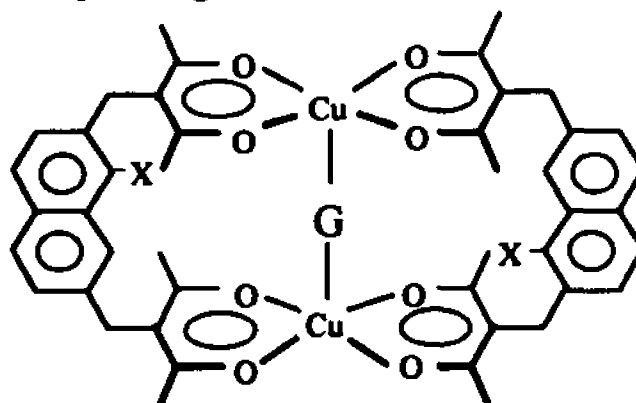

Figure 6.2. $Cu_2(NBA\text{-}X)_2$ (X = H, Br, or CN) host complex with guest (G).

96

We have measured the host-guest interactions using UV-Vis and NMR spectroscopy techniques. The former was used to measure the equilibrium of the paramagnetic copper(II) complexes and the latter for the diamagnetic zinc(II) complexes. In general, the binding constants decrease upon using bulkier substituents on the host complexes (as in the case of the substituted Cu^{2+} complexes), larger guest molecules, or less basic guest molecules unless hydrogen bonding is possible as in the case of the following:

A. The O of $Cu_2(NBA)_2$ interacting with an NH_2 proton of aminopyrazine[38]; or

B. The N of $Cu_2(NBA-CN)_2$ interacting with the NH protons of piperazine.

Although we have yet to mimic the catalytic activity of alkaline phosphatase, we have discovered how to make our complexes more selective when binding small nitrogenous bases. By using substituents, on the naphthalene rings, which are capable of hydrogen bonding with a guest molecule, we have increased the affinity of our host complex for guest molecules containing groups capable of hydrogen bonding. We are one step further toward our goal with the design and synthesis of complexes which preferentially bind one guest over another. Now we can modify the naphthalene substituents to include groups that can undergo chemical reactions with a guest molecule.

6.2 Future work

Even though our binuclear bis(β-diketone) complexes provide a novel example of host molecules, their stability in solution leaves something to be desired. When left in $CHCl_3$ overnight, these complexes begin to decompose. When left in $CHCl_3$ with guest molecules, in some cases, decomposition is apparent after only 12 hours. This low

stability makes it difficult to obtain accurate binding constants. This problem might be alleviated by using a ligand which could provide a more stable complex in solution.

We believe that 6.1, being very similar to the ligand used by McAuliffe et al. as a model for the oxygen evolution center of photosystem II,[79] might be a good candidate.

This macrocyclic octadentate binucleating ligand should be accessible from NBAH$_2$ and its derivatives.

The formation of this octadentate binucleating complex will require the coming together of one ligand and two metal ions

6.1
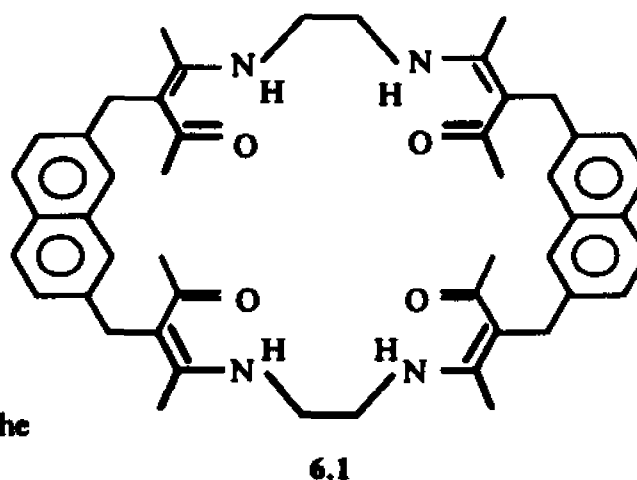
as opposed to two ligand molecules binding two metal ions, as in the case of our complexes. The resulting ΔS for the former will be more favorable and the complex will hopefully be more stable than the corresponding NBA^{2-} complex. The ligand could be synthesized by treating NBAH$_2$ with ethylenediamine. The ligand synthesis will be similar to that of the 3 + 2 nitrogen-donor cryptands.[80] Our version of this reaction will involve slowly adding a dilute solution of our β-diketone to a dilute solution of ethylenediamine at 0 °C. The resulting product will be ligand 6.1 which could also be designed with various substituents at the 1 position of the naphthalene rings.

Other substituents which would prove to be useful at the 1 position of the naphthalene bridge are OH and COOH. Complexes with these groups in the cavity and Zn^{2+} atoms binding to the ligand would resemble the active site of alkaline phosphatase

much more closely. Then with organophosphate ions bound to the Zn^{2+} atoms, it is

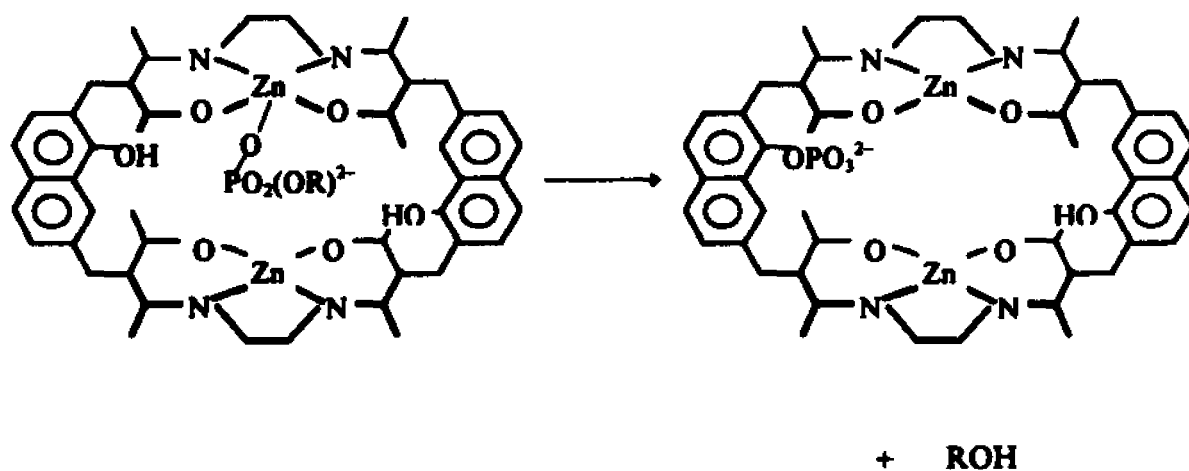possible that hydrolysis could occur as seen in **Figure 6.3**.

+ ROH

Figure 6.3. Hydrolysis of an organophosphate by proposed cofacial binuclear Zn^{2+} complex.

References

1. Lehn, J.-M.; In *Frontiers in Supramolecular Organic Chemistry and Photochemistry*; Schneider, H.-J.; Dürr, H. Ed.; VCH Publishers: New York, NY, 1991, pp. 1-28.

2. Cram, D. J.; Trueblood, K. N. In *Host Guest Complex Chemistry: Macrocycles*; Vögtle, F.; Weber, E. Ed.; Springer: Berlin, 1985, pp. 125-188.

3. Collman, J. P.; Elliott, C. M.; Halbert, T. R.; Tovrog, B. S. *Proc. Natl. Acad. Sci. U. S. A.* **1977**, *74*, 18-22.

4. Ogoshi, H.; Sugimoto, H.; Yoshida, Z. *Tetrahedron Lett.* **1977**, 169-172.

5. Chang, C. K.; Wang, C.-B. In *Electron Transport and Oxygen Utilization*; Elsevier Biomedical, **1982**; pp. 237-243.

6. Chang, C. K.; Takamura, S.; Musselman, B. D.; Kessel, D. *ACS Symp. Ser.* **1986**, 321 (Porphyrins: Excited States Dyn.) pp. 347-361.

7. Chang, C. K.; Sotiriou, C. *J. Org. Chem.* **1987**, *52(5)*, 926-929.

8. Ogoshi, H.; Hatakeyama, H.; Yamamura, K.; Kuroda, Y. *Chem. Lett.* **1990**, *11*, 51-54.

9. Ogoshi, H.; Hatakeyama, H.; Kotani, J.; Kawashima, A.; Kuroda, Y. *J. Am. Chem. Soc.* **1991**, *113 (21)*, 8181-8183.

10. Ogoshi, H.; Suzuki, Y.; Kuroda, Y. *Chem. Lett.* **1991**, *(9)*, 1547-50.

11. Collman, J. P.; Hutchison, J. E.; Lopez, M. A.; Guilard, R. *J. Am. Chem. Soc.* **1992**, *114(21)*, 8066-73.

12. Collman, J. P.; Wagenknecht, P. S.; Hutchison, J. E.; Lewis, N. S.; Lopez, M. A.; Guilard, R.; L'Her, M.; Bothner-By, A. A.; Mishra, P. K. *J. Am. Chem. Soc.* **1992**, *114(14)*, 5654-64.

13. Collman, J. P.; Wagenknecht, P. S.; Lewis, N. S. *J. Am. Chem. Soc.* **1992**, *114(14)*, 5654-64.

14. Collman, J. P.; Hutchison, J. E.; Ennis, M. S.; Lopez, M. A.; Guilard, R. *J. Am. Chem. Soc.* **1992**, *114(21)*, 8074-80.

15. Collman, J. P.; Hutchison, J. E.; Lopez, M. A.; Tabard, A.; Guilard, R.; Seok, W. K.; Ibers, J. A.; L'Her, M. J. *J. Am. Chem. Soc.* 1992, *114(25)*, 9869-77.

16. Collman, J. P.; Wagenknecht, P. S.; Hutchinson, J. E. *Angew. Chem. Int. Ed Engl.* 1994, *33*, 1537-1554.

17. Chang, C. K.; Liang, Y.; Aviles, G.; Peng, S. M. *J. Am. Chem. Soc.* 1995, *117(14)*, 4191-2.

18. Anderson, S.; Anderson, H. L.; Bashall, A.; McPartlin, M.; Sanders, J. K. M. *Angew. Chem. Int. Ed. Engl.* 1995, *34*, 1096-1099.

19. Lehn, J. M. *Pure & Appl. Chem.* 1980, *52*, 2441-2457.

20. Motekaitis, R. J.; Martell, A. E.; Lehn J.-M.; Watanabe, E.-I. *Inorg. Chem.* 1982, *21*, 4253-4257.

21. Nelson, S. M.; Esho, F.; Lavery, A.; Drew, M. G. B. *J. Am. Chem. Soc.* 1983, *105*, 5693-5695.

22. Coughlin, P. K.; Martin, A. E.; Dewan, J. C.; Watanabe, E.-I.; Bulkowski, J. E.; Lehn, J.-M.; Lippard, S. *Inorg. Chem.* 1984, *23*, 1004-1009.

23. Murase, I.; Yeno, S.; Kida, S. *Inorg. Chim. Acta* 1986, *111*, 57-60.

24. Murase, I.; Mikuriya, M.; Sonoda, H.; Fukuda, Y.; Kida, S. *J. Chem. Soc., Dalton Trans.* 1986, 953-959.

25. Murase, I.; Ueda, I.; Marubayashi, N.; Kida, S.; Matsumoto, N.; Kudo, M.; Toyohara, M.; Hiate, K.; Mikuriya, M. *J. Chem. Soc., Dalton Trans.* 1990, 2763-2769.

26. Murase, I.; Vuckovic, G.; Kodera, M.; Harada, H.; Matsumoto, N.; Kida, S. *Inorg. Chem.* 1991, *30(4)*, 728-730.

27. Lehn, J. M.; Vigneron, J. P.; Bkouche-Waksman, I.; Guilhem, J.; Pascard, C. *Helv. Chim. Acta* 1992, *75(4)*, 1069-1070.

28. Lehn, J. M. *Science* 1993, *260(5115)*, 1762-1763.

29. Izumitani, T.; Okawa, H.; Kida, S. *Chem. Lett.* 1981, 483-488.

30. Okawa, H.; Kakimoto, M.; Izumitani, T.; Nakamura, M.; Kida, S. *Bull. Chem. Soc. Jpn.* 1983, *56*, 149-152.

31.   Whitmore, B. C.; Eisenberg, R. *Inorg. Chem.* **1984**, *24*, 1624-1629.

32.   Okawa, H.; Honda, A.; Nakamura, M.; Kida, S. *J. Chem. Soc., Dalton Trans.* **1985**, 59-64.

33.   Mashuta, M. S.; Doman, T. N.; Pierce, W.; Buchanan, R. M. *Inorg. Chim. Acta* **1988**, *145*, 21-28.

34.   Buchanan, R. M.; O'Brien, R. J.; Richardson, J. F.; Latour, J. M. *Inorg. Chim. Acta* **1993**, *214(1-2)*, 33-40.

35.   Lintvedt, R. L.; Ranger, G.; Schoenfelner, B. H. *Inorg. Chem.* **1984**, *23*, 688-695.

36.   Maverick, A. W.; Klavetter, F. E. *Inorg. Chem.* **1984**, *23*, 4129-4130.

37.   Maverick, A. W.; Buckingham, S. C.; Yao, Q.; Bradbury, J. R.; Stanley, G. G. *J. Am. Chem. Soc.* **1986**, *108*, 7430-7431.

38.   Maverick, A. W.; Ivie, M. L.; Waggenspack, J. H.; Fronczek, F. R. *Inorg. Chem.* **1990**, *29*, 2403-2409.

39.   Fujimoto, K.; Shinkai, S. *Tetrahedron Lett.* **1994**, *35*, 2915-2918.

40.   Martin, D. F.; Fernelius, W. C.; Shamma, M. *J. Am. Chem. Soc.* **1959**, *81*, 130-133.

41.   Martin, D. F.; Martin, B. B. *Inorg. Chem.* **1962**, *1*, 404-409.

42.   Kim, E. E.; Wyckoff, H. W. *J. Mol. Biol.* **1991**, *218*, 449-464 and references therein.

43.   Karlin, K. D.; Gultneh, Y. *J. Chem. Ed.* **1985**, *62*, 983-990.

44.   Buchanan, R. M.; Chen, S.; Richardson, J. F.; Bressan, M.; Forti, L.; Morvillo, A.; Fish, R. H. *Inorg. Chem.* **1994**, *33*, 3208-3209.

45.   Kimura, E.; Yamaoka, M.; Morioka, M.; Koike, T. *Inorg. Chem.* **1986**, *25*, 3883-3886.

46.   Kimura, E.; Koike, T.; Toriumi, K. *Inorg. Chem.* **1988**, *27*, 3687-3688.

47.   Kimura, E.; Shiota, T.; Koike, T.; Shiro, M.; Kodama, M. *J. Am. Chem. Soc.* **1990**, *112*, 5805-5811.

48. Kimura, E.; Shiota, T.; Koike, T.; Shiota, T.; Iitaka, Y. *Inorg. Chem.* **1990**, *29*, 4621-4629.

49. Gellman, S. H.; Petter, R.; Breslow, R. *J. Am. Chem. Soc.* **1986**, *108*, 2388-2394.

50. Karlin, K. D.; Cruse, R. W.; Gultneh, Y.; Hayes, J. C.; Zubieta, J. *J. Am. Chem. Soc.* **1984**, *106*, 3372-3374.

51. Karlin, K. D.; Haka, M. S.; Cruse, R. W.; Gultneh, Y. *J. Am. Chem. Soc.* **1985**, *107*, 5828-5829.

52. Gobel, M. W. *Angew. Chem. Int. Ed. Engl.* **1994**, *33*, 1141-1143.

53. Whitmore, B. C.; Eisenberg, R. *Inorg. Chem.* **1984**, *23*, 1697-7703.

54. Turro, N. J.; Lee, P. C. C. *Photochem. Photobiol.* **1980**, *32*, 327-334.

55. Gore, P. H.; Siddiquei, A. S. *J. C. S. Perkin Trans* **1972**, 1442-1445.

56. Maverick, A. W.; Lord, M. D.; Yao, Q.; Henderson, L. J., Jr. *Inorg. Chem.*, **1991**, *30*, 553-558.

57. Friedman, L.; Shechter, H. *J. Org. Chem.* **1961**, *26*, 2522-2524.

58. Brown, L. A.; Kumar, R.; Fronczek, F. R.; Maverick, A. W. *Acta Cryst. Sect. C.* **(1995)** in press.

59. Clar, E.; Wallenstein, H. D. *Chem. Ber.* **1931**, *64*, 2076-2082.

60. Fair, C. K. *MolEN, An Interactive Structure Solution Procedure*; Enraf-Nonius: Delft, The Netherlands, 1990.

61. Cruickshank, D. W. *Acta Crystallogr.* **1957**, *10*, 504-508.

62. Stevens, B. *Spectrochim. Acta* **1962**, *18*, 439-448.

63. Stevens, B.; Dickinson, T. *Spectrochim. Acta* **1963**, *19*, 1865-1870.

64. Iball, J.; Scrimgeour, S. N.; Young, D. W. *Acta Crystallor.* **1976**, *B32*, 328-330.

65. Schulman, S. G. *Fluorescence and Phosphorescence Spectroscopy: Physicochemical Principles and Practice*; Pergamon Press: NY, 1977.

66.   Prince, P.; Fronczek, F. R.; Gandour, R. D. *Acta Crystallogr.*, *Sect. C*, **1989**, *45*, 1256-1258.

67.   Prince, P.; Evans, K. L.; Boss, K. R.; Fronczek, F. R.; Gandour, R. D. *Acta Crystallogr.*, *Sect. C*, **1990**, *46*, 1150-1152.

68.   Prince, P.; Fronczek, F. R.; Gandour, R. D. *Acta Crystallogr.*, *Sect. C*, **1992**, *48*, 2225-2228.

69.   Private communication with Dr. George Stanley.

70.   Rose, N. J.; Drago, R. S. *J. Am. Chem. Soc.* **1959**, *81*, 6138-6141.

71.   pK_b values in H_2O: (a) Budavari, S. Ed. The *Merck Index*; Merck & Co., Inc.: Rahway, N. J. 1989; p 1521. (b) Linde, D. R. Ed. *CRC Handbook of Chemistry and Physics*; Boca Raton, FL 1992; p 8-38. (c) Perrin, D. D. Ed. *International Union of Pure and Applied Chemistry Analytical Chemistry Division Commission on Electroanalytical Chemistry: Dissociation Constants of Organic Bases in Aqueous Solution*; Butterworth and Co.; London 1965; p 201.

72.   The coordinates for **Figure 4.7** were produced by the *PCMODEL* program (Gajewski, J. J.; Gilbert, K. E. PCMODEL, 3.2; Serena Software, Bloomington, IN. 1991).

73.   The coordinates for **Figures 4.9** and **4.10** were produced by the *SYBYL* program (Naruto, S.; Motoc, I.; Marshall, G. R.; Daniels, S. B.; Sofia, M. J.; Katzenellenbogen, J. A. *J. Am. Chem. Soc.* **1985**, *107*, 5262-5270. Clark, M.; Cramer, R. D., III; Van Opdenbosch, N. *J. Comput. Chem.* **1989**, *10*, 982-1012.), using the crystal structure data of $Cu_2(NBA)_2(\mu$-piperazine) as the starting point.

74.   Kimura, E. In *Progress in Inorganic Chemistry*; Karlin, K. D., Ed., John Wiley & Sons, Inc.: New York, 1994.

75.   Cotton , F. A.; Wilkinson, G. *Advanced Inorganic Chemistry*, Fifth Edition; Wiley-Interscience: New York, NY, 1988, pg. 599.

76.   Hirst, S. C.; Tecilla, P.; Geib, S. J.; Fan, E.; Hamilton, A. D. *Israel J. Chem.* **1992**, *32*, 105-111.

77.   Laxman, R. K.; Fronczek, F. R. unpublished results.

78.   Turro, N. J. *Modern Molecular Photochemistry*; Benjamin/Cummings Publishing Co., Inc.: Menlo Park, CA, 1978.

79.   Watkinson, M.; Whiting, A.; McAuliffe, C. A. *J. Chem. Soc., Chem. Commun.* **1994**, 2141-2142.

80.   Smith, P. H.; Barr, M. E.; Brainard, J. R.; Ford, D. K.; Freiser, H.; Muralidharan, S.; Reilly, S. D.; Ryan, R. R.; Silks, L. A.; Yu, W. *J. Org. Chem.* **1993**, *58*, 7939-7941.

Vita

Laurie Ann Brown was born in Slidell, Louisiana on July 17, 1968. She graduated from Northshore High School in Slidell in 1986. She obtained her B.S. degree in Chemistry from the University of Southern Mississippi in 1990. In June of 1990, she came to Louisiana State University in Baton Rouge, where she began her graduate work under the guidance of Dr. Andrew W. Maverick. She will receive the degree of Doctor of Philosophy in Chemistry on December 22, 1995. On December 23, 1995, she will marry Daniel Colvin Johnson and they will live happily-ever-after.

The End

DOCTORAL EXAMINATION AND DISSERTATION REPORT

Candidate: Laurie A. Brown
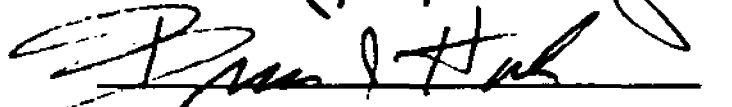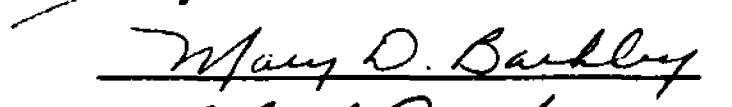
Major Field: Chemistry

Title of Dissertation: Host-Guest Chemistry of Cofacial Binuclear Copper(II) and Zinc(II) Complexes of Bis(Beta-Diketone) Ligands

Approved:

_____
Major Professor and Chairman

_____
Dean of the Graduate School

EXAMINING COMMITTEE:

_____

_____

_____

_____

_____

_____

_____

Date of Examination:

_____

October 20, 1995